JOURNAL OF PETROLOGY | VOLUME 48 | NUMBER 5 | PAGES 951–999 | 2007 | doi:10.1093/petrology/egm007

Compositional Zoning of the Bishop Tuff

WES HILDRETH[1]* AND COLIN J. N. WILSON[2]

[1]US GEOLOGICAL SURVEY, MS-910, MENLO PARK, CA 94025, USA

[2]SCHOOL OF GEOGRAPHY, GEOLOGY AND ENVIRONMENTAL SCIENCE, UNIVERSITY OF AUCKLAND, PB 92019 AUCKLAND MAIL CENTRE, AUCKLAND 1142, NEW ZEALAND

RECEIVED JANUARY 7, 2006; ACCEPTED FEBRUARY 13, 2007
ADVANCE ACCESS PUBLICATION MARCH 29, 2007

Compositional data for >400 pumice clasts, organized according to eruptive sequence, crystal content, and texture, provide new perspectives on eruption and pre-eruptive evolution of the >600 km^3 of zoned rhyolitic magma ejected as the Bishop Tuff during formation of Long Valley caldera. Proportions and compositions of different pumice types are given for each ignimbrite package and for the intercalated plinian pumice-fall layers that erupted synchronously. Although withdrawal of the zoned magma was less systematic than previously realized, the overall sequence displays trends toward greater proportions of less evolved pumice, more crystals (0·5–24 wt %), and higher FeTi-oxide temperatures (714–818°C). No significant hiatus took place during the 6 day eruption of the Bishop Tuff, nearly all of which issued from an integrated, zoned, unitary reservoir. Shortly before eruption, however, the zoned melt-dominant portion of the chamber was invaded by batches of disparate lower-silica rhyolite magma, poorer in crystals than most of the resident magma but slightly hotter and richer in Ba, Sr, and Ti. Interaction with resident magma at the deepest levels tapped promoted growth of Ti-rich rims on quartz, Ba-rich rims on sanidine, and entrapment of near-rim melt inclusions relatively enriched in Ba and CO_2. Varied amounts of mingling, even in higher parts of the chamber, led to the dark gray and swirly crystal-poor pumices sparsely present in all ash-flow packages. As shown by FeTi-oxide geothermometry, the zoned rhyolitic chamber was hottest where crystal-richest, rendering any model of solidification fronts at the walls or roof unlikely. The main compositional gradient (75–195 ppm Rb; 0·8–2·2 ppm Ta; 71–154 ppm Zr; 0·40–1·73% FeO) existed in the melt, prior to crystallization of the phenocryst suite observed, which included zircon as much as 100 kyr older than the eruption. The compositions of crystals, though themselves largely unzoned, generally reflect magma temperature and the bulk compositional gradient, implying both that few crystals settled or were transported far and that the observed crystals contributed little to establishing that gradient. Upward increases in aqueous gas and dissolved water, combined with the adiabatic gradient (for the ~5 km depth range tapped) and the roofward decline in liquidus temperature of the zoned melt, prevented significant crystallization against the roof, consistent with dominance of crystal-poor magma early in the eruption and lack of any roof-rind fragments among the Bishop ejecta, before or after onset of caldera collapse. A model of secular incremental zoning is advanced wherein numerous batches of crystal-poor melt were released from a mush zone (many kilometers thick) that floored the accumulating rhyolitic melt-rich body. Each batch rose to its own appropriate level in the melt-buoyancy gradient, which was self-sustaining against wholesale convective re-homogenization, while the thick mush zone below buffered it against disruption by the deeper (non-rhyolitic) recharge that augmented the mush zone and thermally sustained the whole magma chamber. Crystal–melt fractionation was the dominant zoning process, but it took place not principally in the shallow melt-rich body but mostly in the pluton-scale mush zone before and during batchwise melt extraction.*

KEY WORDS: *Bishop Tuff; ignimbrite; magma zonation; mush model; rhyolite*

INTRODUCTION

The Bishop Tuff, product of one of the world's greatest Quaternary eruptions, was released at 760 ka during an episode about 6 days long from the Long Valley magma chamber in eastern California. Fallout remnants are preserved from the Pacific Ocean to Nebraska, over an area of $>2{\cdot}5 \times 10^6$ km^2. Concurrent with the fallout, ash flows spread >70 km SE down Owens Valley, 40–50 km east to bank against the White Mountains, 40–50 km north into Mono Basin and Adobe Valley, and tens of kilometers SW down the San Joaquin River canyon (Fig. 1). Long Valley caldera collapsed along a 12 km × 22 km elliptical ring-fault zone that became active only after half or more of the erupting magma had escaped from the chamber.

*Corresponding author. Telephone: 650-329-5231. Fax: 650-329-5203. E-mail: hildreth@usgs.gov

Published by Oxford University Press (2007).

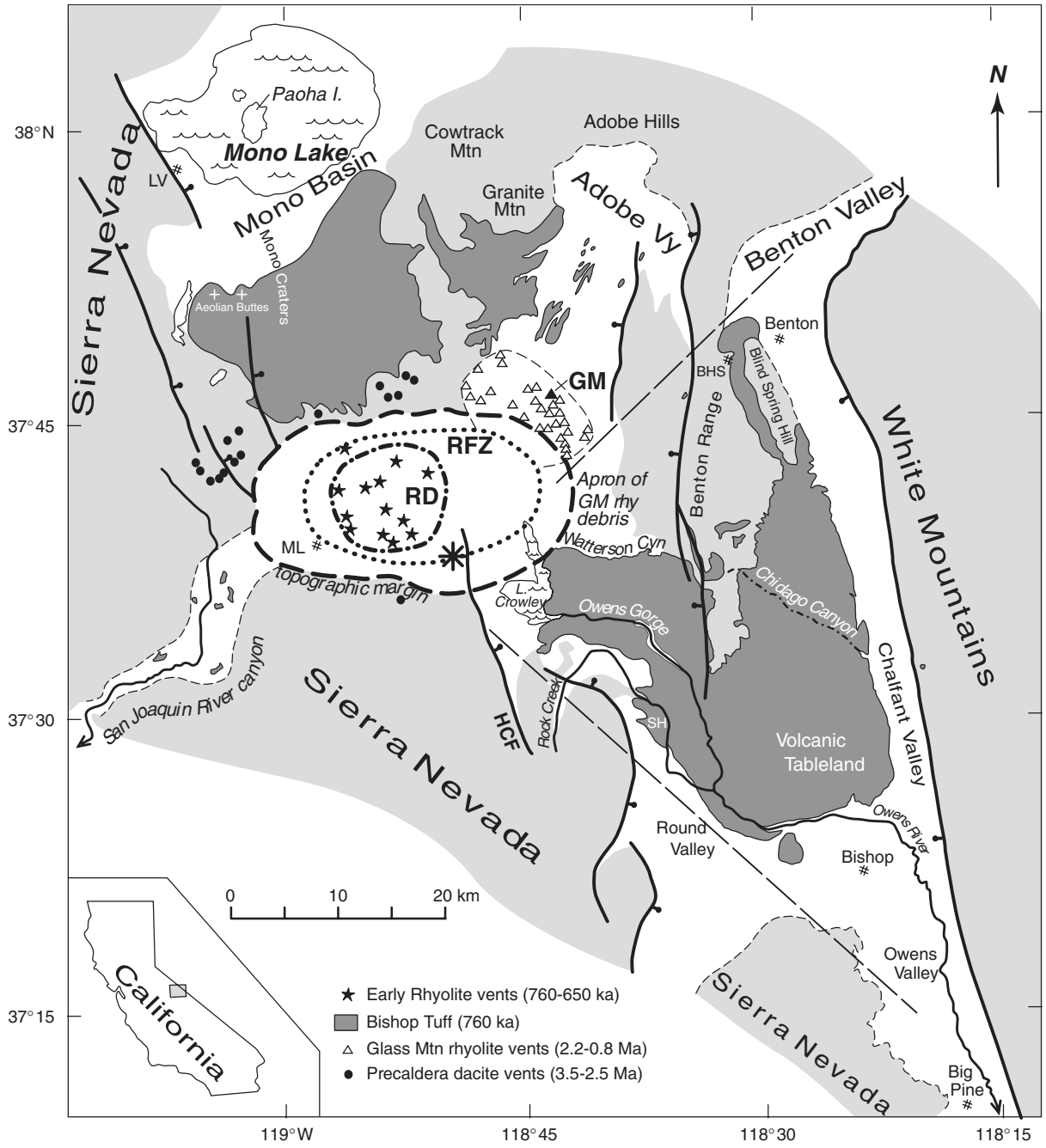

Fig. 1. Outline map of Long Valley caldera and the Bishop Tuff, straddling the extensionally faulted transition from Basin and Range to Sierra Nevada. Dark gray pattern indicates exposed Bishop Tuff; light gray is pre-Quaternary basement; white is Quaternary volcanic and valley-fill deposits. Shown for the caldera are its topographic margin (dashed), ring-fault zone (RFZ; dotted), and limit of structurally uplifted resurgent dome (RD; dash–dot). Exposed vents for precaldera dacites, precaldera Glass Mountain (GM) rhyolites, and early postcaldera rhyolites are identified (after Bailey, 1989; Metz & Bailey, 1993). Separate clusters of pre- and postcaldera rhyolite vents suggest that a shift of magmatic focus took place during growth of the caldera-forming Bishop magma chamber. Drilling has shown subsurface Bishop Tuff to extend NW beneath Paoha Island in Mono Lake, SE beneath Big Pine, and to be as thick as 1500 m beneath the caldera floor. Before erosion and burial, Bishop ignimbrite probably covered all of Mono Basin, Adobe Valley, Benton Valley, Chalfant Valley, Owens Valley at least as far south as Big Pine, and the canyon of the San Joaquin River as far as 50 km downstream; the patterned areas of present-day outcrops thus represent only about half the original ignimbrite distribution (even neglecting thin upland veneers). Plinian pumice-fall deposits are preserved only within the easterly sector confined by the two long-dash lines, though primary plinian ashfall is also recognized outside this sector as far as Owens Lake (160 km SSE) and Friant Dam (110 km SW). Large asterisk indicates initial vent site (for most of Igl and F1–F8 plinian fallout) as inferred by Hildreth & Mahood (1986). Place-name abbreviations: BHS, Benton Hot Springs; HCF, Hilton Creek fault; LV, Lee Vining; ML, town of Mammoth Lakes; SH, Sherwin Hill. Chidago Canyon is normally a dry wash (dot–dash line).

The caldera was enlarged by syneruptive slumping and secular erosive recession of the walls to form the modern 17 km × 32 km depression, which has been the site of many postcaldera eruptions, resurgent structural uplift, hydrothermal activity, and current unrest (Bailey *et al.*, 1976; Bailey, 1989; Sorey *et al.*, 1991; Hill *et al.*, 2002; Hildreth, 2004).

The Bishop Tuff consists predominantly of ash and pumice clasts of biotite–plagioclase–quartz–sanidine high-silica rhyolite (mainly 74–77·7% SiO_2), though scarcer pumice types (reported here) extend the compositional range to dacite. Proximal to medial fall deposits are plinian pumice lapilli and crystal-rich ash, but beyond about 200 km from source the fallout is largely vitric ash that includes both plinian and coignimbrite contributions. Outflow ignimbrite sheets are as thick as 170 m and range from nonwelded to eutaxitic, and from unconsolidated, sintered, or variably welded vitric zones to fully devitrified zones and zones of intense vapor-phase crystallization. Intracaldera Bishop Tuff, not exposed but sampled in many drillholes (Suemnicht & Varga, 1988; Bailey, 1989; McConnell *et al.*, 1995), is devitrified, densely welded, and as thick as 1500 m.

Eruptive volume is not well known owing to (1) erosion, transport, and resedimentation of distal ash, (2) erosion or burial of distal outflow sheets, (3) thick postcaldera fill that conceals the intracaldera tuff, and (4) irregular faulting of the caldera floor beneath it. McConnell *et al.* (1995) estimated 340 km^3 of intracaldera Bishop Tuff; we estimate 200 km^3 initially for the outflow sheets; and application of the method of Fierstein & Nathenson (1992) to sparse data for unreworked downwind ashfall (Izett *et al.*, 1988) gives roughly 250 km^3 of fallout. Recalculating to a density of 2·2 g/cm^3 for hydrous rhyolite magma yields a crude estimate of 600–650 km^3 for the magma that erupted to produce the Bishop Tuff. The two northerly ignimbrite lobes (Fig. 1), emplaced late in the eruptive sequence, account for 10–15% of the total volume erupted.

For simplicity, we restrict use of the term Bishop Tuff to the deposit, and we refer to Bishop magma, crystals, and melt, none of which became tuff until they had ceased being magma. The melt-dominant volume from which the eruption issued is referred to here as the magma body, and what constituted the Bishop magma chamber as a whole and what complex reservoir may have continued beneath it are discussed in the section 'Definition of magma chamber'.

LONG VALLEY MAGMATISM

The Bishop Tuff was by far the largest of more than 200 eruptions in the Long Valley volcanic field during the past 4·5 Myr. Numerous mafic and intermediate magma batches that erupted during the interval 4·5–2·5 Ma were followed by incremental construction of the rhyolitic Glass Mountain complex of lava domes and pyroclastic deposits between 2·2 and 0·79 Ma (Bailey *et al.*, 1976; Metz & Mahood, 1985, 1991; Bailey, 1989, 2004; Metz & Bailey, 1993). Taking into account dispersed pyroclastics (Sarna-Wojcicki *et al.*, 2005), the 60 or more precaldera vents of Glass Mountain erupted 100 ± 20 km^3 (Hildreth, 2004) of high-silica-rhyolite magma, most of it similar to or even more evolved than the most differentiated pumice in the Bishop Tuff (Metz & Mahood, 1991). Early postcaldera phenocryst-poor rhyolites (760–650 ka) include lavas, tuffs, and intrusions that likewise add up to ~100 km^3. In large part coextensive and contemporaneous with growth of a 10 km wide resurgent uplift (Bailey, 1989), these early intracaldera rhyolites (74–75% SiO_2) are less evolved than the precaldera rhyolites, and in most respects they overlap compositionally with the less evolved pumice emplaced late in the zoned Bishop Tuff sequence (McConnell *et al.*, 1995; Hildreth, 2004). Younger rhyolitic, intermediate, and mafic volcanism within and west of the caldera has continued, intermittently and far less voluminously, from 525 ka to the present (Bailey, 1989; Hildreth, 2004). This activity is not dealt with here, as it reflects events and processes subsequent to those that built and organized the magma reservoir that released the Bishop Tuff.

PREVIOUS WORK ON THE BISHOP TUFF

The Bishop Tuff was initially mapped, described, and named by Gilbert (1938), who characterized the pyroclastic-flow origin and welding of its outflow sheets. Bateman (1965) described the basal fall deposit as an integral part of the Bishop Tuff, and Izett *et al.* (1988) documented surviving remnants of the regionally dispersed ashfall. Sheridan (1965, 1968, 1970) recognized the multi-lobate distribution of the ignimbrite, studied its mineralogy, and described its fossil fumaroles. Contrasting suites of basement lithic fragments in sequentially emplaced subunits allowed Hildreth & Mahood (1986) to locate the initial eruption site and to document ring-fault-controlled opening of subsequent vents that influenced sectorial emplacement of outflow sheets.

Compositional zonation of the Bishop Tuff was first recognized and reconnoitered by Hildreth (1977, 1979, 1981, 1983, 1985) and Halliday *et al.* (1984), and the processes that brought about that zoning have remained topics of lively discussion and investigation ever since. Confirmation of zoning in volatiles by analysis of melt inclusions in Bishop Tuff phenocrysts has provided important insights about the pre-eruptive magma body (Anderson *et al.*, 1989, 2000; Skirius, 1990; Anderson, 1991; Lu, 1991; Dunbar & Hervig, 1992; Lu *et al.*, 1992; Wallace *et al.*, 1995, 1999). Investigations of the growth, differentiation, and physical and thermal condition of the pre-Bishop magma reservoir

(Metz & Mahood, 1985, 1991l; Halliday *et al.*, 1989; Mahood, 1990; Sparks *et al.*, 1990: Davies *et al.*, 1994) and of pre-eruptive residence times of magmas that led to the Bishop Tuff (Christensen & DePaolo, 1993; van den Bogaard & Schirnick, 1995; Christensen & Halliday, 1996; Davies & Halliday, 1998; Reid & Coath, 2000; Winick *et al.*, 2001; Simon *et al.*, 2005) have provoked spirited debate.

In this paper we review these contributions and present a revised and expanded database of Bishop analytical data, supplementing and superseding that of Hildreth (1977, 1979). These data are tied to our revisions of the tuff stratigraphy and eruptive sequence (Wilson & Hildreth, 1997). We extend previous studies by (1) documenting the full compositional range of major and minor types of pumice, (2) recording the complexities of magma withdrawal reflected in fluctuating proportions of varied pumice types that were concurrently emplaced, and (3) drawing revised inferences concerning pre-eruptive processes in the magma reservoir.

ERUPTIVE STRATIGRAPHY

The eruptive sequence (Fig. 2; Wilson & Hildreth, 1997) includes a fall deposit (F) divided into nine widely recognizable units (F1–F9) and some 13 packages (or subpackages) of ignimbrite (Ig), which are chronologically or sectorially distinctive bodies of tuff. Most, possibly all (see below) of the ignimbrite packages are demonstrably syn-plinian, rather than post-plinian as previously thought by Hildreth (1977, 1979). Within the fall sequence exposed east of vent (Fig. 1) there is no sign of a time break, except a short one between F8 and F9 when a few centimeters of ash (Fig. 3) had time to settle. Each ignimbrite package contains distinctive lithic and pumice populations, has consistent lithologic characteristics (independent of welding zonation), and was emplaced as a rapid succession of pulses or flow units (Wilson & Hildreth, 1997, 2003).

The sequence of Wilson & Hildreth (1997) is updated and summarized (Fig. 2) as follows. The eruption began in the south–central part of what later became the caldera, feeding a plume that gradually grew from about 18 km to 45 km in height and was largely blown eastward. East and SE of vent, several ignimbrite packages successively offlapped, each one shingling progressively farther away from source. The earlier Ig1Ea and b were coeval with fall units F2–F8; they lack pyroxene phenocrysts and generally lack the rhyolite lithics (derived from Glass Mountain and

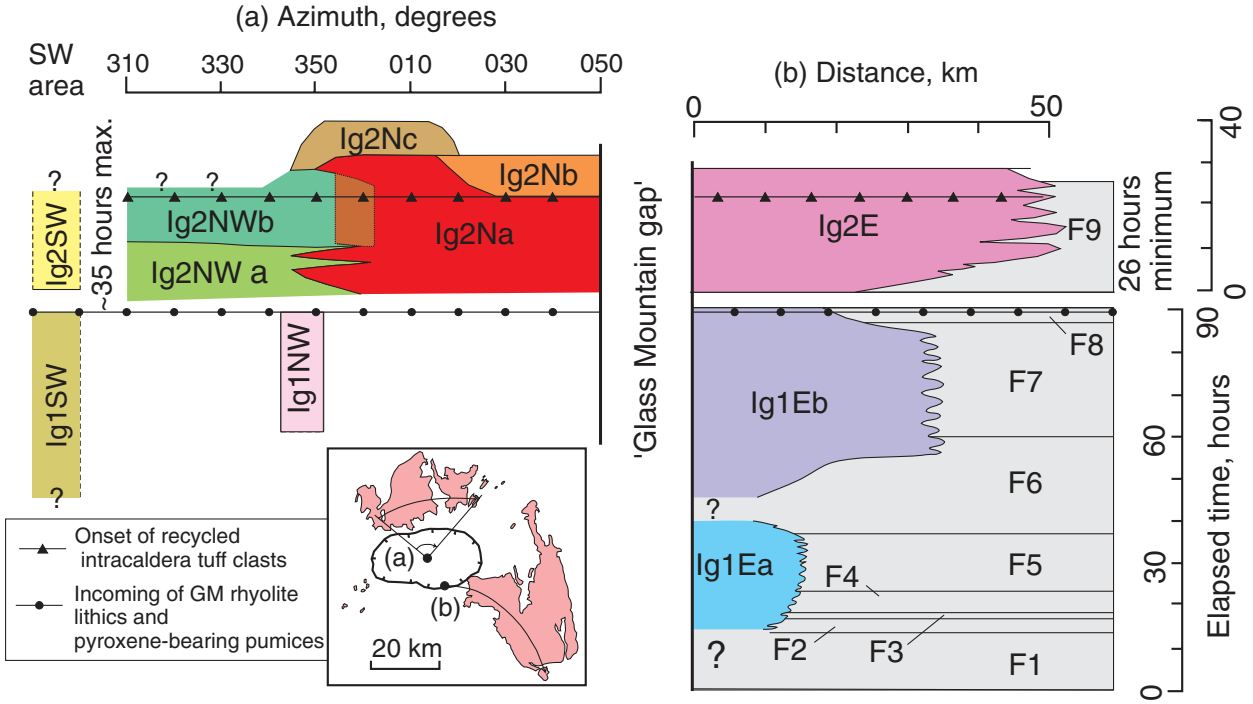

Fig. 2. Summary of stratigraphic relationships and estimated emplacement durations of Bishop fall units and ignimbrite packages, updated from Wilson & Hildreth (1997). 'Glass Mountain gap' represents the gap in information NE of Glass Mountain, where all Bishop deposits have been removed by erosion. Vertical distances are scaled to a composite timescale, which is separated by a short time break between F8 and F9. (a) shows a hypothetical west to east section along an arc from 310° to 050° (relative to grid north, as projected from an arbitrary origin in the center of Long Valley caldera; see inset map), with the northern ignimbrite subpackages drawn to represent their projected dispersal sectors (horizontal scale) and relative stratigraphic positions (vertical scale). Brown unlabeled area represents the mixed zone between Ig2Na and Ig2NWb (Wilson & Hildreth, 1997, Fig. 16). (b) illustrates a section from proximal to distal areas, roughly along the line of Owens Gorge; horizontal axis is distance from the initial vent area (Hildreth & Mahood, 1986). Fall deposits are shaded gray and labeled F1–F9. (a) and (b) are linked by a pair of inferred time-marker planes: (1) the incoming of both Glass Mountain-derived rhyolite lithics (eastern ignimbrite and Ig2N) and pyroxene-bearing pumices (both sides); (2) the incoming of clasts of recycled intracaldera Bishop ignimbrite that itself contains the rhyolite lithics.

its volcaniclastic apron) characteristic of the overlying Ig2E packages, except where they flowed eastward across the Glass Mountain apron. Later eastern packages (Ig2Ea, b, c) were coeval with uppermost F8 and F9, and like those fall layers they do contain pyroxene-bearing pumice and vent-derived rhyolite lithics, the latter indicating northeastward propagation of vents along the ring-fault zone during caldera subsidence. Because the plinian plume was driven strongly eastward, proximal to medial fall deposits are not present in northern and southwestern outflow sectors (Fig. 1), ruling out direct correlation with deposits in the (today noncontiguous) eastern sector. Nonetheless, the northerly packages (Ig2N, Ig2NW) are rich in pyroxene-bearing pumice, overlie a remnant of pyroxene-free ignimbrite (Ig1NW) near the north margin of the caldera, and have suites of pumice types that partly overlap with that of Ig2E. In the San Joaquin canyon to the SW, lithic suites were in large part picked up locally, but pumice suites and mineral chemistry link the lower of two packages (Ig1SW) to the Ig1E eruptive interval and the upper (Ig2SW) to the Ig2 interval.

Recognition that fall and flow deposits were emplaced synchronously permitted estimates of accumulation time for each plinian layer to be applied for the intercalated synplinian ignimbrite packages as well (Wilson & Hildreth, 1997, table 4). Accumulation times

Fig. 3. Some key stratigraphic relationships: (a) Horton Creek left-bank section (685/401) near Location 57 of Wilson & Hildreth (1997), 38 km SE of vent. Several meters of nonwelded distal Ig2Ea rest conformably on fall unit F9. White fine-ash-bearing 3 cm marker separates 35 cm F9 from ~50 cm F8, beneath which lies ~60 cm F7 and (whiter-appearing) 1·8 m F6. Fall units F1–F5 are scree-covered here. Igl flow units failed to reach this location, terminating a few kilometers north. Geologist is 163 cm high. (b) Chalfant Valley pumice quarry (792/466), 42 km ESE of vent, showing several meters of nonwelded distal Ig2Ea conformably resting on 65 cm fall unit F9 (gray, stratified), which overlies the same white fine-ash-bearing marker seen in (a), here ~5 cm thick. Beneath the white marker, part of fall unit F8 is interbedded with and replaced by a lobate flow unit of Ig1Eb, which in turn rests on ~1·1 m F7 and whiter-appearing F6 at base of exposure. Standing geologist is 1·8 m high. (c) Fall unit F9 intercalated between Ig1Eb below (base not exposed) and Ig2Ea above (15–20 m thick); along a southern tributary of Chidago Canyon (697/594), 33 km east of vent. F9 was variably shaved by overriding ignimbrite but is persistently 40–55 cm thick along the gorge wall. All units are intensely vapor-phase altered. F9 and ignimbrite above contain rhyolite lithics; ignimbrite below does not. Geologist is 1·8 m high.

so estimated are: 90 h for fall units F1–F8, inclusive; 25 h for IglEa; 36 h for IglEb. Accumulation of fall unit F9 was originally estimated to occupy at least 8 h, but new data from the west side of the White Mountains, where F9 is 207 cm thick, imply an accumulation time of roughly 26 h. For the northern Ig2 packages, their generally massive nature was taken, by analogy with deposition patterns in IglE, to indicate that their thickest parts (120–140 m) accumulated in no more than 35 h. Evidence discussed by Wilson & Hildreth (1997) and data gathered since imply that F9, Ig2E, and the northern packages erupted synchronously and that the whole eruption thus took less than 6 days.

The importance of this chronostratigraphic framework is threefold. (1) Because much of the Bishop Tuff underwent devitrification and vapor-phase crystallization, many phenocrysts are exsolved, oxidized, or otherwise altered. Detailed understanding of the emplacement sequence allows sampling of pumice from fresh glassy parts of every emplacement package. (2) Proportions of pumice clasts of different characteristics or composition can be estimated by clast counts of each eruptive subunit, permitting assessment of the time–volume–compositional progress of the eruption. (3) Understanding the opening and migration of successive vents around the caldera and the changing proportions of different compositions that erupted from each vent segment provides evidence important for attempting to reconstruct the distribution of magma in the pre-eruptive reservoir or to model dynamic processes of magma withdrawal.

TYPES AND PROPORTIONS OF PUMICE

Pumice clasts in the Bishop Tuff (Figs 4 and 5) range continuously in phenocryst content from <1% to 25 wt %, as determined by mineral separations in heavy liquids (Electronic Appendix 1, available for downloading at http://www.petrology.oxfordjournals.org). There is a variety of primary textures in glassy nonwelded pumice that, in combination with differences in phenocryst (hereafter, crystal) contents, is used to divide the pumices into a dominant 'normal' spectrum (which ranges widely in crystal content), plus a number of variant types (summarized in Table 1). Banded and composite pumice are sparsely present (Table 1) but were not analyzed. In addition to >400 pumices, a few dense vitrophyric blobs and glassy fiamme were sampled. Proportions of the pumice types were determined by clast counts at ~110 outcrops (Fig. 5), supplemented by laboratory counts of material bagged in the field. Within a chosen outcrop area, we tried to count all pumice clasts larger than 4 cm (Fig. 5), resorting to counting 2–4 cm pumices only when required to achieve adequate numbers. For chemical analysis, most pumices taken from ignimbrite were 10–25 cm in diameter; those from fall deposits mostly 4–7 cm. There is no evidence in our observational or chemical data for any correlation between composition and size of pumices. Ash and pumice granules are created by fragmentation and comminution of all pumice types.

There are systematic variations in proportions of the different pumice types through the tuff, as summarized in Fig. 6 and detailed in Electronic Appendix 2. The main continuum of crystal-poor (xp: 0–6%) through medium (xm: 6–12%) to crystal-rich (xr: >12%) normal pumice (Table 1) generally makes up 93–99% of the juvenile clasts in all deposits, except where diluted by a few spatially restricted influxes of swirly pumice in IglEb (Watterson subunit—see below). The proportion of xr pumice, however, increased drastically from <5% in IglEa to ~30% at the Igl–Ig2 transition, and to as much as 90% in the latest ignimbrite packages (Fig. 6). Conversely, xp pumice was predominant in Igl, remained abundant throughout much of Ig2E, but dropped to about 5% of the final packages (Electronic Appendix 2). Of the variant pumice types, the glistening variety of xp pumice is sparsely present throughout Igl and Ig2E but is rare north of the caldera (Electronic Appendix 2). Swirly pumice occurs in the earliest ignimbrite (IglEa) and throughout the eruptive sequence, typically at 1–5% of the clast count, but is especially enriched in the Watterson subunit (Fig. 6; see below) and locally elsewhere in IglEb and Ig2Ea. Dark gray pumice is also represented in IglEa and irregularly throughout the sequence of emplacement units. Local spikes in the count fractions of low-density dark, swirly, and glistening pumice (Electronic Appendix 2) are interpreted to reflect buoyant concentration during outflow.

New data collected since Wilson & Hildreth (1997) lead us here to define two distinctive local lithofacies of IglEb, the Watterson and Sherwin subunits (Electronic Appendix 2; Fig. 6). The Watterson subunit is (like most of Igl) poor in xr pumice (2–12%) but is atypically rich in swirly pumice (5–28%), and much of it further contrasts with the rest of IglE in containing significant amounts of rhyolite lithics. The subunit lies in the middle of IglEb, below the upper zone of dense welding that is prominent along Owens Gorge [welding zone c of Wilson & Hildreth (2003)] and in Chidago Canyon, and it is sandwiched between ignimbrite that is virtually devoid of rhyolite lithics. The subunit is poorly represented in Owens Gorge but is well expressed in an east–west strip about 20 km long and a few kilometers wide (between Lake Crowley and Chidago Canyon) of non-welded to poorly welded ignimbrite that forms the northern edge of the ignimbrite plateau where it laps onto the Glass Mountain debris fan along Watterson Canyon. Available data do not discriminate between deposition by flows directed eastward from the initial vent

Fig. 4. Variant pumice clasts. (a) Dark crystal-poor low-silica rhyolite pumice, 15 cm long, streaked with white high-silica rhyolite; Ig2NWb, Aeolian Buttes. (b) Swirly foliated, fragile, crystal-poor, Ba-rich rhyolite pumice, 20 cm long, showing pale gray core and characteristic yellow or orange-to-tan oxidized rind; Watterson subunit (576/666). (c) Lineated crystal-rich rhyolite pumice block, 25 cm long, split open, showing white core and oxidized exterior; Watterson subunit (576/666); brown welded-tuff matrix adheres to left margin. (d) Typical crystal-rich Adobe-type pumice block, illustrating the characteristic lineation defined by extended vesicles and stringers of feldspar and quartz phenocrysts (many broken). (e) Swirly crystal-poor pumice, 12 cm long, showing characteristic wavy foliation and pale gray streaky color; Alpers Canyon; Ig2NWb (301/809); at left, basaltic lithic in hard-sintered, case-hardened, pumice-rich ignimbrite matrix. (f) Vitrophyric crystal-rich densely welded ignimbrite at Aeolian Buttes (15 km NNW of caldera margin at Crestview); Ig2NWb (173/929). The compositional problems of bulk ash-flow vitrophyres, subject to glass–crystal fractionation and contamination during eruption and outflow, are well known. Even collapsed pumices (fiamme), here as long as 25 cm, sometimes fail to retain magmatic compositions (especially if small and crystal-rich), as phenocrysts can be concentrated in fiamme cores during welding and glass preferentially extruded to the rind, as seen here. A single wispy, pale gray, crystal-poor collapsed pumice clast, 10 cm long, lies ~10 cm above the 8·5 cm knife.

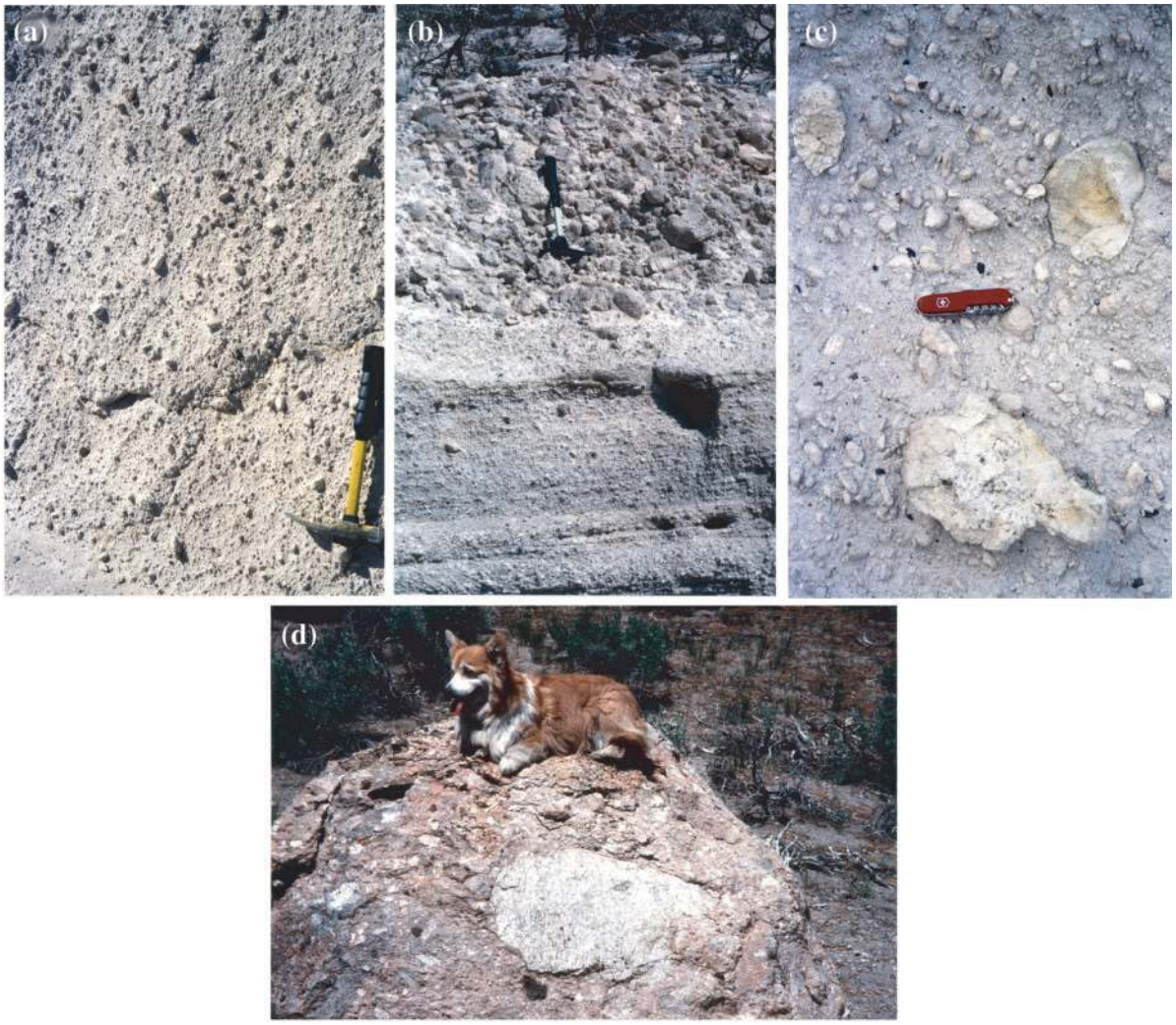

Fig. 5. Some typical Bishop Tuff outcrops counted and sampled. Hammers are 30 cm long; knife is 8·5 cm long. (a) Glassy nonwelded ignimbrite rich in pumice clasts; roadcut at pass on Old Sherwin Grade near Sherwin Hill; (560/530) in Sherwin subunit of IglEb; a wide variety of pumice types is present (see site 73 in Electronic Appendix 2). (b) Pumice concentration zone in a distal flow unit of Ig2Ea, left bank of Horton Creek (683/401). Finer-grained basal 20 cm of ignimbrite rests on stratified fall unit F9 (35–40 cm thick), beneath which is seen top of F8. (c) Nonwelded ignimbrite in roadcut at pass just west of Little Round Valley; IglEb (477/585); pumice clasts are mostly high-silica rhyolite with low to medium crystal contents, but also unusually abundant here are nearly aphyric, relatively Ba-rich, swirly pumices (~12 count%; see site 451 in Electronic Appendix 2) like the three largest in the image; such clasts are typically fragile and finely vesicular, but commonly have inflated frothy cores (as does the largest one here). (d) Pumice-rich ignimbrite poor in ash-grade matrix, 1 km north of caldera margin, at Alpers Canyon (302/808); dark brown basaltic lithics at left; large pale gray dense pumice is 60 cm long; 70 cm long corgi for scale.

site that scoured that fan (Fig. 1) vis-à-vis flows representing a short-lived precursory outburst from a vent farther east that directly penetrated the Glass Mountain debris fan. In contrast, the Sherwin subunit is more typical of IglE in containing few rhyolite lithics and only modest amounts of swirly pumice, but it is exceptional in having large fractions of xr pumice (27–64%; Electronic Appendix 2), including Adobe-type textures. This subunit forms the topmost part of IglEb, above welding zone c, principally near the rim of Rock Creek gorge in the area of Sherwin Hill, though scattered outliers occur farther east. It is absent from Chidago Canyon, and, as such, its distribution is distinct from that of the Watterson subunit.

COMPOSITIONAL RANGES OF PUMICE TYPES

Each pumice type identified has a significant range of composition (Table 2; Figs 7–10). The range is least conspicuous for SiO_2—only 73·4–77·9% for the main array of normal pumice that makes up >90% of the Bishop Tuff. However, the ranges of FeO* (0·40–1·73%),

Table 1: Summary of juvenile clast types in the Bishop Tuff

Type	% of clasts	Sub-type	wt % crystals	SiO_2 range	Comments
Normal	See Electronic Appendix 2 and Fig. 6	xp	<6	75·6–77·9	We define three ranges, used for field pumice counts (Electronic Appendix 2 and Fig. 6). Although the boundaries are arbitrary, we have calibrated visual field estimates against quantitative mineral separations in the laboratory (Electronic Appendix 1). Along this continuum, the styles of vesicularity are similar (i.e. pumice of any crystal content can exhibit much the same range of textures). Vesicularity is commonly seriate from <0·1 to 1 mm, though extremes are also common—crisp, microvesicular (most <0·1 mm) pumice vis-à-vis frothy pumice with abundant 1–2 mm vesicles. Vesicles are predominantly stretched, yielding a finely lineated fabric, which ranges from thinly tubular to silky if extreme. For normal pumice, lineation is more common than sheared (platy or wavy) foliated fabrics and far more common than equant vesicularity. A common variant is finely lineated pumice with scattered equant 1–10 mm vesicles superimposed. White in color, unless oxidized (Fig. 4)
		xm	6–12	74·5–77·7	
		xr	12–25	73·4–77·6	
Normal	See Electronic Appendix 2 and Fig. 6	Adobe	xr	73·4–77·6	Dominant in Ig2NW and Ig2N and scattered elsewhere (Electronic Appendix 2); crystal-rich (most with pyroxene), white (wherever unoxidized; Fig. 4), characterized by a coarsely fibrous lineated fabric that is typically wavy or crimped and encloses stringers or schlieren of clustered crystals, many of them broken. Schlieren are typically 10–80 mm long, several mm thick, and commonly associated with lenticular gas vugs. The Adobe textural style is gradational to xr pumice in which it is only weakly developed, and occasionally is present in xm clasts. Because Adobe-type pumice and other xr pumices are gradational texturally and indistinguishable in bulk composition, they are dealt with hereafter as a single xr group as part of the normal pumice
Variant	0–4	Glistening	1·4–6·4	77·0–78·2	Moderately lineated pumice with tubular vesicles (0·1–1 mm diameter) with thicker than average walls of translucent pale gray glass, which reflect a sparkling shimmer as if from a wet surface. Lacks pyroxene
Variant	0–28	Swirly	0·7–9·1	71·5–76·8	Intrinsically pale gray, but usually oxidized yellow, pale orange, or tan, only rarely pink. Has a lineated microvesicular (<0·1 mm) fabric, which is typically wavy, twisted, or contorted and, less commonly, sheared into a planar or undulating microfoliation. Clast cores are often inflated by late growth of coarse equant vesicles (10–30 mm). Some clasts have 1–3 mm denser rinds, which are typically fissured or incipiently breadcrusted. Lowest-density clasts in the Bishop, they tend to be locally enriched by rafting into pumice concentration zones in the ignimbrite. Ba-rich
Variant	0–12	Dark	0·4–6·6	67·0–76·1	Dark gray, black, or dull smoky gray, showing no obvious discoloration by oxidation. Densities and fabrics are more similar to the normal pumice rather than to the low-density swirly pumice. Characteristically contains commingled blebs, streaks, and bands of normal white pumice (Fig. 4). Ba-rich
Variant	rare	Dacite	n.m.	65·0, 68·6	Rare, found only in Ig2NWb in the eastern knolls of Aeolian Buttes (Fig. 1). Black glassy blocks (14–43 cm), finely vesicular and rich in quartz and in feldspars up to 13 mm long. Vesicles generally <0·2 mm, equant or locally stretched, overprinted by sparse vugs up to 4 mm. Interpreted as juvenile from commingled white rhyolite pumice and by adhering rinds of fused tuff

(continued)

Table 1: Continued

Type	% of clasts	Sub-type	wt % crystals	SiO_2 range	Comments
Variant	rare	Trachy-andesite	n.m. (xp)	56·9, 57·0	Rare, found only in fall layer F7 near Blind Spring Hill (Fig. 1). Dull medium-gray cauliflower lapilli (3–5 cm), crystal-poor. Moderately dense, with relatively few scattered vesicles (0·1–1 mm), sparse olivine microphenocrysts, plus rare olivine crystals up to 1·5 mm. Interpreted as juvenile from the cauliform shape and compositional affinity with the dacite clasts (see Figs 9 and 10) but might be xenoliths entrained by plume
Dense	<0·1	Vitrophyre	n.m.	75·2–77·3	Blobs and variably breadcrusted clasts, poorly vesicular, typically 1–5 cm, rarely 20 cm. Dense glassy rinds (2–10 mm) are black to dark gray–brown. Clast interiors have equant vesicles and are variously microvesicular and pale gray, coarsely vesicular and black, or black with sparse small vesicles seriate up to 2 mm. These clasts are a textural, not a compositional, type inferred to represent magma that partially degassed before ejection
Dense	n.m.	Fiamme	n.m.	72·4–77·2	Glassy fiamme sampled from dense welded vitric tuff
Banded	<0·1	Banded	(xp–xr)	n.m.	Blebs, streaks, and layers of white xp to xr material are abundant in the dark pumice (Fig. 4), uncommon in the swirly pumice, and inconspicuous elsewhere. Mutual commingling of crystal-richer and -poorer white normal pumice is rare. In swirly pumice, streaking and banding of subtle color shades are common, but reflect physical, rather than compositional differences, as all components are equivalently crystal-poor
Composite	<0·1	Reassembled	(xp)	n.m.	Lithic-free, shattered-then-healed lapilli to blocks, mostly derived from swirly pumice, interpreted to have been derived from zones of crushing and milling near conduit walls after initial vesiculation of the magma
Composite	<1	Recycled	n.m.	n.m.	Lapilli to blocks of lithic-bearing welded tuff recycled from coeruptive intracaldera deposits. Occur mostly in later emplacement packages and have proven useful stratigraphically (Fig. 2; Wilson & Hildreth, 1997). Vary widely in degrees of welding, some showing evidence of secondary revesiculation and chilling as free clasts

n.m., not measured.

MgO (<0·01–0·48%), CaO (0·42–1·61%), TiO_2 (0·08–0·25%), Zr (71–154 ppm), and Rb (75–195 ppm) for the main array are proportionately far more extensive, and the ranges for Ba (2–614 ppm) and Sr (9–185 ppm) are extraordinary. All such ranges are continuous, not bimodal or otherwise clustered. At the evolved ends of their ranges, the main xp, xm, and xr arrays are all compositionally similar (Table 2; Figs 9 and 10): 77·6–77·9% SiO_2, 0·08% TiO_2, 12·2% Al_2O_3, ≤0·01% MgO, ≤75 ppm Zr, and ≤10 ppm each Ba and Sr. At the less evolved ends, however, the crystal-rich arrays extend to less differentiated compositions than the crystal-poor arrays; in this respect, the xm arrays consistently end at intermediate values for all elements (Table 2).

Such extensive overlap of the compositional ranges for main-suite pumices signifies that major- and trace-element compositions are to some degree independent of crystal content (Electronic Appendix 1), there being at best a crude correlation for a few elements (Fig. 7). This, in turn, suggests (1) that the main body of high-silica rhyolitic magma that erupted to form the Bishop Tuff had been compositionally zoned before the observed spectrum of crystal contents developed, and (2) that crystal accumulation within the magma erupted was not a leading compositional control.

Data for the dense vitrophyric clasts and fiamme extensively overlap the compositional ranges of the main xp–xm–xr arrays described above (Table 2), consistent with these being dense equivalents of normal Bishop pumice. Exceptions are two or three dense fiamme that may once have been Ba-rich swirly pumice. Whole-rock welded-tuff vitrophyre has generally been avoided owing

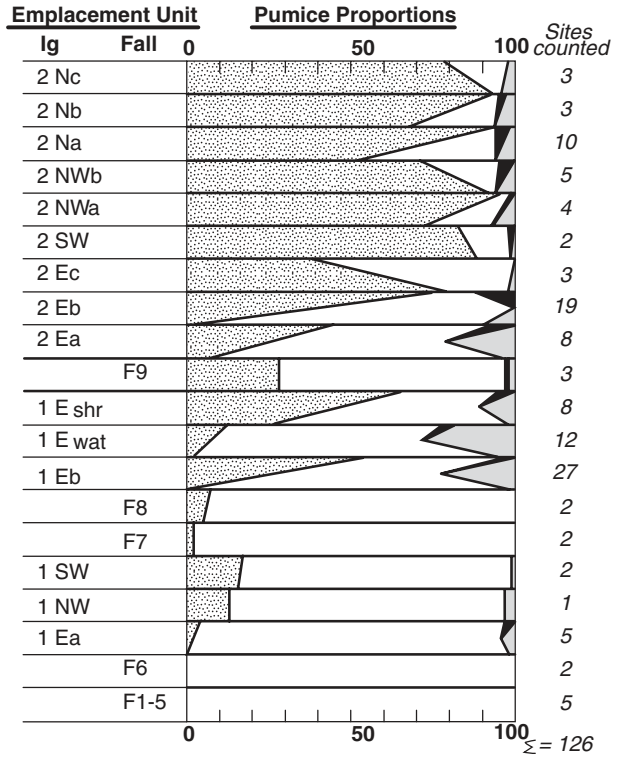

Fig. 6. Pumice clast proportions for Bishop emplacement units of Fig. 2. Clasts counted at indicated number of field sites for each unit; data are given in Electronic Appendix 2. Sherwin (shr) and Watterson (wat) subunits of Ig1Eb were counted separately. Black, dark variant pumice; gray, swirly variant pumice; stipple, normal xr pumice with ≥12% crystals; unornamented white, normal pumice with 0·5–12% crystals (xp + xm lumped). Diagonal lines indicate ranges of within-unit variability.

to the obvious potential for contamination and crystal–glass sorting during eruption and emplacement. We note, however, that compositions of the four such samples in our data set are monotonously normal: 76·1–76·4% SiO_2, 12·7–12·9% Al_2O_3, 0·94–1·04% FeO*, 3·48–3·55% Na_2O, 4·97–5·06% K_2O, 0·5–2·1% weight loss on ignition (LOI), 116–129 ppm Rb, 48–65 ppm Sr, 179–255 ppm Ba, and 105–127 ppm Zr. Because the four were lithic-free and from low in thick welded emplacement packages, they may have lost little glass-enriched elutriate and suffered little sorting. Their lesser hydration and limited alkali variability suggest that carefully selected samples of bulk ignimbrite vitrophyre can (in such special circumstances) offer some advantages over badly hydrated pumice.

Of the variant pumice types, glistening pumice shows a limited compositional range, consistently at or near the extreme end of Bishop arrays, and it includes the highest SiO_2 (78·2%) and lowest Al_2O_3 (12·1%) values recorded for fresh clasts in the Bishop Tuff (Table 2). Swirly pumice is by far the most abundant Bishop component not belonging to the main xp–xm–xr continuum. It differs in texture, color, and in combining low phenocryst content with generally elevated Ba and Sr abundances. For most elements determined, the swirly pumice spans the same compositional ranges as the normal xr (including Adobe-type) pumice of the main array, but it extends to still higher values of FeO*, MnO, MgO, CaO, Ba, and Sr (Table 2), and to lower SiO_2. Dark gray pumice is likewise crystal-poor and rich in Ba and Sr; most elements span ranges similar to those of the swirly pumice (to which it may be magmatically related), but a few of the dark gray clasts extend the ranges to extreme (non-rhyolitic) values: 67% SiO_2, 4·14% FeO*, 3·85% CaO, 1350 ppm Ba, and 460 ppm Sr.

Hydration and alteration

Nearly all samples analyzed were single clasts or fiamme, unaffected by the crystal–glass fractionation and lithic contamination intrinsic to emplacement of bulk ignimbrite. To minimize effects of post-emplacement vapor transport and secular alteration, we avoided taking clasts from devitrified or vapor-phase zones, or from exposures displaying case-hardening (i.e. potentially leached and/or silicified). Although the samples thus approach the compositions of magma erupted, all consist of 75–99% glass, which has been variably hydrated. Water content was not measured directly, but LOI at 900°C provides a fair approximation to the degree of hydration of the (FeO-, CO_2- and halogen-poor) glass. The hydrous phenocrysts, biotite and allanite, together make up <1 wt % of the pumice, so their water contributions are negligible.

Most of the vitrophyre clasts and fiamme give LOI values of 1–3 wt % and most pumice clasts yield 2–5 wt % (Fig. 8). (The two low-LOI samples of Fig. 8 are partly devitrified phenocryst-rich fiamme.) Because hydration of volcanic glass usually results in Na loss and, also commonly, in K gain (Lipman, 1965; Noble, 1967), probably in part by ion exchange between groundwater and glass (Truesdell, 1966), the Na–K data for the Bishop Tuff sample suite have been scrutinized. The wide scatter in Na_2O and K_2O contents (Fig. 8) certainly in part reflects alkali mobility, both groundwater leaching and ion exchange, but much of the spread also reflects magmatic zoning and real differences among the types of pumice coerupted. Glassy melt inclusions sealed in unbroken quartz crystals contain 3·0–3·8 wt % Na_2O ($n = 55$; Wallace *et al.*, 1999). Main-suite (xp–xm–xr) pumices having Na_2O <2·8 wt % and K/Na > 2·3 have probably lost some Na, whereas those with Na_2O contents greater than ~4 wt % may have gained Na. Notably, however, there is no simple relationship between Na loss (or K/Na ratio) and LOI (Fig. 8). Many of the highest LOI values are for samples within the main range of K/Na ratios.

A few additional points can be observed in Fig. 8. (1) For the normal pumice suite, LOI tends to be lower for xr

Table 2: Summary of the compositional ranges of Bishop juvenile clasts

Clast type		*n*	SiO_2	Al_2O3	FeO*	MgO	CaO	Na_2O	K_2O
	xr	95	73·4–77·6	12·2–15·1	0·71–1·73	0·01–0·48	0·46–1·61	2·5–3·9	4·8–6·0
Normal								(2·2–4·1)	(4·8–6·5)
Pumice	xm	123	74·5–77·7	12·2–15·1	0·56–1·26	0·01–0·35	0·42–1·15	2·5–3·9	4·6–5·8
Suite							(2·2–3·9)	(4·6–6·3)	
	xp	75	75·6–77·9	12·2–13·9	0·40–1·00	0·01–0·23	0·45–1·02	2·6–3·9	4·5–5·8
								(2·4–4·0)	(4·5–6·4)
Glistening		7	77·0–78·2	12·1–12·6	0·65–0·81	<0·01–0·01	0·44–0·90	3·4–3·8	4·7–4·9
Swirly		71	71·5–76·8	12·6–15·1	0·79–2·57	0·11–0·69	0·58–2·39	2·9–3·8	4·1–5·8
				[15·6]				(1·9–4·3)	(4·1–6·2)
Dark		25	69·5–76·1	12·2–15·0	1·06–2·87	0·29–1·02	1·09–2·62	2·5–3·8	3·9–5·7
			[67·0]	[16·4, 17·6]	[4·14]		[3·85]	(2·1–4·0)	(3·6–5·7)
Dacite		2	65·0, 68·6	14·8, 15·5	2·77, 3·68	1·64, 2·57	3·16, 4·45	3·4, 3·6	3·8, 4·5
Trachyandesite		2	56·9, 57·0	17·8, 17·9	5·6, 5·7	3·98, 4·03	7·15, 7·28	3·6, 3·9	2·40, 2·43
Vitrophyre		17	75·2–77·3	12·4–13·5	0·43–1·23	0·01–0·25	0·47–0·93	2·8–3·8	4·7–5·8
Fiamme		12	72·4–77·2	12·3–13·8	0·67–1·84	0·01–0·82	0·42–1·85	2·9–3·8	4·5–5·9

Clast type		TiO_2	MnO	Rb	Sr	Ba	Y	Zr	Nb
Normal	xr	0·08–0·25	0·02–0·05	75–183	10–185	5–614	8–27	71–154	7–25
Pumice	xm	0·08–0·21	0·02–0·06	85–195	9–116	2–474	9–33	75–138	9–31
Suite	xp	0·08–0·12	0·03–0·05	125–198	9–49	2–140	20–31	75–102	14–26
Glistening		0·08–0·09	0·03–0·04	152–181	11–29	5–34	24–29	77–98	21–27
Swirly		0·09–0·26	0·03–0·08	82–196	21–256	41–686	11–34	76–150	8–25
Dark		0·12–0·33	0·02–0·11	83–190	117–263	259–1347	13–27	89–146	9–22
		[0·40]			[462]				
Dacite		0·52, 0·68	0·05, 0·07	56, 63	338, 494	759, 950	13, 16	170, 179	13, 14
Trachyandesite		1·09, 1·10	0·10, 0·11	99, 113	800, 823	1100, 1140	17, 23	224, 243	16, 18
Vitrophyre		0·08–0·21	0·02–0·05	81–178	11–109	15–499	11–30	80–128	10–26
Fiamme		0·09–0·34	0·02–0·07	78–190	9–222	5–598	9–27	76–158	8–23

Definitions and descriptions of clast types have been given in Table 1. Vitrophyres are dense glassy juvenile ejecta, not welded tuff. *n*, number of samples analyzed. Square brackets enclose outliers beyond continuous range of data; parentheses enclose ranges of Na_2O and K_2O extended by strongly hydrated samples. Major oxides in wt %, normalized to 99·6 wt % (leaving 0·4 wt % for trace oxides and halogens), determined by wavelength-dispersive XRF at USGS laboratory in Lakewood, Colorado, D. F. Siems, analyst. Trace elements in ppm, by energy-dispersive XRF; D. F. Siems and P. E. Bruggman, analysts. Procedures, standards, accuracy, and precision of these longstanding USGS methods have been detailed by Baedecker (1987) and Bacon & Druitt (1988). Precision is estimated by numerous repeat analyses of internal standards. For major elements, absolute standard deviation, in wt %: SiO_2 0·3, Al_2O_3 0·1, FeO* 0·03, MgO 0·01, CaO 0·01, Na_2O 0·05, K_2O 0·04, TiO_2 0·02, MnO 0·01. For trace elements, standard deviation of repeat determinations on standards, in per cent of the amount present (Siems, 2000): Rb 0·6, Sr 4·2, Y 2·7, Zr 1·4, Nb 2·7, Ba 2.

samples and higher for xp ones, despite much overlap. (2) Few samples have patently excess K_2O (>6 wt %) or Na_2O (>3·8 wt %). (3) There is little evidence for K loss. (4) For the normal pumice suite, there is a rough tendency toward lower K_2O abundances with increasing SiO_2, presumably related to separation (at some stage) of melt from sanidine (± biotite). A negative K–Si correlation is opposite to expectation if K gain by ion exchange were linked with greater hydration of higher-silica samples. (5) If any of the low-Na pumice also lost silica, the loss was limited to 1–2 wt % SiO_2 and affected few samples. There is no correlation between SiO_2 and LOI (plot not shown). (6) The suites of dark and swirly pumice have ranges of Na_2O similar to that of the main xp–xm–xr suite, but both of the subordinate suites extend to lower K_2O and SiO_2 abundances. All three suites overlap at the high-silica ends of the arrays.

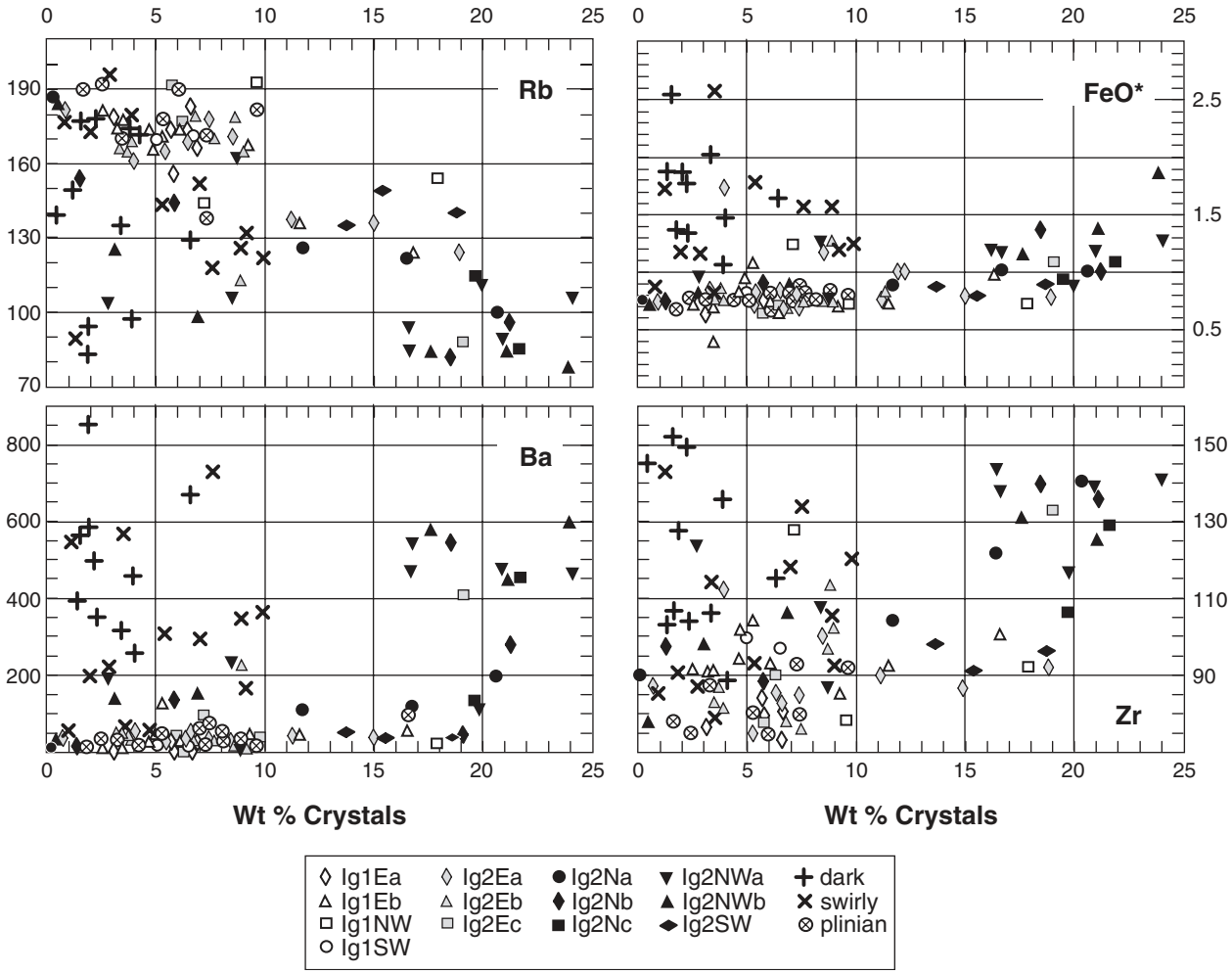

Fig. 7. Crystal contents of 118 pumice clasts vs whole-pumice contents of Rb, Ba, and Zr (in ppm) and FeO* (in wt %). Weight per cent crystals was determined by separations in heavy liquids as tabulated in Electronic Appendix 1. Inset identifies emplacement unit (as in Fig. 2) for each sample of main pumice suite. Dark and swirly pumices (from all units; see Fig. 6 and Electronic Appendices 1 and 2) are identified separately.

Plotting LOI vs every other element determined revealed no evidence for preferential mobilization in high-LOI samples. In particular, no systematic gains or losses of TiO_2, FeO*, MgO, CaO, Y, Zr, Nb, Ba, or even Rb are discernible with progressive hydration for any clast type in the data set. Scrutiny of LOI and inter-element plots identified five samples that appear to have lost SiO_2 and five more that have gained Ca and Sr; these 10 samples were omitted from the data set discussed below. Two samples of the dark gray pumice that may have lost SiO_2 and another that may have gained SiO_2 have been retained, owing to uncertainties about the primary compositional range of this highly varied suite.

Discussion of compositional ranges

A general feature of major- and trace-element plots of Bishop Tuff pumice data is an absence of narrow compositional arrays. Instead, all *x–y* plots show broadly scattered trends for the main suite of normal xp–xm–xr pumices and generally different trends (typically even more scattered) for the subordinate suites of variant swirly and dark pumices. Processes that might have contributed to such scatter could include: (1) heterogeneous incremental assembly and growth of the laterally and vertically extensive zoned magma body; (2) varied degrees of mixing among three or more magma domains that had evolved, at least for a time, separately; (3) spatially inhomogeneous crystal–melt–vapor fractionation within the zoned magma reservoir; (4) meter-scale (or smaller) melt–crystal segregation and/or crystal accumulation by convective sorting, either preeruptive or in syneruptive magma flow toward or within conduits; (5) posteruptive alteration.

Variation vs SiO_2 of key major and trace element contents are shown in Figs 9 and 10. Data for the normal xp pumices cluster at the high-silica low-Ca–Fe–Ti ends of

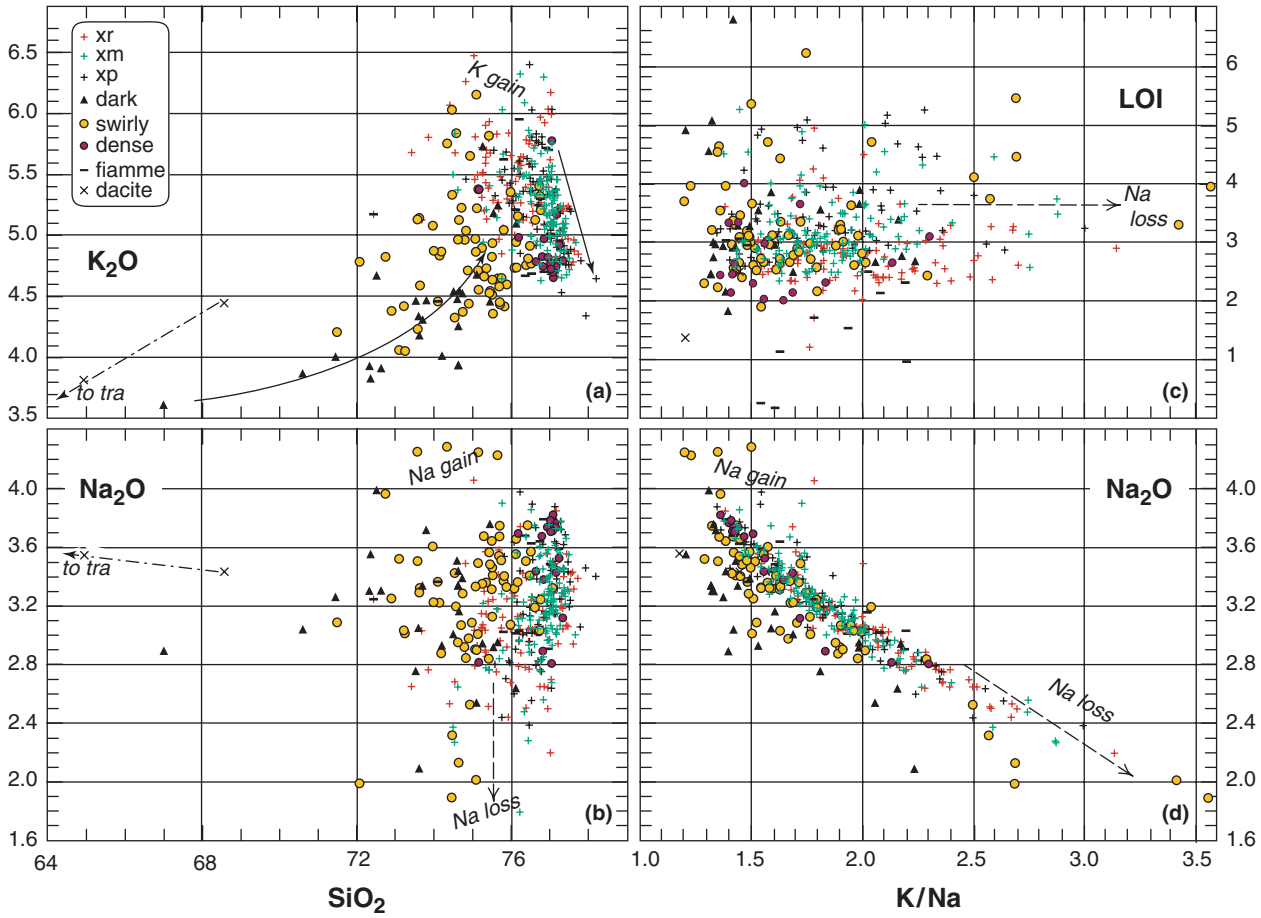

Fig. 8. Alkali variation and mobilization for pumiceous and dense clasts in the Bishop Tuff. Clast types described in text are identified in inset. Alkali and SiO_2 data are normalized to 99·6 wt % anhydrous (leaving 0·4 wt % for trace oxides and halogens). (a) K_2O vs SiO_2 in wt %. Lines suggest gross evolutionary trends for (1) main high-silica array (xp–xm–xr); (2) dark and swirly pumice arrays; and (3) trachyandesite–dacite array, for which trachyandesites (tra) are off-scale at 57% SiO_2. (b) Na_2O vs SiO_2 in wt %. Na_2O values $<2·8\%$ or $>3·8\%$ probably reflect varied degrees of Na loss or gain during secular hydration. (c) LOI (wt %) vs K/Na wt ratio. LOI at 900°C is a rough measure of degree of hydration, with which apparent Na mobility correlates poorly. (d) Na_2O (wt %) vs K/Na ratio. [Compare with (a)–(c) and note that dark and swirly pumice arrays have generally lower K_2O, but Na_2O similar to that of the main high-silica (xp–xm–xr) array.]

the arrays (Fig. 9), whereas the xm and xr pumices range from near the same high-silica terminations to as low as 73·4% SiO_2, where their CaO and TiO_2 contents are three times greater and their FeO* twice that of the most evolved pumices. The scattered arrays of dark and swirly pumice extend to still less silicic compositions, but both overlap extensively the main xp–xm–xr array in CaO and TiO_2. At high silica, the swirly pumice array has FeO* similar to the main array, though dark pumice tends to have higher FeO* at given values of SiO_2.

Comparable relationships for Ba, Zr, and Rb are illustrated in Fig. 10. Data for the high-silica xp normal pumice are concentrated at the high-Rb (175 ± 25 ppm), low-Zr (75–100 ppm), low-Ba (<50 ppm) ends of the main arrays, whereas crystal-richer normal pumice trends toward far less evolved compositions, filling broad fields that overlap the fields of the subordinate dark and swirly pumice. Despite considerable overlap, the dark and swirly pumice arrays tend to have higher Rb and lower Zr, Ba, and Ti (at equivalent SiO_2) than the xr segments of the main arrays (Figs 9 and 10).

Data arrays for swirly pumice converge with the main xp–xm–xr array at 76–77% SiO_2 for all elements determined (Figs 9 and 10). Of the dark gray pumice, only five of 25 samples analyzed have >75% SiO_2, and because those data are scattered, specifying the high-silica evolutionary path of this variant is more equivocal. At the low-silica end, the array of xp swirly pumice extends to 71·5% SiO_2 and that of xp dark pumice also to 71·5% (with a single homogeneous dark outlier at 67% and two strongly hydrated suspect samples at 69·5 and 70·6%). In the FeO* and Ba panels (Figs 9 and 10), the SiO_2 scale is extended down to 56%, to show the dark outlier, plus two dacite and two trachyandesite clasts (Table 1), which appear to

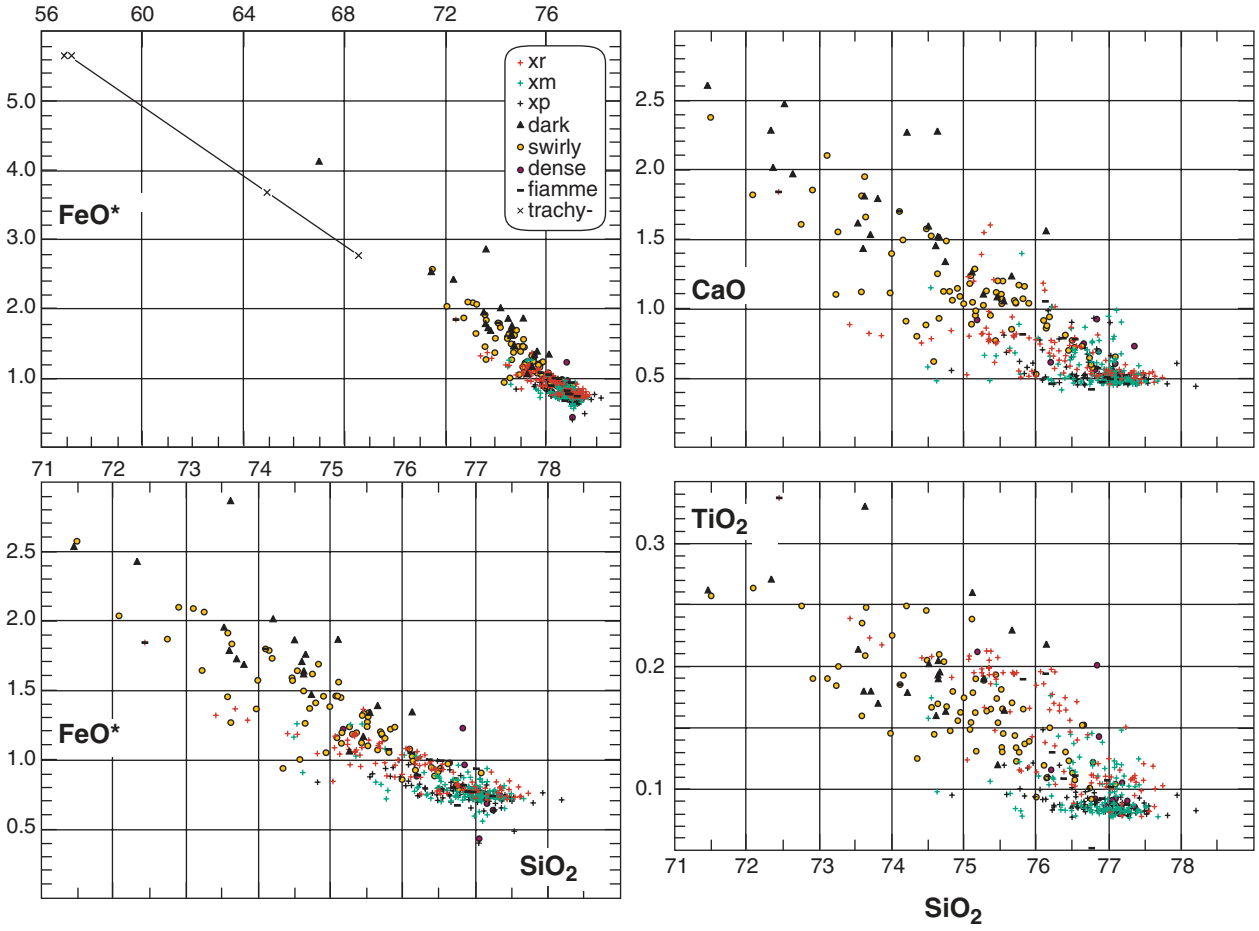

Fig. 9. FeO*, CaO, and TiO_2 contents vs SiO_2 (all in wt %) for pumice clasts in the Bishop Tuff. Clast types described in text are identified in inset. Major-element data normalized to 99·6 wt % anhydrous (leaving 0·4 wt % for trace oxides and halogens). FeO* is total iron calculated as FeO. Main xp–xm–xr suite represents >90% of pumice clasts in the Bishop Tuff. Other clast types are sparse or only locally common (see Electronic Appendix 2). (For dark and swirly pumice types, see text.) Fiamme are welded lenticles of any collapsed pumice-clast type. Most dense clasts are crystal-poor. The upper-left panel is extended to include five clasts with <71% SiO_2: one dark gray crystal-poor pumice, and (×, trachy-) two crystal-poor trachyandesites and two plagioclase-rich dacites.

be roughly collinear with the dark and swirly pumice arrays.

Many trace-element plots exhibit fairly coherent arrays for the main suite but broadly scattered fields for the swirly and dark pumices (Figs 11–13). At equivalent Ba contents (Fig. 11), the main suite has lower Rb, generally lower Sr, and (despite more overlap) a tendency toward higher Zr than the swirly and dark pumices. It should be noted, however, that no dark and few swirly pumices have <100 ppm Ba, whereas two-thirds of the normal pumices have <100 ppm and, of the 50 main-suite samples with >250 ppm Ba, nearly all are crystal-rich (Fig. 11).

Figure 12 shows that, at any given FeO* content, the swirly and dark pumices tend to have lower Zr and Ti but similar or higher Nb abundances than the crystal-richer parts of the normal pumice arrays. Conversely, however, the evolved (low-Fe) ends of the main arrays extend to somewhat lower Zr and Ti and slightly higher Nb than the swirly and dark pumices. Apart from clusters of highly evolved samples (predominantly but not exclusively xp pumice) that terminate the main-suite arrays, the scattered fields of swirly and dark pumice nonetheless exhibit essentially the same ranges in Nb, Ti, and Zr abundances as the main suite (Fig. 12).

Trace-element ratios plotted against FeO* (Fig. 13) further illustrate relationships among the suites, presumably reflecting fractionations dominated by feldspars, Fe–Ti oxides, and zircon. The extended field of Rb/Zr values for swirly and dark pumice spans almost the same fivefold range as the narrowly curved main array. For Zr/Nb ratios, discrete arrays for the crystal-richer normal pumice and for the swirly and dark xp pumices converge upon the evolved cluster of low-FeO* (predominantly crystal-poor) samples; the scattering of some data between

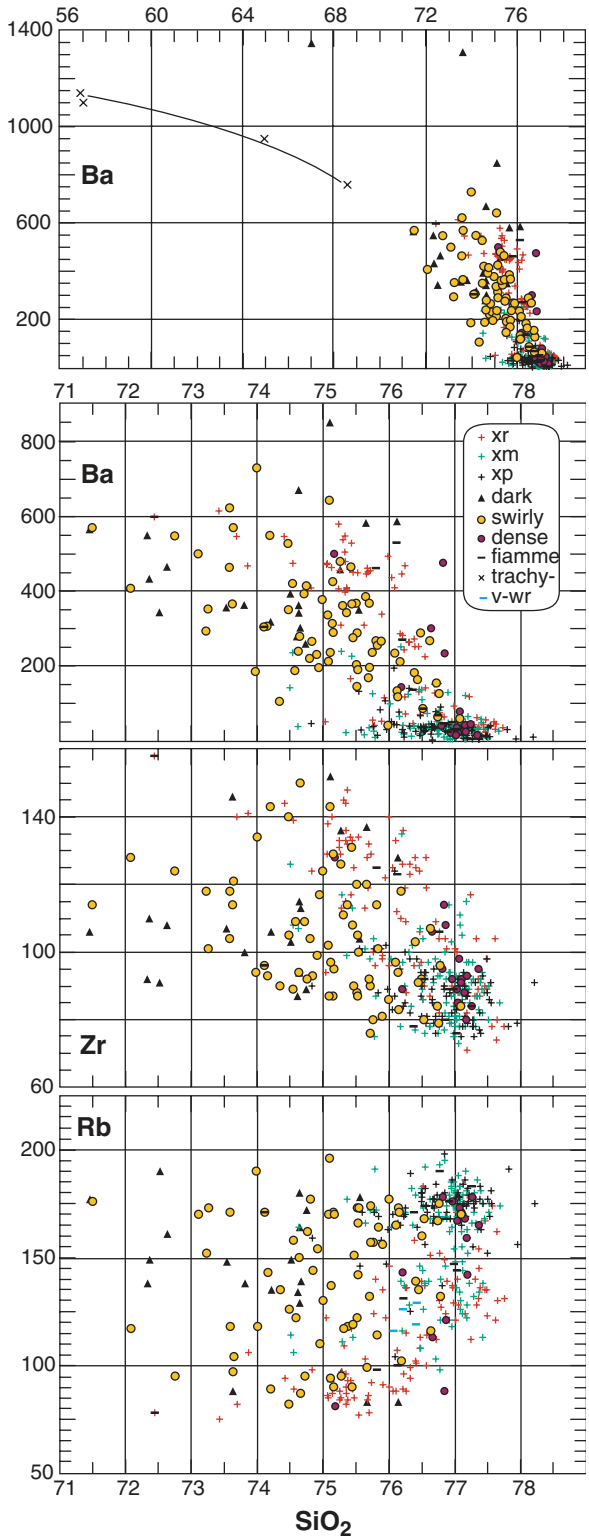

Fig. 10. Ba, Zr, and Rb (in ppm) vs wt % SiO_2 for pumice clasts in the Bishop Tuff. Clast types identified in inset, as in Fig. 9; also plotted are four whole-rock welded-tuff vitrophyre samples (v-wr). The top panel is extended as in Fig. 9 to include the rare trachy-andesites and dacites (curved tie-line).

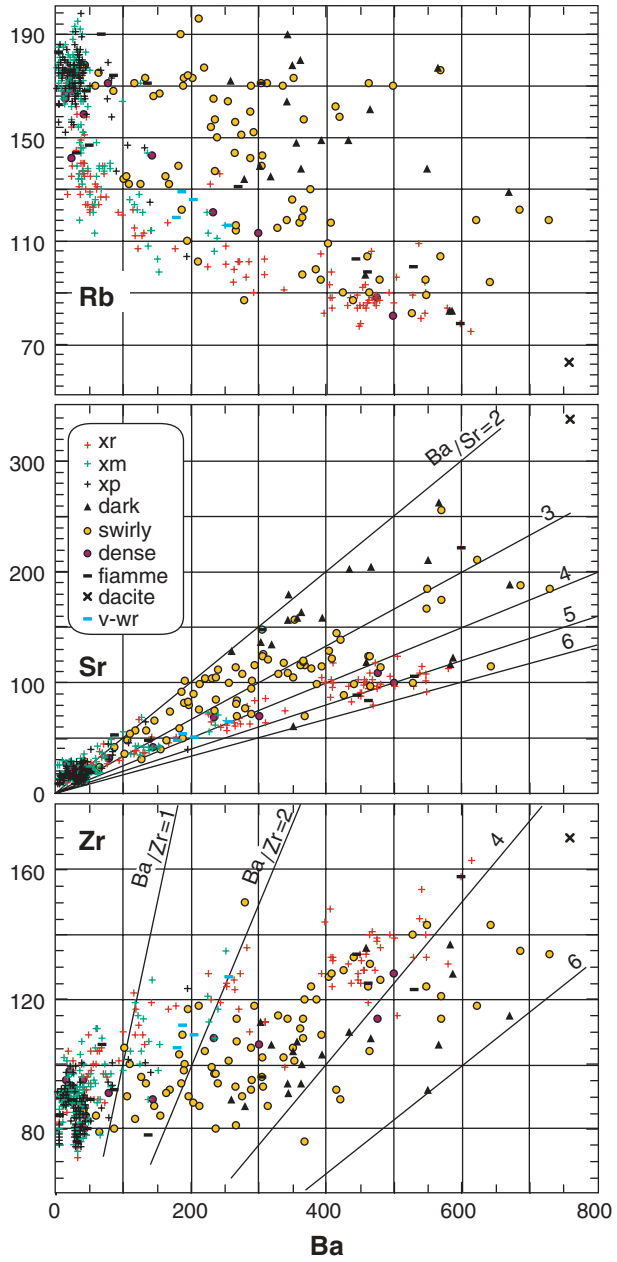

Fig. 11. Variations of Rb, Sr, and Zr vs Ba (all in ppm) for pumice clasts in the Bishop Tuff. Clast types identified in inset, as in Fig. 9; also plotted are four whole-rock welded-tuff vitrophyre samples (v-wr).

arrays may reflect mutual mixing. For Ba/Sr ratios, the two principal arrays are nearly perpendicular; the low-FeO* end of the main array is essentially vertical, dropping to values of Ba/Sr < 0·5, whereas the dark and swirly pumice array is nearly horizontal, with most Ba/Sr ratios in the range 2–4. There is a kink in the main array of normal pumice near Ba/Sr ~ 3, above which a subset of predominantly xr pumice trends with increasing

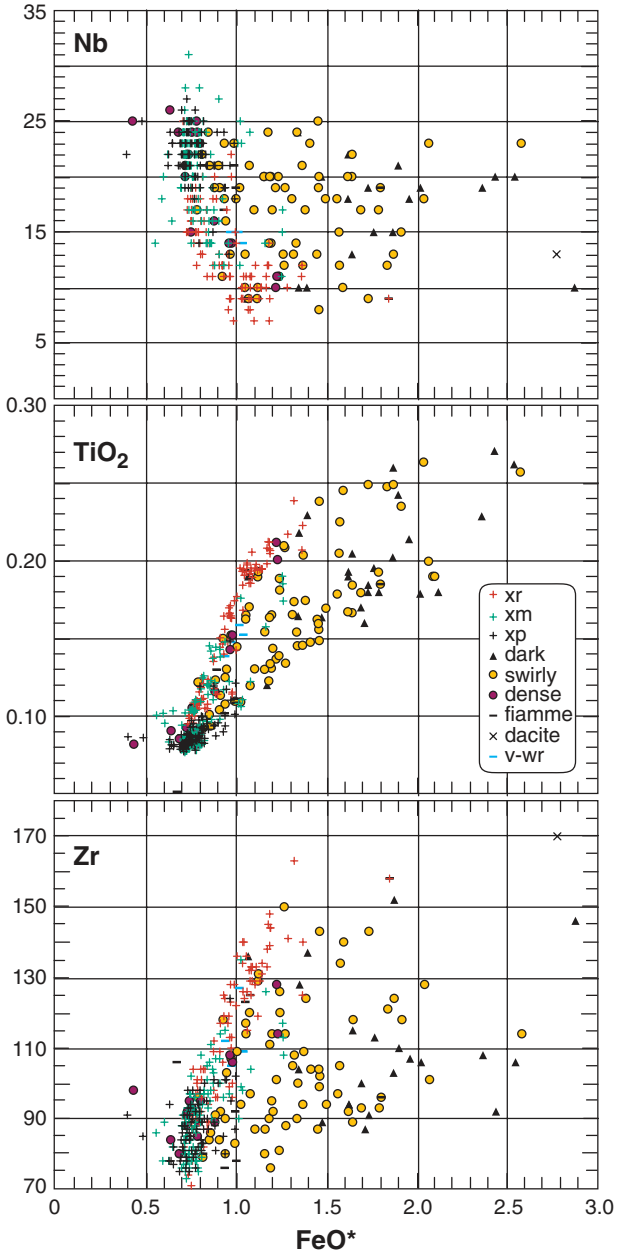

Fig. 12. Variations of Nb, TiO_2, and Zr vs FeO* for pumice clasts in the Bishop Tuff. Oxides in wt %; elements in ppm. Clast types identified in inset, as in previous figures.

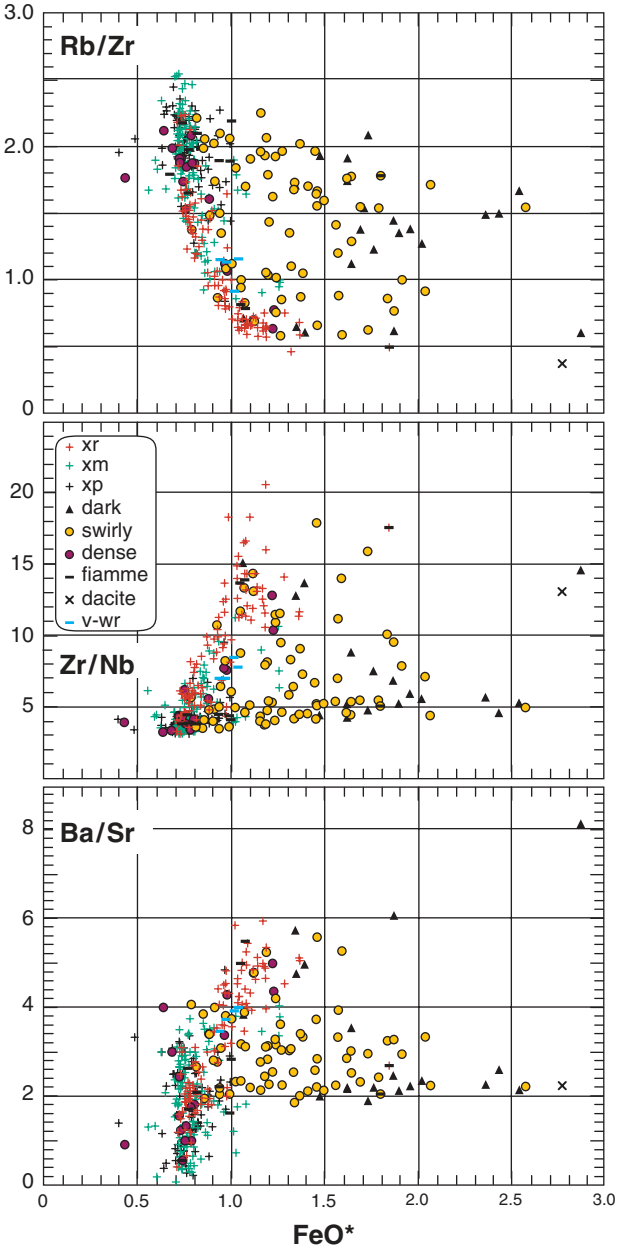

Fig. 13. Rb/Zr, Zr/Nb, and Ba/Sr ratios vs wt % FeO* for pumice clasts in the Bishop Tuff. Clast types identified in inset, as in previous figures.

FeO* to Ba/Sr ~ 6. The observation that a dozen or more samples of dark and swirly pumice also follow this (positively sloping) trend (Fig. 13) is unlikely to reflect crystal accumulation because those pumices are all crystal-poor.

Compositional arrays of successive emplacement packages

Each successive emplacement package (Fig. 2) had a variety of pumice types (Fig. 6; Electronic Appendix 2) and a range of pumice compositions (Figs 8–13), but proportions of the various pumice types coerupting changed markedly during the eruption. In Fig. 14, we show the range of pumice compositions sampled within each of 14 emplacement units.

Considering first the main suite of (xp–xm–xr) normal pumice (which makes up >90% of the Bishop Tuff), the plinian deposit and Igl represent only the more evolved half of the compositional spectrum erupted. For example, these deposits have normal pumices that range only from

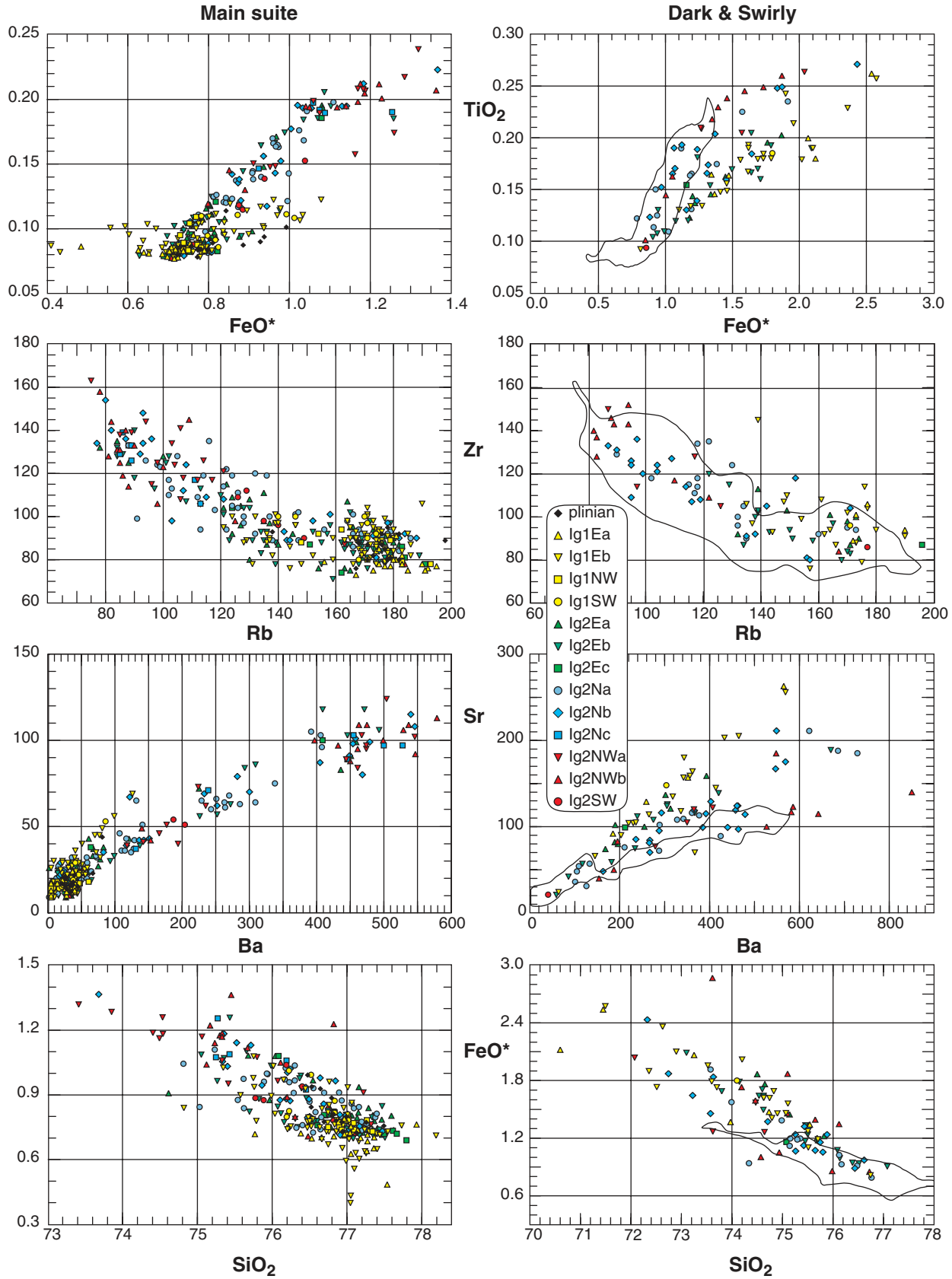

Fig. 14. Compositional variations with eruption progress: ranges of SiO_2, FeO*, and TiO_2 (in wt %) and Zr, Ba, Sr, and Rb (in ppm) for each emplacement package (as in Fig. 2). Symbols identified in inset. For clarity, paired panels separate the main suite of xp–xm–xr white pumice from the combined suite of subordinate dark and swirly pumice. To facilitate comparison, the field outlines of the former are reproduced in panels of the latter.

0·08 to 0·12% TiO_2, from 73 to 106 ppm Zr, from 9 to 69 ppm Sr, and from 2 to 126 ppm Ba. In contrast, the Ig2 packages, though likewise containing the highly evolved pumices, have much wider ranges of these and other elements, extending to 0·24% TiO_2, 163 ppm Zr, 124 ppm Sr, and 579 ppm Ba (Fig. 14). Comparable partial overlaps exist for plots of Y, Nb, and other major and trace elements not shown. For SiO_2 contents, normal (plus glistening) pumice in Igl ranges from 78·2 to 74·8%, though only seven of 120 samples have <76%. On the other hand, normal pumice in Ig2 ranges from 77·8% down to 73·4% but 50 of 200 samples have <76% SiO_2, and for the Ig2NW packages alone, 17 of 27 normal pumices have <76%. Most of the least evolved pumices are in Ig2N and Ig2NW, though several are also in Ig2E. It is important to observe (Fig. 14) that Ig2E [the Tableland sheet of Hildreth (1977, 1979)] contains pumice clasts that span most of the compositional range of the entire Bishop Tuff.

Considering next the crystal-poor suite of swirly and dark pumices (Fig. 14), there are few tendencies toward systematic compositional change with eruption progress. These pumices tend to have higher Rb and lower Zr in Igl than later in the eruptive sequence, but there are exceptions. There are also tendencies for swirly and dark pumices in Igl to have lower Ba/Sr and higher Fe/Ti than in Ig2 (Fig. 14). Many (but not all) of the swirly and dark pumices with low Rb and high Zr and Ba are from the northern outflow sheets (Ig2N, Ig2NW). Figure 14 also shows that the swirly and dark pumices extend to lower SiO_2 and to higher Fe, Ti, Ba, and Sr contents than the main suite. However, the main and subordinate suites exhibit similar ranges of Rb and Zr as well as of Y (both suites 8–33 ppm) and Nb (7–31 vs 8–25 ppm, respectively). Overall, the wide compositional range of the subordinate magma that produced the swirly and dark pumices remained available throughout the eruption, having been released unsystematically as a small but fluctuating fraction (Fig. 6) that accompanied eruption of the zoned rhyolite that produced the main suite.

Fluctuating proportions of pumice types throughout the eruptive sequence—especially marked in Ig2E (Fig. 6)—might reflect any of several processes: (1) coeruption of varied magmas drawn concurrently into conduits from different parts of a zoned chamber; (2) coeruption from separate nearby chambers, each contributing to a common conduit system; (3) intrusion of the subcaldera chamber by one or more new magma batches from deeper in the crust, soon enough before eruption that intra-chamber distribution remained inhomogeneous; (4) circum-vent convective entrainment of earlier-emplaced pumice swept back up into the eruption column; (5) surficial incorporation of earlier pumice by ash flows sweeping the caldera floor or scouring previously emplaced fallout and outflow sheets. The concurrent emplacement of most kinds of pumice virtually from start to finish strongly suggests the importance of processes (1) and (3); and, in a later section below, we provide abundant evidence for a unitary chamber, thus rejecting process (2). Processes (4) and (5) are unavoidable at some scale during an eruption of this magnitude and duration, and the welded-tuff clasts in Ig2 (Fig. 2; Table 1) clearly demonstrate the reality of syneruptive recycling.

CRYSTALS AND LITHICS

Although the main purpose of this paper is to document the extent and continuity of the Bishop pumice (magmatic) compositional zoning, crystals contribute to bulk magma composition and inevitably warrant discussion. Conceptually, it is useful to distinguish among crystals in a magma that are (1) xenocrysts, accidentally entrained from contrasting magmas or older rocks during intrusion, storage, eruption, or outflow; (2) phenocrysts, which grew in the magma containing them and may have had long or short residence times; and (3) antecrysts, which were inherited by the magma now containing them but had grown as phenocrysts in a discrete but kindred magmatic precursor, known or inferred to have been an earlier component of a waxing–waning multi-stage system. Crystals introduced by recharge batches of similar but not identical magma, crystals re-entrained from floor cumulates or mushy enveloping rinds, and the crystals liberated from precursor batches that had nearly but temporarily solidified provide examples of antecryst-vs-xenocryst ambiguity that require microbeam data and thoughtful interpretation.

Crystal suites

Even though the Bishop crystals are largely unzoned, reflect the bulk zonation, and thus appear to have crystallized after the chamber became zoned (Hildreth, 1977, 1979), attributes of the crystals (and their melt inclusions) nonetheless bear significantly on interpretation of the origin of the zoning.

Total crystal contents of pumices range from <1 to 24 wt % (Electronic Appendix 1; Fig. 7). Across the main xp–xm–xr continuum, sanidine and quartz always predominate in roughly equal proportions, and plagioclase is consistently subordinate, making up only 10–15% of the three tectosilicate species, which together constitute 98–99% of the assemblage. Titanomagnetite and biotite are next in abundance, each increasing from trace amounts (<500 ppm) in crystal-poor pumice to ~5000 ppm in crystal-rich pumice. Zircon is ubiquitous, both as free crystals and as inclusions in most other species, and reaches a maximum abundance of ~50 ppm. Likewise ubiquitous, but sparser still, is apatite (≤10 ppm), which forms inclusions in most others species (especially Fe–Ti oxides and pyroxenes). Euhedral allanite, with a maximum abundance of ~50 ppm, occurs in all sectors but is absent in samples

that give Fe–Ti-oxide temperatures >763°C (Hildreth, 1977, 1979); it appears to be far sparser in pyroxene-bearing than in pyroxene-free pumice.

Where present, euhedral augite and hypersthene virtually always occur together, in roughly equal amounts. They are restricted to Ig2 (and F9), but not all Ig2 pumices contain pyroxenes. Hildreth (1977) found them in 26 of 36 Ig2 samples, and for the broader suite (including swirly and dark pumices: Electronic Appendix 1) separated for the present study, pyroxenes were identified in 24 of 69 Ig2 pumices and in one of five pumices from F9. Pyroxene abundances increase from ~25 ppm of each in some Ig2E (xm–xr) pumices to as much as 2000 ppm each in xr Adobe-style pumices. Both pyroxenes contain tiny inclusions of ilmenite, titanomagnetite, zircon, apatite, sulfide and, rarely, allanite and monazite. Sulfide blebs (<1 ppm, largely pyrrhotite), occur as inclusions in oxides, pyroxenes, allanite, and zircon, but were found only in pyroxene-bearing pumice.

It should be noted that only a subordinate proportion of the Bishop Tuff is pyroxene-bearing. There is great uncertainty about the fractions of pyroxene-bearing material in the intracaldera tuff and distal ash-fall, but both are likely to be modest. For exposed ignimbrite, if 60% of the pumice is pyroxene-bearing in the northern lobes and 20% in Ig2E and Ig2SW, as we estimate, then the overall fraction of pyroxene-bearing material in Bishop outflow sheets is less than 30%. For proximal to medial plinian pumice-fall deposits, it is no more than 1%, represented by uncommon clasts of pyroxene-bearing pumice found only in F9.

Crystals are generally solitary and euhedral, whereas crystal aggregates are very rare. Tiny mineral and glass inclusions are common in most crystal species. Compositional data for each mineral species in the main pumice suite have been tabulated by Hildreth (1977), whose principal observations (adapted to our detailed stratigraphic framework) were the following.

(1) Ranges of FeTi-oxide temperature for coerupted glassy material extended to higher values as the eruption progressed, viz. 720–725°C for plinian pumice ($n = 9$; F5–F7); 720–740°C for Ig1 ($n = 25$); 722–763°C for Ig2E ($n = 16$); 745–773°C for Ig2SW ($n = 3$); 748–781°C for Ig2N ($n = 10$); and 756–790°C for Ig2NW ($n = 6$). There was extensive overlap in the ranges of temperature given by the pumice suites in successive emplacement units. Temperatures correlated well with mineral and bulk-pumice compositions, but with eruptive withdrawal sequence only in the gross sense of an increasing proportion of higher-temperature ejecta with time.

(2) Within any sample, each mineral species is unzoned or nearly so, but with rising FeTi-oxide temperature, the compositions of sanidine, plagioclase, biotite, titanomagnetite, ilmenite, zircon, and apatite are progressively less evolved. Along with declining proportions of highly evolved pumice across the eruptive sequence, the progressive addition of less evolved, higher-temperature pumices was accompanied by attendant shifts in mineral compositions. For example, average plagioclase shifted from An_{14} to An_{23}; the Ca content of sanidine doubled; Mn contents of biotite, titanomagnetite, and ilmenite dropped threefold; Y contents of zircon and apatite dropped twofold or more; and the Zr/Hf ratio of zircon increased from ~40 to 55 (Hildreth, 1977, 1979).

(3) Allanite, hypersthene, augite, and pyrrhotite crystals are likewise unzoned, but, in contrast to the other mineral species, compositions change little with emplacement sequence or across the limited temperature range over which each species occurs.

The quantitative mineral separations undertaken (Electronic Appendix 1) illustrate a weak tendency within the normal pumice suite for crystal content to correlate crudely with whole-pumice Zr, Fe, Ba, and Sr contents and negatively with Rb (Fig. 7). The swirly and dark pumices, on the other hand, exhibit only wide compositional scatter at low to moderate crystal contents (Fig. 7). Crystal contents of the main-suite pumice increased with eruption progress, in the general sense of a progressive advance in the proportion of crystal-rich pumice. Nonetheless, sparse crystal-rich pumices were also ejected early, and subordinate crystal-poor pumices remained part of the eruptive mixture until the very end (Figs 6 and 7).

Crystals in dark and swirly pumice

The dark pumices were first reported by Hildreth (1985), who noted that most are crystal-poor and commingled with bands and blebs of white rhyolite pumice. Dark pumice contains small amounts (0·02–0·08 wt %) of non-carbonate carbon with a $\delta^{13}C$ value of −25‰, suggesting a biogenic origin, perhaps ingested from metapelitic xenoliths. Mineral separations from dark pumices (Electronic Appendix 1) yield 0·4–6·6 wt % crystals, resembling the same suite of phenocrysts as present in coerupted white normal pumice (and potentially derived in part therefrom). Touching ilmenite–titanomagnetite pairs ($n = 11$) from three dark clasts (one each from Ig2Eb, Ig2Nb, and Ig2NWb) gave Fe–Ti oxide temperatures of 795–820°C (Electronic Appendix 3; discussed below). The lowest-silica sample (67% SiO_2) of dark pumice, crystal-poor dacite B-443, lacks pyroxenes and its Fe–Ti oxides are disturbed, but (uniquely for the Bishop Tuff) it contains traces of homogeneous euhedral amphibole as well as quartz, sanidine, plagioclase, and biotite (Scaillet & Hildreth, 2001). The amphibole has 11–12% Al_2O_3, suggesting equilibration at 5–6 kbar (Johnson & Rutherford, 1989).

Mineral separations from swirly pumice (Electronic Appendix 1) yield 0·7–9·8 wt % crystals, again resembling the crystal suite in the normal pumice, with which swirly pumice is seldom visibly commingled. No Fe–Ti oxide temperatures were obtained for any of 13 swirly pumice samples separated, owing either to lack of ilmenite or to alteration of one or both oxide minerals.

Lithics, xenocrysts, and antecrysts

Lithic fragments entrained during eruption and outflow make up modest fractions of all emplacement units (0·2–4 wt % of fall units; 0·2 to >10 wt % of ignimbrite), but the main macroscopic xenoliths we noticed inside pumice clasts are metasediments, which are sparse, commonly schistose, and mostly <5 mm; our impression is that they are less rare in dark and swirly pumice than in white normal pumice. With rare exceptions among granitoids, lithic fragments lack evidence of partial melting, a generalization that pertains even to obsidian clasts of precaldera high-silica rhyolite.

Mineral concentrates from pumice include sparse anhedral quartz, hornblende, cloudy feldspars, and various intergrowths of the three, which we infer to have disaggregated from granitoid xenoliths. Broken anhedral sphene and monazite xenocrysts are likewise present (at sub-ppm abundances) within pumice clasts (Hildreth, 1977). Many mineral separates from pumice contain distinguishable xenocrysts at parts-per-mil concentrations; a few also have traces of millimeter-sized xenoliths, mostly schistose metapelite but also rare volcanic, metavolcanic, and hornfelsed (silicic and calc-silicate) metasedimentary grains. Dark and swirly pumices carry the same kinds of xenoliths as the main suite. Ion-probe U–Pb analysis (Reid & Coath, 2000; Simon & Reid, 2005; Simon *et al.*, 2005) identified a few Triassic zircons in pumice from F6, Ig1Eb, and Ig2NWb, derived presumably from the large Triassic pluton cut by the eastern part of the caldera (Hildreth & Mahood, 1986; Bailey, 1989). Microprobe analyses (Hildreth, 1977) of plagioclase (mostly unzoned or poorly zoned oligoclase) identified rare crystals in Ig2 that have irregular $An_{32–48}$ cores, suggesting xenocrystic inheritance and overgrowth. Engulfment of part of the Glass Mountain apron of high-silica-rhyolite pyroclastic debris during the Ig2 stage of the caldera-forming eruption would inevitably have contaminated the Bishop magma with entrained xenocrysts of biotite, quartz, and feldspar difficult to distinguish from the juvenile phenocrysts. It needs to be emphasized that during a complex 6 day eruption and collapse sequence, xenocrysts and xenolithic debris would enter the magma itself as well as be entrained in the erupting ejecta. Truly accidental material is certainly present in Bishop pumice, though rather sparsely.

Rb–Sr isotope data for Bishop crystals and glass led Christensen & DePaolo (1993) to infer (1) that some small fraction (<1%) of the biotite was entrained as roof-rock xenocrysts during the eruption and (2) that some feldspar crystals were resident in the magma for up to 500 kyr prior to the eruption. Christensen & Halliday (1996) presented several Rb–Sr model ages, for melt-inclusion-bearing quartz (MIBQ), interpreted to represent melt-differentiation events ranging from 2·5 to 1·4 Ma for MIBQ in plinian pumice and from 1·2 to 1·0 Ma for MIBQ in Ig2. They also reported Rb–Sr feldspar–glass model ages of 1·8 to 1·2 Ma for plinian feldspar and 900–800 ka for feldspar in Ig2.

Davies & Halliday (1998) undertook single-crystal Nd and Sr isotope work on separates from two Bishop samples, determining that feldspars and glass from Ig2NWb were in mutual isotopic equilibrium and gave glass–feldspar model ages of 1·1–0·9 Ma. On the contrary, in their plinian pumice sample, several isotopically heterogeneous feldspar crystals were identified. Adjusted to the time of eruption, $^{87}Sr/^{86}Sr$ ranged from 0·7062 to 0·7110 for coexisting feldspar grains, a few of which were shown to be more radiogenic internally. The same plinian feldspars yielded ε_{Nd} values from −1 to −3·5, even though numerous data for MIBQ, titanomagnetite, bulk sanidine separates, glass, and whole rocks have shown the Bishop Tuff to yield nearly constant ε_{Nd} values of −1 (Halliday *et al.*, 1984; Christensen & Halliday, 1996; Davies & Halliday, 1998). Despite this isotopic variability (for one sample), abundant microprobe data for plinian feldspars from many samples have identified only virtually homogeneous sanidine ($Or_{62–66}$) and plagioclase ($An_{13–16}$), unzoned in major and trace elements (Hildreth, 1977; Lu, 1991; Anderson *et al.*, 2000). All the isotope studies interpreted the results in terms of long pre-eruptive residence times for melts and crystals; in particular, that many were inherited from precaldera batches of Glass Mountain rhyolite of various ages that range from 2·2 to 0·8 Ma (Metz & Mahood, 1985; Halliday *et al.*, 1989; Davies *et al.*, 1994). At odds with such a conclusion, however, are two pieces of new data. First, Simon *et al.* (2005) reported that feldspars from older Glass Mountain rhyolites are distinct in Pb-isotope composition from younger Glass Mountain and Bishop feldspars, precluding phenocryst status for feldspars older than ~1·1 Ma in the Bishop Tuff. Second, the scarcity in the Bishop of zircon crystals more than ~160 kyr older than the eruption (Reid & Coath, 2000; Simon & Reid, 2005) renders puzzling how any Glass Mountain sanidine crystals might have survived so much longer. We address issues raised by the Rb–Sr isotope systematics in the later section 'Residence time of Bishop magma'.

Fe–Ti oxide data revisited and expanded

Hildreth (1977, 1979) presented T–fO_2 data for the Bishop Tuff, based on methods of Buddington & Lindsley (1964), from coexisting oxide pairs in 68 samples (53 pumices and 15 welded-tuff vitrophyres). We supplement and recalculate

this data set here, with data from additional locations and lithologies, and extending coverage to the variant pumices. However, only 34 of our 71 new samples separated yielded homogeneous titanomagnetite–ilmenite pairs (see notes to Electronic Appendix 3). Analytical data for 201 new pairs that satisfy Mg–Mn distribution criteria of Bacon & Hirschmann (1988) are summarized in Electronic Appendix 3 and Fig. 15.

Hildreth's (1977) samples gave values of T ranging continuously from 714 to 790°C and of log fO_2 from −16·5 to −13·6, using the Buddington & Lindsley (1964) calibration. Recalculation of those data by the QUILF95 program based on Andersen & Lindsley (1988) modifies individual T values by −9 to +26°C and raises fO_2 by 0·2–0·9 log units. The recalculated pairs now extend from 714 to 798°C and from −16·2 to −13·0 (NNO to NNO + 1, where NNO is nickel–nickel oxide buffer), not large changes, and are plotted along with the new samples in Fig. 15. Unlike the 1977 data, where each ilmenite or titanomagnetite analysis reported was an average of two or more spot analyses of five or more similar homogeneous grains, the new data involve no averaging, each representing a point analysis of a single grain. Touching pairs were preferred but not always found. Inhomogeneous grains were rejected, and all the pairs accepted (whether touching, or embedded together in a pyroxene crystal, or occurring as free glass-enveloped crystals) plot well inside the 2σ error envelope of Bacon & Hirschmann (1988). For most samples, multiple coexisting pairs yield T ranges that span several degrees or (uncommonly) as much as 35°C. When the range is <10°C, a single mid-range analysis is given in Electronic Appendix 3, but for samples containing pairs that yield wider ranges (suggesting mixing shortly before or during eruption), the divergent data are tabulated individually. The 112 T–fO_2 values plotted (Fig. 15) span the range of all 201 new pairs accepted.

For the main xp–xm–xr suite of normal pumice, 172 new pairs yield temperatures ranging continuously from 714 to 818°C (with two outliers at 702 and 834°C) and of log fO_2 from −15·9 to −12·6. This range is essentially identical to those estimated using the Ti-in-quartz geothermometer (720–810°C; Wark *et al.*, 2004, 2007) and $\Delta^{18}O$ (qz–mt) fractionation thermometry (715–815°C; Bindeman & Valley, 2002). All pairs that gave temperatures higher than the 798°C upper limit of the recalculated 1977 data were in crystal-rich pyroxene-bearing pumices from Ig2E, Ig2N, and Ig2NW. Pairs from six new samples of xp pumice, from Ig1E, Ig2E, and Ig2N, gave a range from 702 to 748°C; those from 10 xm pumices gave 716–796°C; and pairs from 10 xr pumices gave 737–834°C. It should be noted that temperatures obtained for three xp Ba-poor pumices in Ig2 (Electronic Appendix 3) are all low (702–747°C). No T–fO_2 data were obtained for xr pumices in Ig1, but of those for which mineral separates were undertaken (Electronic Appendix 1), none were pyroxene-bearing.

Of the variant pumice types (Table 1), pairs in a glistening xp pumice from Ig2Ea gave 718–736°C at −15·8 to −15·2. None of the 13 swirly pumices separated contained homogeneous Fe–Ti oxide pairs. It can be inferred, nonetheless, that the magma they represented had little thermal contrast to the resident magma it invaded, because it remained phenocryst-poor and the pumice ejected was glassy. For dark pumices, 26 pairs from three clasts (in Ig2Eb, Ig2Nb, and Ig2NWb) gave ranges of 795–816°C and −13·3 to −12·6. Three pairs from a single dark pumice in Ig1Eb gave 756–758°C at −14·4.

For 10 new pyroxene-bearing samples, 84 pairs gave temperatures in the range 716–834°C, of which only four are <750°C. For 24 pyroxene-free samples, 117 pairs gave a range of 702–816°C, of which only three pairs from dark pumice and seven pairs from normal pumice yield values >775°C. Although there are significant overlaps and lack of any simple correspondence, the new data support the old in indicating generally coordinated trends toward greater crystal content, higher pre-eruptive temperatures, and an increasing proportion of pyroxene-bearing pumice as the eruption progressed. The pyroxene-bearing domain in the magma reservoir seems not to have been simply bounded by an isothermal surface, however, because several pyroxene-free pumices yield FeTi-oxide temperatures overlapping the main range for the pyroxene-bearing assemblage.

Pyroxenes and oxides in equilibrium?

Whether the pyroxenes present in many Ig2 and F9 pumices were in equilibrium with the coexisting Fe–Ti oxides and silicate phenocrysts was questioned by Ghiorso & Sack (1991) and Frost & Lindsley (1992). The former cited: (1) lack of Fe–Mg exchange equilibrium between Bishop biotite (which ranges compositionally with temperature) and coexisting orthopyroxene, which is of virtually constant composition across the temperature range; and (2) independence of the Bishop T–fO_2 trend (Fig. 15) from the presence or absence of pyroxene. Ghiorso & Sack (1991) attributed the smooth divergence of the Bishop trend away from the FMQ (fayalite–magnetite–quartz) oxygen buffer curve (Fig. 15) to internal buffering by the assemblage biotite–feldspar–magnetite, which depends on fH_2O but apparently not on the incoming of the pyroxenes. Frost & Lindsley (1992) stated that, according to their solution model, all 22 Bishop pyroxene pairs were in mutual equilibrium, yielding an average two-pyroxene temperature of 824 ± 15°C, whereas the Fe–Ti oxides in the same 22 samples gave them a range of 764–811°C. They suggested that ilmenite composition may have been modified, either just before, during, or after eruption, by some thermal event not recorded by the pyroxenes.

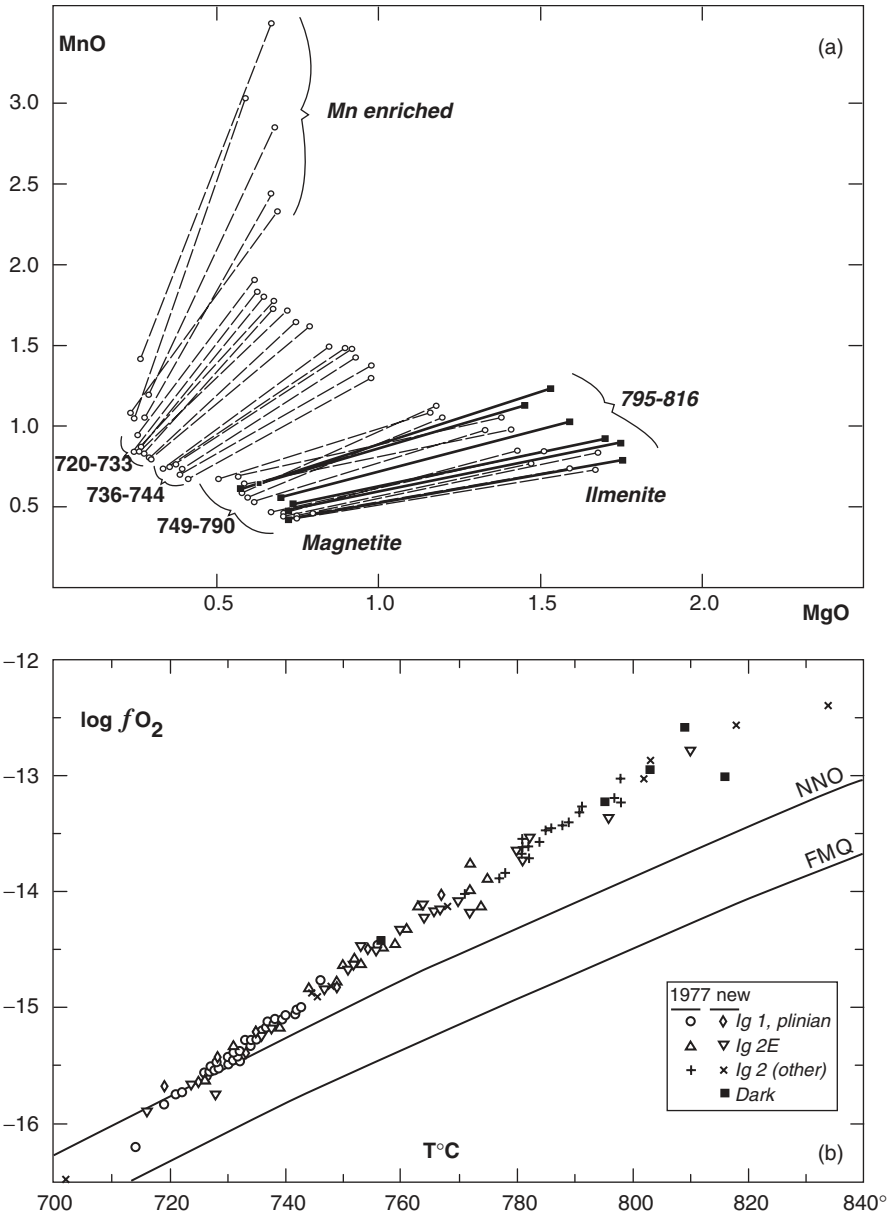

Fig. 15. FeTi-oxide data for the Bishop Tuff. (a) MnO vs MgO in wt % determined by electron microprobe for selected titanomagnetite–ilmenite pairs. Temperature ranges calculated by the method of Andersen & Lindsley (1988) are indicated for subsets of samples. Anomalously Mn-enriched subset illustrates probable vapor-phase modification, which yields suspect T–fO_2 results (not used). Square symbols indicate oxide pairs from dark gray pumice clasts (795–816°C). (b) Temperature and oxygen fugacity calculated for titanomagnetite–ilmenite pairs from 111 samples by the method of Andersen & Lindsley (1988). Plotted are 68 samples recalculated from Hildreth (1977) and 43 from the new data of Electronic Appendix 3. Symbols are identified in inset; the wide range of transitional package Ig2E should be noted. NNO buffer curve after Huebner & Sato (1970); FMQ after Myers & Eugster (1983); both determined at 1 bar.

The possibility that pyroxene or oxide compositions were modified by post-eruptive processes can be ruled out because (1) both pyroxenes are euhedral (e.g. Michael, 1988, fig. 2), homogeneous, and nearly constant in composition in all samples studied, whether in rapidly cooled pumice or in densely welded tuff; and (2) only chilled unoxidized glassy samples with homogeneous oxide pairs were used for the T–fO_2 determinations. The same homogeneity cannot be claimed for Bishop biotites, which may have interacted with a pre-eruptive (or syneruptive) gas phase (Hildreth, 1977). Cooling rates for our samples are inferred to have been rapid (see Zhang *et al.*, 2000; Wallace *et al.*, 2003), dropping non-oxidized pumice below closure temperature for diffusive modification of the FeTi

oxides (Tait *et al.*, 1998) within minutes to a few hours. In such circumstances, ilmenite, titanomagnetite, and pyroxenes remained as pristine as erupted.

Another possibility suggested by both Ghiorso & Sack (1991) and Frost & Lindsley (1992) is inheritance of un-reequilibrated pyroxenes (antecrysts in the sense introduced above) from a rhyolitic precursor, presumably originally deeper and slightly hotter than when erupted. Constraints bearing upon such a hypothesis include the following. (1) The pyroxenes are euhedral and lack zoning, resorption, or overgrowths. (2) In any particular sample, euhedral ilmenite, titanomagnetite, and zircon trapped as microphenocryst inclusions in or on augite and hypersthene grains are compositionally virtually identical to corresponding crystals remote from the pyroxenes, whether free or included in biotite or feldspars (Hildreth, 1977). (3) Augite and hypersthene from Ig2E and Ig2NWb were shown by Bindeman & Valley (2002) to be in oxygen-isotopic equilibrium with coexisting quartz, zircon, titanomagnetite, and melt at temperatures (758–814°C) calculated on the basis of the $\Delta^{18}O$ (qz–mt) calibration of Chiba *et al.* (1989). (4) Across the Fe–Ti-oxide temperature range for the Bishop, apatite exhibits large temperature-correlated ranges in Y, Mn, light rare earth elements (LREE), F, and Cl, as does zircon in Y, Th, and Hf; yet, in any particular sample, compositions of apatite and zircon inclusions in pyroxenes, oxides, and feldspars are indistinguishable (Hildreth, 1977). (5) Minor-element compositions (Al, Mg, Mn, V) of both ilmenite and titanomagnetite are strongly correlated with their mutual equilibration temperatures (Hildreth, 1977, 1979), whether in pyroxene-bearing or pyroxene-free pumices. As such correlations are also documented globally (Ghiorso & Sack, 1991, fig. 8), they cast doubt here on the suggestion of fortuitous inheritance of Bishop pyroxenes studded with mutually equilibrated (Bacon & Hirschman, 1988) oxide inclusions that conformed to the reservoir-wide thermal and compositional systematics (Fig. 15). We conclude that, at the time of eruption, both pyroxenes and both oxides were indigenous to the zoned Bishop reservoir.

New observations on Bishop crystals

Mineralogical observations on the Bishop Tuff subsequent to Hildreth's (1977, 1979, 1981) reports include the following.

(1) Rare monazite, reported by Hildreth only as anhedral xenocrysts, was found by Michael (1988) as 25–40 μm euhedra included within or adhering to augite and hypersthene in Ig2NWb.

(2) Traces of allanite were separated by Izett *et al.* (1988) from a few pumices in Ig2N and Ig2NW, suggesting that allanite, though far sparser than earlier in the eruption, might also have been present in magma with temperatures higher than the 763°C limit observed by Hildreth (1977). Temperatures for their samples were not reported, but it is well established that the northerly packages contain a range of pumices with varied crystal contents and temperatures of 749–790°C (Hildreth, 1977), now extended to 702–834°C (Electronic Appendix 3).

(3) Rims enriched in Sr and strongly so in Ba were identified on sanidine crystals from several pumices in Ig2E, Ig2N, and Ig2NW (Lu, 1991; Dunbar & Hervig, 1992). For some of these crystals, Fe and Ca also increase slightly in the Ba-rich rims (Lu, 1991; Anderson *et al.*, 2000). Sanidine from plinian and Igl pumices, in contrast, was shown (by ion probe) to be nearly homogeneous in trace and major elements. Although all the Ig2 sanidines analyzed are likewise unzoned in major elements, many in Ig2E have cores with 50–150 ppm Ba overgrown by rims with >2000 ppm Ba. Even stronger Ba zoning typifies sanidines from Ig2N and Ig2NW, where some rims have 5000–9000 ppm Ba. Indicative of independent early histories as well as final crystallization environments, however, the cores of Ba-rimmed sanidines in Ig2 contain ~200 ppm Sr, about 10–15 times more than in the unzoned sanidines from the plinian and IglE pumices (13–19 ppm Sr; Lu, 1991).

(4) Six grains of high-Mn (low-Mg + Al) titanomagnetite, similar to those in some Glass Mountain rhyolites (Metz, 1987) and in early erupted Bishop pumice (Fig. 15), were identified as inclusions in quartz crystals from three pumices in Ig2 (Lu, 1991; Anderson *et al.*, 2000). Whether the host quartz crystals were xenocrysts, antecrysts, or Bishop-age phenocrysts transferred by mixing within the magma reservoir or by syneruptive engulfment of earlier-erupted material is unresolved.

(5) Zircon crystals in the Bishop Tuff were shown by ion-probe U–Pb analysis to have crystallization ages as much as 160 kyr older than the 760 ka eruption (Reid & Coath, 2000; Simon & Reid, 2005). Different grains yielded ages ranging from near that of the eruption back to 926 ± 36 ka, but none gave the still older ages (2·2–1·0 Ma) that would be expected for zircon antecrysts inherited from the numerous Glass Mountain rhyolite predecessors. Several Triassic zircons were apparently derived from local granitoid roof rocks, showing that old zircons could survive in the low-temperature Bishop magma. The ion-probe determinations of U concentrations in F6, Igl, and Ig2 zircons are consistent with electron-probe and instrumental neutron activation analysis (INAA) evidence (Hildreth, 1977, 1979) that these zircons crystallized from magma that had already become zoned in U, as well as in Zr/Hf, Y, and Th.

(6) Ion-probe analysis of melt inclusions (MI) trapped in quartz and feldspar crystals identified ranges of

incompatible-element enrichments (for sets of MI within single eruptive packages, commonly within single pumices, and even within a few individual host crystals) consistent with degrees of fractional crystallization (of the evolving, intermittently trapped, host melt) that range from ~7% to as high as 33–40% (Dunbar & Hervig, 1992; Lu, 1992; Anderson *et al.*, 2000), reconsidered by Wallace *et al.* (1999) to be largely in the range $15 \pm 5\%$. Because the larger values are 2–10 times greater than the wt % crystals present in Bishop pumices (Fig. 7), some kind of crystal–melt separation is implicit, as is some enormous cumulate repository. No straightforward mechanism of monotonic compositional evolution of melt composition emerges from the MI data, however, because entrapment sequences are compositionally inconsistent and often nearly random (Lu *et al.*, 1992, fig. 1; Peppard *et al.*, 2001, fig. 14), both within clasts and within crystals.

(7) Infrared spectroscopic analysis of MI in quartz crystals (Anderson *et al.*, 1989, 2000; Wallace *et al.*, 1995, 1999) demonstrated a pre-eruptive gradient of H_2O dissolved in the melt that ranged from ~3·2 to ~6 wt %, similar to the range calculated by Hildreth (1977) on the basis of mineral equilibria. CO_2 contents of the MI analyzed extend from 19 to 1085 ppm (Skirius, 1990; Wallace *et al.*, 1999). Inverse correlations between incompatible trace elements and CO_2 in sets of MI from plinian, Igl, and earliest Ig2 pumices permit the inference of gas-saturated crystallization, which would be accompanied by progressive preferential partitioning of CO_2 into the gas phase. Using the FeTi-oxide temperatures of Hildreth (1977), this inference in turn allowed (1) estimation of gas-saturated total pressures at times of MI entrapment (calculated on the basis of experimentally calibrated pressure-dependent solubilities of H_2O and CO_2) that range from ~1·5 to ~2·1 kbar for the first three-quarters of the eruption; and (2) calculation of a pre-eruptive gradient in exsolved gas content, from ~1 wt % at depth to ~6 wt % near the reservoir roof, where bubbles would thus have been equivalent in mass to the total dissolved volatile content of the host melt (Wallace *et al.*, 1999). Why such a mass of bubbles, if real, would not rise to the roof and escape was not addressed.

(8) Analyses of MI from pumice at two sites indicate a more complex history for the quartz host crystals in Ig2NW (Wallace *et al.*, 1999; Anderson *et al.*, 2000). There is little overlap of H_2O contents of MI in Ig2NW with those of the MI erupted during the volumetrically dominant earlier sequence. In Ig2NW, H_2O is lower ($\sim 4{\cdot}1 \pm 0{\cdot}5$ wt % vs 4·8–6·3 wt % in earlier units), and CO_2 extends much higher (150–1085 ppm vs 19–208 ppm in earlier units). Gas-saturation pressures extensively overlap those for the earlier units, but seven of 41 MI analyzed from Ig2NW yield higher values in the range 2·2–2·8 kbar. [P. J. Wallace (personal communication, 2004) suggested that most of the 41 MI from Ig2NW may have lost H_2O diffusively, thereby lowering their estimated entrapment pressures.] Most of the highest-CO_2 MI are near the rims of their quartz hosts. Ion-probe analyses of the same sets of MI document positive correlations of Ba, Sr, Zr, and Mg abundances with CO_2 contents, thus demonstrating joint rimward increases in successively trapped MI of these compatible trace elements and incompatible CO_2. Such reverse trace-element zoning contrasts with that recorded for quartz MI from earlier in the Bishop sequence, where these elements and CO_2 either decrease slightly or scatter randomly in successively rimward MI. Moreover, importantly, most MI analyzed from their Ig2NW samples, even those in the cores of quartz grains, have higher CO_2 contents than do MI from earlier in the eruptive sequence (Wallace *et al.*, 1999), apparently requiring separate environments of early (as well as final) quartz crystallization.

(9) Cathodoluminescence (CL) imaging identified oscillatory growth zones in Bishop quartz grains (Peppard *et al.*, 2001) that were used to estimate the entrapment sequence of MI in individual crystals. For Igl, plinian, and Ig2Ea quartz, neither compatible (Ba, Zr, Mg) nor incompatible (U, Nb) elements (determined by ion probe) showed any systematic compositional evolution of MI with entrapment sequence; the within-crystal concentrations variously increased, decreased, reversed, or remained constant for core-to-rim sequences of MI. For two sites in Ig2NW, however, bright-CL rims on 20 of 21 quartz grains (from 10 pumice lumps) indicated late overgrowths that are rare on grains in Ig2E and apparently absent earlier in the eruptive sequence. Ion-probe analysis showed that MI in the sharply bounded bright-CL outer zones of Ig2NW quartz are enriched in Ba and Zr (and depleted in Nb) relative to MI in their own interiors as well as compared with MI in quartz grains from earlier in the sequence. This reinforces the evidence from items (3) and (8), above, that the final growth stage of these Ig2NW quartz grains took place after an abrupt change of the rhyolitic host melt to one that was less evolved, richer in Ba, Sr, Ti, Zr, and CO_2, and presumably somewhat hotter than had been the host melt when the interior zones had grown (Peppard *et al.*, 2001). Peppard *et al.* suggested settling of the crystals into deeper magma that subsequently erupted (late in the sequence) as Ig2NW, but modification of the host melt is more

plausible and more consistent with other observations. Compositions of the virtually unzoned Ig2NW crystals (biotite, plagioclase, both FeTi oxides, zircon, and apatite) differ markedly from those erupted earlier from shallower levels of the chamber, and only the quartz and sanidine carry the thin overgrowths that indicate late elevation of Ba, Sr, Ti, Zr, and CO_2 contents in some (but by no means all; Fig. 14) of the Ig2 host magma.

(10) Application of the Ti-in-quartz geothermometer (Wark & Watson, 2006) to a spectrum of Bishop pumices (Wark *et al.*, 2004, 2007) yielded 720–750°C for quartz cores but a wider range of 720–810°C for quartz rims, the latter correlating well with our FeTi-oxide eruption temperatures. The bright-CL rims so common on Ig2 quartz grains contain roughly twice the Ti of their dark-CL cores, yielding temperatures of 750–810°C. These data suggest that a thermal pulse caused resorption, truncating the outermost CL zones (Peppard *et al.*, 2001), followed by overgrowth of Ti-richer bright-CL quartz rims from a host magma that was hotter, richer in Ba, Sr, Ti, and Zr, and had much higher CO_2 contents (which may have promoted overgrowth by reducing H_2O activity). These shifts are recognized only in Ig2 pumice and are pronounced mainly for crystal-rich pumice of Ig2NW and Ig2N, ejection of which terminated the eruption. These processes had little or no effect on the lower-temperature rhyolite at shallower levels of the chamber that supplied the first three-quarters of the eruptive volume. Estimates of Ti diffusivity in quartz suggest that the sharply bounded Ti-enriched bright-CL rims grew no earlier than a century or so before eruption (Wark *et al.*, 2007).

CONTINUITY OF THE ERUPTIVE SEQUENCE

All lines of evidence indicate physical continuity of the Bishop eruptive sequence. We infer that accumulation of Bishop fall layers F1–F8 required about 90 h (Wilson & Hildreth, 1997).

The F1–F8 sequence brackets all of Ig1E and (beyond the distal limits of coeval ignimbrite) contains no discernible hiatus in plinian deposition. A short break in activity, probably representing at most a few hours, occurred at the F8–F9 boundary. The shortness of the break is indicated by pristine preservation of the fine-ash-bearing top of F8 (Fig. 3), by conformity of the Ig1–F9–Ig2 sandwich in Owens Gorge (with no evidence for erosion or reworking; Wilson & Hildreth, 1997, fig. 10), and by the mutual compound welding of Ig1 and Ig2 (Wilson & Hildreth, 2003). Although Snow & Yund (1988) suggested, from thicknesses of cryptoperthite lamellae in sanidine crystals, that 1–2 years separated emplacement of Ig1 and Ig2, such an interpretation is undermined by their earlier proposal (Snow & Yund, 1985) of a 1–5 year hiatus in emplacement within the demonstrably unitary Ig2Eb.

Our newer data show that fall unit F9 was synchronous with most or all of Ig2E emplacement (see above). Moreover, failure of ash flows consisting of undiluted northern material to cross the caldera floor and join the easterly outflow sector may best be attributable to blockage by synchronous outpouring of Ig2E material from the eastern and southeastern ring-vent segments. Conversely, the presence of Ig1NW material at the northern caldera margin (Wilson & Hildreth, 1997, fig. 15) and absence of Ig2E at the same site, even though the later Ig2E flows were more energetic and farther-traveled than those of Ig1NW, suggest that synchronous eruption of the northerly Ig2 packages prevented northward emplacement of Ig2E. Concurrent foundering of the caldera floor may also have been a contributing factor, but it would not change the implications of these observations. We conclude that any plausible time breaks in deposition of the Bishop Tuff were short, local, and, on the 6 day timescale of the eruption, trivial.

In central Utah, 660 km ENE of Long Valley [location 45 of Izett *et al.* (1988)], ~2 m of white to buff, fine-grained Bishop Ash is preserved locally. Unlike most distal Bishop remnants, which are reworked and contaminated (Izett *et al.*, 1988), the basal meter there appears to be undisturbed primary fallout. This 1 m massive interval grades up from pyroxene-free white ash in its lower two-thirds to pale tan ash of similar grainsize, which contains traces of euhedral augite and hypersthene (along with quartz, feldspars, biotite, oxides, and allanite). The continuous gradation implies continuous deposition from a downwind ash cloud that included co-ignimbrite ash entrained into the plinian column. The large fraction of pyroxene-bearing ash (as much as the upper third of the Utah section) is inferred to be equivalent to proximal–medial fall unit F9, along with ash elutriated from the coeval Ig2E and Ig2NW and Ig2N flows. A composite column around Chalfant Valley (Fig. 1) would include 207 cm of F9 and 480 cm of F1–F8, implying that F9 forms ~30% of the total medial fall thickness, comparable with the Utah proportion. We infer that pyroxene-bearing magma joined the erupting mixture about two-thirds of the way (volumetrically) through the eruption. It came to dominate the mixture, however, only in the northern outflow lobes, contributing ≤20% of the pumice in F9, Ig2E and Ig2SW, and probably a still smaller fraction in the upper part of the distal ash deposit.

CONTINUITY OF ZONATION IN A SINGLE MAGMA CHAMBER

In addition to the physical evidence for continuity of the Bishop eruption, abundant and varied chemical and mineralogical evidence supports the notion of a single integrated magma reservoir prior to the eruption. Evidence is compelling that the Bishop Tuff represents magma that had been stored in a unitary zoned chamber that was most differentiated, lowest in temperature, richest in gas, and poorest in phenocrysts at the roof, where withdrawal began. Not long before the eruption, the chamber was injected by batches of crystal-poor, Ba-rich, less-evolved rhyolite and dacite that were dispersed sparsely but widely throughout the zoned resident magma, with which they mixed and mingled, probably in part syneruptively, ultimately forming the swirly and dark pumice.

(1) If two or more discrete rhyolitic magma bodies had underlain the caldera, then initial breakout of each one would be expected to have contributed its own fall deposit as well as ignimbrite. No proximal to medial fall deposits with an independent distribution pattern, or with pumice and lithic suites matching the northern packages, have been found.

(2) Crystal-poor pumice is dominant and crystal-rich pumice is sparse in F1–F8 and in most of Igl, whereas the opposite holds for most of Ig2 (Electronic Appendix 2; Fig. 6). For the mid-eruption packages, in the Sherwin subunit of Igl and in Ig2E, xp and xr pumice proportions are comparable. The overall trend from early xp-dominated ejecta toward later suites increasingly dominated by crystal-richer ejecta is unmistakable. The data indicate a general (not strict) positive correlation between FeTi-oxide temperature and crystal abundance (Hildreth, 1979) for the main pumice suite.

(3) Pyroxene-bearing (generally higher-temperature) pumice is absent or rare in Igl, common in Ig2E and Ig2SW, and dominant in Ig2NW and Ig2N. Stratigraphic conformity, temporal continuity, and otherwise similar pumice proportions of IglEb and Ig2Ea (Fig. 6) suggest that the incoming of higher-temperature pumice by gradual incremental increase (rather than by an overwhelming influx) reflected progressive tapping of a single magma body. Similar observations and conclusions apply to the xr Adobe-type pumices (Table 1; Fig. 4d).

(4) Swirly and dark, variant xp pumices are present in small amounts in all ignimbrite packages throughout the eruption, with the only major influx of swirly pumice being in the Watterson subunit, nearly midway through the sequence in terms of magma volume erupted. The sparser dark pumices joined the eruptive mixture in sporadic pulses, widely spaced across the sequence, resulting in local concentrations (Electronic Appendix 2) at a few scattered outcrops. The ubiquity and persistence of these variant pumices also tie the main zoned sequence to a common chamber.

(5) Allanite, augite, hypersthene, and pyrrhotite are compositionally identical in all sectors. Allanite is ubiquitous in Igl and is also widespread in Ig2 pumices that yield magma temperatures up to ~763°C. The other three phases all coexist in pumices that yield temperatures of 737°C or higher, thus overlapping extensively with coexisting allanite in F9, Ig2E, Ig2SW, Ig2NW, and Ig2N. These relations are easily reconciled with magma withdrawal from adjacent zones of a single chamber but only by special pleading from separate ones.

(6) The continuity of the T–fO_2 data (Fig. 15), the concomitant progressive compositional changes of sanidine, plagioclase, biotite, titanomagnetite, ilmenite, apatite, and zircon (Hildreth 1977, 1979), and the overall increasing proportions of xr pumices in the eruption mixture (Fig. 6) are consistent only with a single magma body.

(7) Zircons show systematic compositional trends (in Zr/Hf, Y, Th, and U) across the eruptive sequence (Hildreth, 1977, 1979). The mean U–Pb zircon ages, however, are indistinguishable at ~850 ka (Simon & Reid, 2005) for suites of zircons separated from IglEb, Ig2NW, and plinian pumice (Reid & Coath, 2000). Reid & Coath's three samples also have in common the presence of sparse Triassic zircons and the absence of cognate zircons older than 926 ± 36 ka, despite proximity of potentially inheritable zircons as old as 2·1 Ma in the precaldera rhyolites (Simon & Reid, 2005). The similarity of zircon age spectra is most consistent with a unitary magma chamber.

(8) Incompatible-element contents of the melt phase, represented by the matrix glass of main-suite pumices, define coherent compositional arrays (Fig. 16), which are continuous across the entire bulk thermal–compositional spectrum, straightforwardly related to phenocryst–melt partitioning in each sample, but clearly distinct from arrays for swirly and dark pumice (Fig. 16).

(9) Gas-saturation pressures estimated for MI in quartz crystals from Igl and Ig2 show extensive overlap (between 1·1 and 2·1 kbar; Wallace *et al.*, 1999), though a subset in Ig2 extends to pressures 0·4–0·7 kbar still greater, implying withdrawal of Ig2 magma from crystallization depths similar to those of Igl and down to as much as 2 km deeper. Such relations are consistent with complex but generally progressive withdrawal from a unitary chamber.

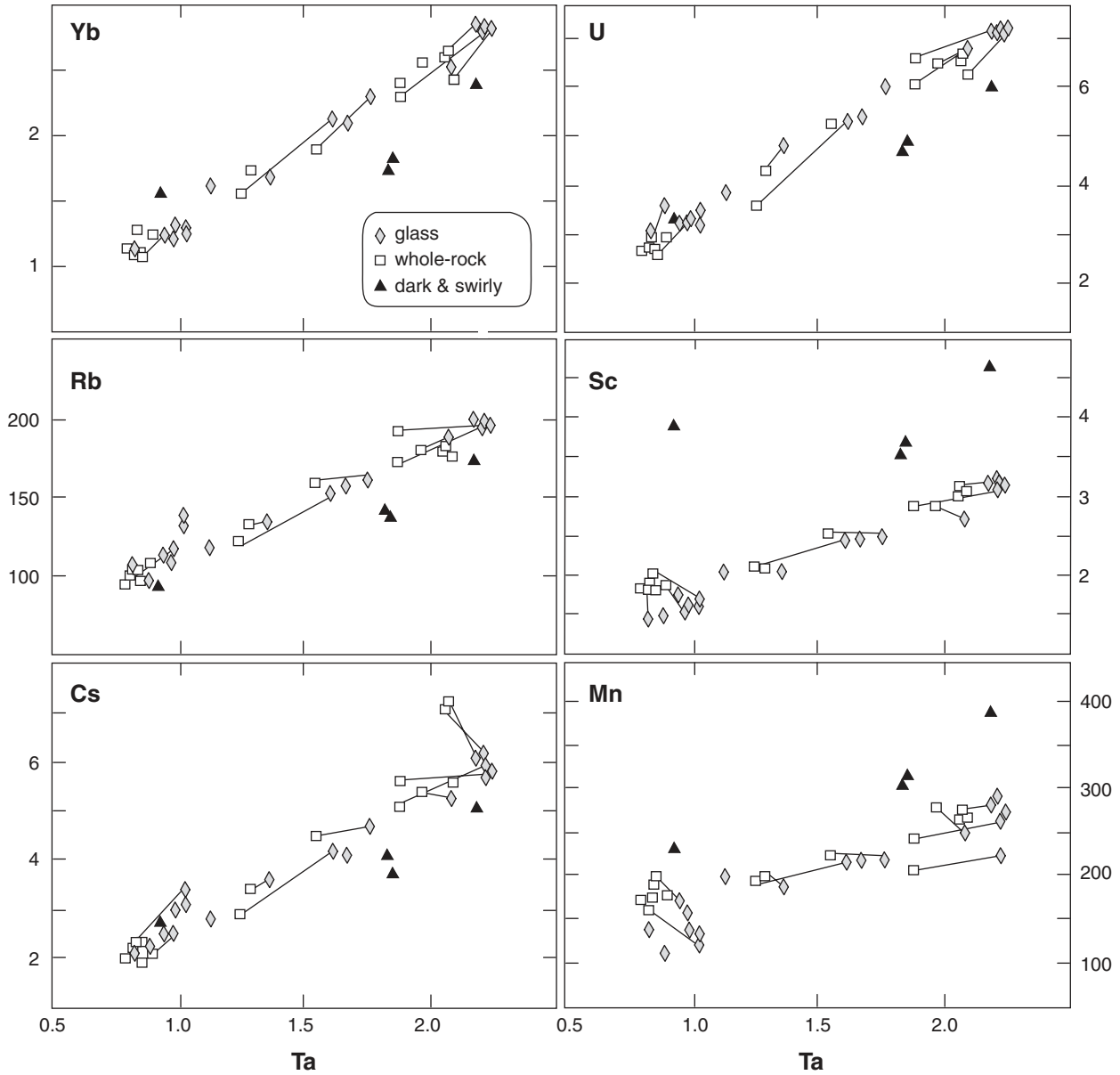

Fig. 16. Variation vs Ta of Yb, Rb, Cs, U, Sc, and Mn (all in ppm) for melt (glass) and whole-rock pairs for 16 samples that span the thermal and compositional ranges of main-suite rhyolite. For illustrative samples, tie-lines connect the pairs. Data are also plotted for crystal-poor (Ba-rich) samples of one swirly pumice (0·9 ppm Ta) and three dark pumices (higher Ta), which generally fall well off the main zoned array. Symbols identified in inset. All seven elements shown (and Th, Tb, Dy, and Lu, not shown) were enriched roofward in the melt as well as in the bulk magma. The apparently compatible intra-sample behavior of Sc and Mn (negatively sloping tie-lines) in some samples reflects crystallization (and retention) of biotite, pyroxenes, allanite, and zircon [see Hildreth (1977) for high concentrations of Sc and Mn in those phenocryst phases]. Anomalous behavior of Cs in a few low-temperature (high-Ta) samples probably reflects pre- or post-eruptive vapor-phase transport, which strongly enriched Cs and Rb in many Bishop biotites (Hildreth, 1977). Data by INAA (Hildreth, 1977; Lawrence Berkeley Laboratory under supervision of Frank Asaro and H. R. Bowman). Precision of individual determinations has been given by Hildreth (1977); typical uncertainties (in ppm) are Cs ± 0·1, Mn ± 2, Rb ± 6, Sc ± 0·02, Ta ± 0·01, U ± 0·04, and Yb ± 0·02 (Perlman & Asaro, 1969). Error bars would be no larger than the symbols plotted.

(10) Despite diverse Nd-isotope ratios for precaldera rhyolites ($\varepsilon_{Nd} = -0{\cdot}5$ to $-3{\cdot}9$) and local mafic lavas ($\varepsilon_{Nd} = +2{\cdot}6$ to $-4{\cdot}8$), Bishop whole-pumice, glass, and titanomagnetite samples from F6, Ig1Eb, Ig2Eb, Ig2SW, Ig2Nb, and Ig2NWb are nearly invariant at $\varepsilon_{Nd} = -1$ (Halliday *et al.*, 1984, 1989; Cousens, 1996; Davies & Halliday, 1998). Pb-isotope determinations for sanidine separates from F6 and Ig2NWb

(early and late in the eruptive sequence) likewise gave identical ratios: $^{206}Pb/^{204}Pb = 19{\cdot}17$; $^{207}Pb/^{204}Pb = 15{\cdot}67$; and $^{208}Pb/^{204}Pb = 38{\cdot}92$ (M. Delevaux & W. Hildreth, unpublished USGS data, 1979), consistent with the data of Simon *et al.* (2005). Oxygen-isotope ratios of 15 quartz separates from all packages are virtually constant at $\delta^{18}O$ (quartz) $= 8{\cdot}2 \pm 0{\cdot}2$ (Hildreth *et al.*, 1984, table 7); and sanidine, titanomagnetite, biotite, and orthopyroxene gave appropriately small temperature-dependent fractionations (W. Hildreth & J. R. O'Neil, unpublished USGS data, 1984). A constant Bishop Tuff value of $\delta^{18}O$ (melt) $= 7{\cdot}8$ was likewise calculated on the basis of mineral determinations for nine plinian and 10 ignimbrite samples by Bindeman & Valley (2002). Initial $^{87}Sr/^{86}Sr$ ratios for bulk sanidine separates indicate isotopic zoning, ranging from 0·7060 to 0·7064 in Ig2 and from 0·7064 to 0·7079 in Igl and the plinian deposit (Noble & Hedge, 1969; Hildreth, 1981; Halliday *et al.*, 1984; Christensen & DePaolo, 1993; Christensen & Halliday, 1996; Davies & Halliday, 1998). [Roof rocks are Paleozoic metasediments (0·709–0·725) and Mesozoic Sierran granitoid plutons (0·707–0·711) (Goff *et al.*, 1991; Hurley *et al.*, 1965).] For Sr, the trend of the zonation itself, from lowest initial $^{87}Sr/^{86}Sr$ ratios for the last material erupted to high and varied initial ratios for early erupted low-Sr magma from the chamber roof zone, again provides good evidence for a single zoned magma body.

(11) Pincer-style convergence of paired ring faults that propagated along opposite sides of a collapsing caldera (Wilson & Hildreth, 1997), producing a single ovoid depression with a smoothly continuous margin, is interpreted most simply as subsidence of a roof plate into a unitary chamber, as is the early postcaldera uplift of a single large resurgent dome (Bailey, 1989; Hildreth, 2004).

DISCUSSION OF THE MAGMA WITHDRAWAL SEQUENCE

The reconnaissance sampling and emphasis on (early vs late) extremes of the Bishop zonation in Hildreth's (1977, 1979) initial investigation conveyed an oversimplified notion of orderly drawdown of the zoned reservoir during magma withdrawal. Because the tuff is multi-lobate, because compositional differences among main-suite rhyolite pumices cannot be judged visually, and because the presence or absence of pyroxenes cannot be reliably determined by hand lens, the expanded data sets assembled here were required to appreciate the complexity of the evacuation sequence.

Early to middle withdrawal interval: Igl

Pumices in fall layers F1–F8 and contemporaneous Igl are quite evolved and for most elements show ranges of concentration that, though limited compared with the whole Bishop sequence, are nonetheless significant (Fig. 14). Our new data for individual F1–F8 pumices yield such ranges as 0·72–0·99 wt % FeO*, 12–23 ppm Sr, 76–91 ppm Zr, 18–24 ppm Nb, and 21–67 ppm Ba, nearly identical to the ranges of 24 plinian samples analyzed by Gardner *et al.* (1991). Because pumices representing all or much of each such range coexist within particular plinian layers, there is no systematic correlation with stratigraphic height in the fall deposit for any element analyzed. Moreover, compositions of pumices in Igl fully overlap those in the fall deposit and, for most elements, extend to compositions even slightly more evolved than those of any plinian pumice analyzed (Fig. 14).

For that and the following reasons, we do not consider the plinian withdrawal scenario of Gardner *et al.* (1991) nor the derivative roof-contamination model of Duffield *et al.* (1995) to be viable. (1) Because the fallout was contemporaneous with all of Igl and much of Ig2 (Wilson & Hildreth, 1997), the plinian deposit is not representative of roof-zone magma alone but, rather, is a partial sampling of the first three-quarters of the volume of the entire Bishop Tuff. (2) Because Gardner *et al.* (1991) miscorrelated the plinian stratigraphy (Wilson & Hildreth, 1997, p. 433), the compositional sequence relied on by Duffield *et al.* (1995) is disarranged. (3) In the data set of Gardner *et al.* (1991), the scatter of trace-element concentrations at several of the eight plinian horizons they sampled is nearly as great as for the plinian deposit as a whole. This heterogeneity is in accord with our own chemical data (Fig. 14) and with the wide range of crystal contents in plinian pumice (1·7–16·7 wt %; Electronic Appendix 1), from which we infer that magmas tapped from various parts of the reservoir were ejected simultaneously during accumulation of the plinian deposit. (4) The grainsize of plinian layers F1–F4 is too fine to provide pumices large enough to yield reliable analytical data for detailed whole-pumice comparisons. The idea that roof contamination might occur is not at all unreasonable and is indeed suggested by us as a possible cause for the old Rb–Sr model ages (see section below on 'Residence time of Bishop magma'), but the existing plinian whole-pumice data do not demonstrate it, and the pre-eruptive relative distribution of magma parcels that produced particular pumice clasts is unknown.

The role of Ig2E

Along with the preceding pulse of xr pumice in the Sherwin subunit late in IglEb, the Ig2E packages represent a complexly varied but progressively changing compositional suite, from predominance of lower-temperature crystal-poorer pumice in Igl toward increasing abundances

of higher-temperature crystal-richer pumice (Fig. 6). All vent segments issued a variety of pumice types and compositions, but the variability was most pronounced in Ig2E, which erupted from the east-to-southeast segments. Pumice clasts in Ig2Ea alone yield a continuous range in crystal content from 0·7 to 19 wt % (Fig. 7; Electronic Appendix 1). Pyroxene-bearing pumice is sparse at the base of Ig2Ea and in lower F9 but common in Ig2Eb and c (though nowhere dominant in Ig2E). Almost the full ranges of Fe, Ti, Zr, Rb, Ba, and Sr contents for main-suite Bishop pumice are represented by homogeneous pumice clasts in Ig2E alone (Fig. 14). The same point was shown for the continuous ranges of Ta, Sc, and Yb by Hildreth (1981, fig. 9) despite the less extensive sampling at that time.

Nearly all the intermediate FeTi-oxide temperatures determined for the Bishop Tuff are from Ig2E (Tableland) pumices, 15 samples of which gave 733–763°C (Hildreth, 1977), here recalculated to 742–775°C. New temperature data (Fig. 15; Electronic Appendix 3) for Ig2E include 46 oxide pairs from pyroxene-free pumice that yield 739–766°C (plus five pairs that give 718–736°C) and 30 pairs for pyroxene-bearing pumices that give 736–810°C. In comparison, temperatures lower than 740°C dominate Igl, and those higher than 770°C dominate Ig2NW and Ig2N.

Although the Igl–Ig2 transition may have been two-thirds or more of the way through the eruption in terms of time elapsed and volume erupted, it was medial (or before) in terms of the full thermal and compositional spectra represented in the Bishop Tuff. The mix of pumice types in Ig2Ea still resembled that of IglEb, whereas those of Ig2Eb and c are closer to the contrasting assemblage present in the northerly sheets of Ig2 (Fig. 6). Stratigraphic considerations, however, strongly suggest that the onset of venting along the northern caldera margin was contemporaneous with vent migration from the initial (Igl, F1–8) southerly vent area (Fig. 1) eastward around the ring fracture, and that emplacement of Ig2E was therefore largely synchronous with (not earlier than) emplacement of the northern packages (Fig. 2; see section above, 'Continuity of the eruptive sequence'). Appearance in Ig2E of magmatic components that are dominant in Ig2NW and Ig2N (Adobe-type textures, pyroxene-bearing pumice, Ba-enriched rims on sanidine, Ti-enriched rims on quartz, and Fe–Ti oxides yielding temperatures of 760–810°C) suggests withdrawal from common storage domains for the eruptive mixtures released concurrently from the southeastern and northern ring-vent segments. Ig2E therefore reflects a transition in tapping successive domains of the zoned reservoir in two ways. First, it provides evidence from Ig2Ea to Ig2Ec of a progressive shift around the eastern caldera margin in proportions of different materials withdrawn from different depths or domains having contrasting ranges of magma temperature. Second, Ig2E represents a compositional and thermal linkage between the dominantly cooler assemblages that erupted earlier at the southern margin to form IglE and the assemblages with overlapping and higher temperatures that erupted coevally along the northern margin to form Ig2N and Ig2NW.

Withdrawal of the northern ignimbrite lobes

Although eruption of the Ig2NW (Mono Basin) packages began slightly before eruption of the Ig2N (Adobe Valley) packages a few kilometers farther east, mutual interfingering shows that their emplacement overlapped in time (Wilson & Hildreth, 1997, figs 15–18). The ranges in crystal contents, pumice types, oxide temperatures, phenocryst suites, and pumice compositions are virtually the same in Ig2NW and Ig2N (Figs 6, 7, 14 and 15), suggesting derivation from a common domain in the magma body despite vent segments aligned for ~15 km along the northern margin. Subordinate highly evolved crystal-poor pumice continued to contribute to both packages (Figs 6 and 14), but their mutual hallmark is the predominance of the least evolved, highest-temperature (main-suite) pumice found in the Bishop Tuff (Figs 14 and 15). Moreover, the highest gas-saturation pressures calculated for melt inclusions in quartz (Wallace *et al.*, 1999) and the highest equilibration pressures calculated for the phenocryst assemblage orthopyroxene–titanomagnetite–quartz (Hildreth, 1977; Ghiorso & Sack, 1991) are for pumices from Ig2NW and Ig2N, suggesting derivation from layers or domains deeper as well as hotter than the sources of previously erupted material.

The presence exclusively in Ig2NWb of rare blocks of glassy dacite (65–68% SiO_2) rich in coarse quartz and feldspar further supports withdrawal of magma from the deepest level tapped. The crystal-rich dacite might represent either a sample of floor mush or a recharge batch lodged and crystallizing somewhere deeper in the reservoir, whence it was drawn up (and commingled) with the voluminous (~100 km^3) crystal-rich rhyolite that dominates the northern lobes of Ig2.

Toward the end of the eruptive sequence, withdrawal of the highest-temperature, crystal-richest magma from the deepest level tapped can be rationalized in terms of several mutually supportive processes. (1) If the chamber roof had dipped northward (Wallace *et al.*, 1999), it could have been intersected by northerly ring faults at a magma level deeper than those that fed earlier vents in other sectors. (2) By the time the late-opening northern ring-vent segments became active, ~400 km^3 of magma had already been withdrawn, some of it probably drawn southward toward the initial plinian–Igl vent (Fig. 1), thereby depleting the northern part of the reservoir in the lower-temperature magma that had previously occupied

its roof zone. (3) Asymmetric subsidence of the caldera floor (Hill, 1976; Bailey, 1989) may have promoted expulsion of deeper magma when the northern ring vents finally opened, especially if the upper levels had previously been withdrawn preferentially toward southerly vents. Seismic refraction profiles (Hill, 1976; Hill *et al.*, 1985) and gravity models (Kane *et al.*, 1976; Carle, 1988) indicate that the caldera fill thickens substantially toward the north and east. What fractions of the deepening reflect precaldera topography, tilting of the cauldron block during collapse, or differential magma withdrawal remain uncertain.

Some consequences of withdrawal dynamics

Concurrent withdrawal of magma from different levels or domains of the reservoir seems certain, but much less certain is the extent to which the heterogeneity of co-emplaced material may also reflect syneruptive recycling and contamination. Nonwelded pumice and crystals deposited on proximal surfaces could be swept back into the convective eruption column by powerful radial winds (Wilson & Hildreth, 1998), persistently or repeatedly during the 6 day sequence. Structural collapse and avalanching during caldera subsidence would also promote such recycling as well as inevitable entrainment of crystals and pumice of Glass Mountain rhyolite, which can be hard to distinguish from Bishop Tuff equivalents.

Even for crystals within single pumice clasts (presumed to have formerly coexisted in magma), there can likewise be considerable uncertainty in assessing the history and origin of anomalous crystals or of chemically or isotopically distinguishable subpopulations of given species. Mixing of hard-to-distinguish subpopulations of euhedral quartz, feldspars, biotite, oxides, zircon, or allanite could take place by any of the following processes: (1) ingestion by Bishop magma of Glass Mountain or earlier-erupted Bishop phenocrysts during the 2–3 km vertical collapse of the chamber roof; (2) confluent mixing of magma from different layers or domains during eruptive withdrawal; (3) interface mixing between adjacent layers or domains within the reservoir, during either pre-eruptive convection or syneruptive disturbance; (4) interzonal mixing in response to disturbances caused by ascent of batches of recharge magma like those that led to the dark and swirly pumices; (5) ascent of crystals entrained from floor cumulates by batches of interstitial melt arising from an underlying mush reservoir; (6) interzonal sinking of large individual crystals or avalanching of masses of crystals that had been growing on steep or overhanging surfaces. A little mixing of crystals by one or more such mechanisms almost certainly took place. Rare pyroxenes are found in F9 and early Ig2Ea pumices, well before they become common in the withdrawal sequence; rare allanite is present in some crystal-rich pyroxene-bearing pumices late in the sequence; and Lu (1991) identified rare sodic cores in a few Ig2 plagioclase crystals as well as a few low-Mg titanomagnetite inclusions coexisting in Ig2 quartz grains with the predominantly higher-Mg titanomagnetite crystals. In view of the complexity of caldera subsidence and the disorderly sequence of concurrent withdrawal from various compositional domains, however, it is remarkable that mixing and contamination failed to obscure the fundamentally systematic trends.

Following eruption of the Bishop Tuff, scores of eruptions of Early Rhyolite (Bailey, 1989) took place in the central part of the caldera from 751 ± 16 ka to 652 ± 14 ka. The resulting lavas and pyroclastic deposits amount to $\sim 100\ km^3$ of magma (Hildreth, 2004) and are all crystal-poor (0–3%), devoid of the quartz and sanidine that dominate the Bishop crystal assemblage. Compositions of the Early Rhyolite (74–75% SiO_2), however, are similar in most respects to the last-erupted part of the Bishop Tuff, except for a few elements (Zr and Ba) that slightly extend the range of Bishop zoning (Hildreth, 2004, fig. 4). Although numerous vents for the Early Rhyolite (Bailey, 1989) were in the central and southern parts of the caldera (where the Bishop eruption began; Fig. 1), the highly evolved magma that dominated the first two-thirds of the Bishop sequence did not reappear. Either the roof-zone high-silica rhyolite magma so strongly depleted in compatible elements had been exhausted during the Bishop withdrawal, or it was thoroughly mixed with less evolved deeper magma (and most of its crystals resorbed) during post-collapse reorganization of the reservoir [see Hildreth (2004) for discussion].

THE BISHOP MAGMA RESERVOIR

Depth and configuration of the Bishop magma chamber are loosely constrained as follows. The area of subsidence enclosed by the ring-fault zone is $\sim 220\ km^2$ (Hildreth, 2004), providing a minimum plan-view area of the reservoir. Vertical subsidence, as shown by circumcaldera topography and numerous drillholes through the intracaldera fill (Bailey, 1989), ranges between ~2 and ~3·3 km, averaging 2·7 km. This yields $>600\ km^3$ of magma displaced, roughly equivalent to the magma volume estimated from the eruptive products. Gas-saturation pressures in MIBQ (Wallace *et al.*, 1999) suggest that the reservoir roof had been 5–6 km beneath the paleosurface and that quartz in the deepest magma withdrawn had trapped MI at 10–11 km. Because this 5 km depth difference is about twice that indicated by the measured subsidence, magma drawdown was not uniformly distributed, as concluded by Hildreth (1977) from equilibration pressures calculated for the assemblage quartz–orthopyroxene–FeTi oxides. It appears that much of the $\sim 500\ km^3$ of magma that produced F1–F8, Ig1, and the pyroxene-free majority of Ig2E could have been withdrawn fairly uniformly from the top ~2 km of the

whole (>220 km^2) reservoir, followed by an areally more restricted upsurge of 100–150 km^3 of pyroxene-bearing Ig2 magma from depths as much as 3 km greater.

Such volume estimates are crude because there is little or no control on the proportions of pumice types nor on the thermal and compositional increments represented in the concealed and altered intracaldera welded tuff, and no evidence at all for the unknown volume of unerupted magma left behind in the reservoir. Although ejecta resulting from the late upsurge were in large part released from northerly vents, there is no obvious way to constrain how localized or, alternatively, how laterally extensive was the magma domain withdrawn from the 8–11 km deep level of the reservoir. Asymmetric subsidence of the roof plate late in the eruption (discussed above) may have initiated a shift from relatively uniform reservoir-wide drawdown to more localized expulsion of crystal-richer magma from deeper levels.

Definition of magma chamber

For purposes of the following discussion, Fig. 17 presents a definition sketch of the various zones we envisage to form a magma chamber and its surroundings. Although magma can be defined simply as any naturally molten material that consists of melt, crystals, and gas in any proportion, ambiguities arise when solid phases predominate or when a long-lived chamber waxes and wanes by magma recharge and zoned crystallization. Around the chamber margins, any melt-bearing zone that had rigidified (Marsh, 2000) might no longer be thought of as magma, but it needs still to be treated as part of the magma chamber by virtue of its physical and thermal continuity with other melt-bearing zones, and because it remains susceptible to remelting during thermally prograde events induced by recharge. Such a rigidified zone retains subordinate interstitial melt that is physically continuous with free magma and can be expelled by compaction or deformation (e.g. Vigneresse *et al.*, 1996) or by gas-driven filter pressing (Sisson & Bacon, 1999) into the non-rigid interior, and thus it can contribute components to the mush or melt-dominant zones. Any model that fails to include the dominant mush and rigid zones as part of the chamber is self-limiting in that it divorces the evolving melt-rich body (or bodies) from the mushy parent zones on which they depend (Hildreth, 2004).

Incremental assembly and growth

Incremental assembly and growth as well as thermal waxing and waning by recharge are likely to be general processes intrinsic to long-lived upper-crustal magma chambers. Recurrent disturbances and mixing appear to be inevitable, resulting in alternating crystallization and resorption episodes as well as in complex secular blending of varied inputs. Although inputs of high-silica rhyolite directly from the deep crust are unlikely (see below), the many magma

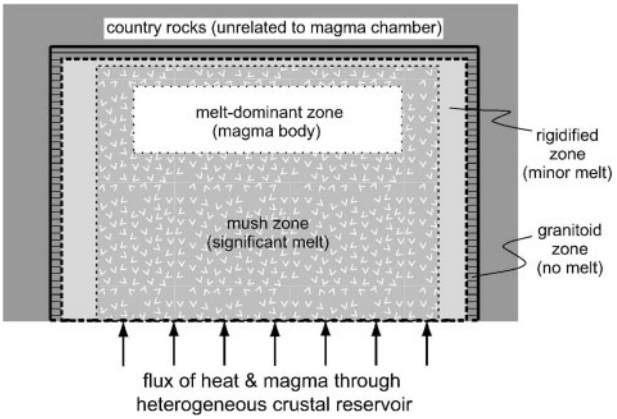

Fig. 17. Definition sketch illustrating terms used in this paper and by Hildreth (2004) to describe zones within, around, and beneath a silicic magma chamber. The thick continuous line encloses the magma chamber (where melt is present) as well as its own crystallized rind (the granitoid zone), which remains physically and chemically linked to melt-bearing zones and subject to resorption. Within the chamber, the melt-rich zone represents the magma body that would be partly or completely tapped during typical eruptions; as in Fig. 18, it may in some chambers (like the Bishop) extend to the roof. The mush zone, which is crystal-rich but carries enough melt to permit mixing and hybridization with recharge magmas, can also sometimes be partially tapped by extraordinary eruptions. Boundaries between zones fluctuate with thermal and fluid flux and are controlled by rheological differences that reflect changing melt/crystal ratios. The greater magma reservoir (in the sense of stored reserves or extra supply) further includes the chamber's feeder zone and the heterogeneous crustal column (dikes, pods, and permeable mush) from which recharge batches sporadically augment the chamber. The magma system (not fully sketched) would still further include partially molten supply domains in the deepest crust and underlying mantle.

batches energizing and augmenting a large upper-crustal chamber over a million-year lifetime may range from mafic to silicic (Wiebe, 1987, 1993; Sisson *et al.*, 1996; Weinberg, 1997; Wiebe & Collins, 1998; Weinberg & Leitch, 1998). Convective self-mixing (Couch *et al.*, 2001) of crystal mush can promote general textural and compositional homogenization of large domains of pluton-sized bodies during their assembly and can, at the same time, preserve disequilibrium features at the scale of mineral grains, yet retain little evidence for crystal accumulation or for mutual intrusion of multiple magma batches. Mush convection can also promote escape of buoyant interstitial melt and its progressive concentration upwards in the chamber.

Such an incremental growth model implies the following: (1) the crystallinity of a pluton-scale granitoid magma chamber fluctuates with depth as well as time, decreasing with mafic recharge but increasing locally with melt loss to a rhyolitic roof zone; (2) each new batch added, by partly crystallizing, contributes to both melt-dominant and mush zones (Bacon & Druitt, 1988); (3) melt-dominant zones of a large chamber need never be volumetrically dominant (Smith, 1979); (4) a melt-dominant upper zone can persist indefinitely in a crystal-poor condition, owing to secular

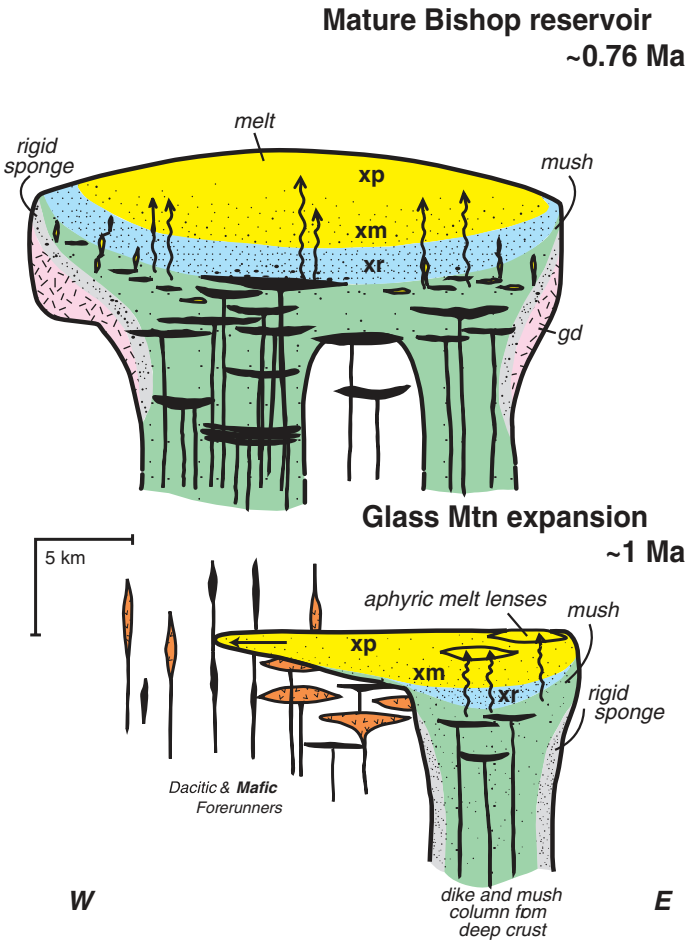

Fig. 18. Conceptual schematic illustrations of mush model of rhyolite melt extraction from plutonic crystal mush of intermediate to silicic hybrid composition, scaled roughly to late Glass Mountain (below) and mature Bishop (above) evolutionary stages. The magmatic water gradient imposes a gradient in crystallinity inverse to temperature. Phenocryst contents of zoned mobile magma are proportional to stipple density: xp, crystal-poor (0–6%); xm, intermediate crystal content; xr, crystal-rich (12–25%; mush = 25–55%). Black dikes and lenses represent the few mafic magmas reaching the upper crust and penetrating the mushy granitoid reservoir (e.g. Wiebe & Collins, 1998); most batches of mantle-derived basalt are thought to lodge in the deep to mid-crust, there inducing partial melting and hybridism, thermally sustaining the system, and replenishing the upper-crustal reservoir via a mushy root zone (Hildreth & Moorbath, 1988; compare fractionation column of Hildreth, 1981, and mush column of Marsh, 2000). Lower illustration additionally depicts mafic and dacitic batches (mostly 3·5–2·5 Ma; Bailey, 1989) that predated growth of the rhyolitic system. During early and middle stages of the subsequent Glass Mountain rhyolitic system (2·2–0·79 Ma), many aphyric melt lenses segregated from enveloping crystal mush, as depicted for two of ~60 crystal-poor batches of high-silica rhyolite melt that erupted during its magmatic lifetime. After ~1·1 Ma, however, the reservoir expanded, integrated any lenses already formed, and yielded crystal-poor eruptive batches of more uniform composition (Metz & Mahood, 1991) from a chamber of intermediate size. Upper illustration depicts Bishop Tuff reservoir at 0·76 Ma. Westward shift of the active mantle-driven focus fed a new root zone beneath central Long Valley, and its upper-crustal reservoir merged with the dying Glass Mountain focus, which ceased being mantle-sustained and crystallized after the caldera-forming eruption. The larger western focus continued to segregate eruptible crystal-poor melt lenses during Early Rhyolite postcaldera time (760–650 ka) and as late as 300 ka, but has since likewise largely crystallized (Hildreth, 2004). Root zones depict mush columns of quartz + feldspar-rich (melt-poor) cumulates laced with varied dikes of mafic, hybrid, or silicic composition, extending to zones of partial melting in the mid- and lower crust. At least one late batch invaded the melt-dominant zoned chamber not long before eruption, providing the swirly and dark pumices. Model illustrates key points: (1) that silicic plutons as well as their segregated melt lenses grow incrementally; (2) that rhyolite melt grades down into silicic crystal mush that can be kilometers thick; (3) that a hybrid mixed zone, fed by persistent deep recharge, underlies reservoirs at all scales and is more likely to be tapped during eruption of smaller chambers than large; (4) that large silicic chambers can be much thicker than averaged drawdown of caldera-forming eruptions, such that most of the crystal-rich resident magma stays behind to supply melt for subsequent eruptive cycles or to solidify ultimately as a granitoid (gd) pluton.

replenishment of heat, water, and rhyolitic melt derived from subjacent granitoid mush kilometers thick; (5) the floor of a large silicic magma chamber is in general a hot plate, not a heat sink (in contrast to sills, laccoliths, and floored lateral lobes of some shallow intrusions; Fig. 18).

In systems like Long Valley with large long-lived silicic magma reservoirs, it is unlikely that the rhyolite magma ascends directly from zones of partial melting in the deep crust. For circum-Pacific and Cordilleran rhyolites, minimum-melt extraction from metasedimentary

protoliths is an uncommon mode of origin, and radiogenic isotope studies typically indicate large immature mantle contributions to hybrid crustal sources (Hildreth & Moorbath, 1988; Mahood & Halliday, 1988; Hildreth *et al.*, 1991*l*; Johnson, 1991*l*). Basalt-induced intracrustal dehydration melting of amphibole-bearing mafic to tonalitic meta-igneous rocks generally yields intermediate (dacitic–rhyodacitic) melts (Helz, 1976; Conrad *et al.*, 1988; Carroll & Wyllie, 1990; Beard & Lofgren, 1991*l*; Rushmer, 1991*l*; Roberts & Clemens, 1993; Skjerlie & Johnston, 1993; Wolf & Wyllie, 1994; Rapp & Watson, 1995; Sisson *et al.*, 2005), not rhyolitic melts, except at very low melt fractions, or unusually high fO_2, or from source rocks already somewhat felsic (e.g. Beard *et al.*, 1993).

Voluminous high-silica rhyolite is more likely to evolve in the mid- to upper crust than to ascend directly from the deep crust for several additional reasons. (1) In many long-lived volcanic fields, intermediate and mafic eruptives predate the rhyolitic episodes (Hildreth, 1981*l*). Thermal models of basalt-driven deep-crustal melting indicate long incubation times (10^5–10^6 years) for major melt production and pluton-scale mobilization (Annen & Sparks, 2002). During the waxing stage, ascent of forerunning basalts, and of scattered batches of the crustal and hybrid melts they induce, would create a hybrid column of mushy pods and trailings of 30 km height, effectively a gauntlet that any ascending rhyolite would later have to run, without entrainment or mixing. Many upper-crustal intermediate plutons separate their own leucogranite pods and dikes, but rarely are they cut by rhyolitic dikes from below, though mafic and intermediate dikes from below are abundant. (2) Great volumes of rhyolite require large source domains, raising problems of deep-crustal heterogeneity and hybridism, and of progressive source depletion and dehydration. The widespread retention of high-silica leucosomes in anatectic migmatites suggests that water-saturated minimum melts are seldom extracted cleanly and that those that do segregate into pods and dikes soon freeze. High-temperature dehydration melting is generally necessary to permit segregation of large melt volumes, which with advancing melt fraction would seldom any longer be rhyolitic. (3) Although batches of water-saturated tonalite to granodiorite mush could achieve neutral buoyancy in the upper crust, an independent batch of high-silica-rhyolite melt is unlikely to do so in any consolidated wallrock. Moreover, if such an isolated batch stalled in the upper crust it would soon cool and crystallize (still more rapidly if exsolving vapor)—in contrast to most high-silica rhyolites observed, which are crystal-poor. (4) Excluding the strongly peraluminous intracrustal magmas (e.g. Andean macusanite and Himalayan leucogranite), rhyolites carrying restite or high-pressure phenocrysts are rare. If from the deep crust, the rapid ascent needed to maintain their aphyric condition would be expected to entrain restite or crystals from older mush along the ascent path. (5) Low-Ba–Sr–Eu rhyolites cannot be derived directly by partial melting, because extensive feldspar fractionation is required, thus demanding voluminous intermediate–granitoid magma as both proximate parent and cumulate remainder. (6) Water-saturated MI sealed in rhyolite crystals yield entrapment pressures of 1–3 kbar (whether the rhyolite be crystal-poor or crystal-rich), indicating upper-crustal crystallization.

In our view, few large shallow magma reservoirs (and particularly that of the Bishop Tuff) originate quickly. A rhyolite-rich upper-crustal reservoir is more likely to start as a plexus of pods, laccoliths, sills, and dikes, the advance facies of a much larger intermediate plutonic complex that arises piecemeal from a long-lived deep crustal MASH zone (Hildreth & Moorbath, 1988; Annen & Sparks, 2002). Each magma batch ascends to its threshold of water-saturation in the mid- to upper crust, where gas exsolution then induces extensive crystallization. Interstitial rhyolitic melt escapes from the accumulating granitoid mush, intrudes upward as a vanguard of dikes and pods, and (in silicic systems grown large) may coalesce into a substantial zone of crystal-poor rhyolitic magma that overlies the mush. The sequence of melt extraction, coalescence, and eruption might be repeated serially from any batholith-scale mush domain subjected to sustained replenishment from below.

Evidence from Long Valley is consistent with such a model (Fig. 18). Basalt and dacite eruptions were common from 4·5 to 2·5 Ma, after which intermediate and more mafic eruptions ceased (Bailey, 1989, 2004). Beginning at ~2·2 Ma, eruptions were exclusively of Glass Mountain rhyolite, released in numerous batches in two successive episodes. (1) From 2·2 to 1·3 Ma, at least 24 eruptive units, all high-silica rhyolite and mostly crystal-poor but chemically varied, were tapped sporadically from several discrete pods at different stages of evolution, including some units considerably more enriched than the Bishop Tuff in incompatible trace elements. (2) From 1·1 to 0·79 Ma, at least 35 more crystal-poor units erupted, all of them high-silica rhyolite chemically similar to the evolved end of the Bishop compositional spectrum and interpreted (Metz & Mahood, 1991*l*; Metz & Bailey, 1993) to have been tapped from a common, expanding magma chamber. Two of the youngest Glass Mountain rhyolites have been shown to have zircon age spectra that overlap that of the Bishop Tuff (Simon & Reid, 2005).

The earlier interval of dacite eruptions reflected crustal magmatism beneath a large westerly area that was wholly separate from that beneath Glass Mountain. Although both these precaldera foci (Hildreth, 2004) were apparently contiguous with the later site of the Bishop magma reservoir, both also extended well outside it (Fig. 1). A major expansion and integration of what became the

Bishop magma chamber beneath Long Valley evidently took place within the last few hundred thousand years before the caldera-forming eruption (Fig. 18). Because evidence is lacking for eruption or storage of pre-Bishop rhyolite anywhere west of Glass Mountain (Fig. 1), we infer that roof rocks for the Bishop chamber that expanded under Long Valley were predominantly pre-Cenozoic basement and that any rhyolitic to granitic precursors of Glass Mountain affinity were subordinate and limited to the eastern sector (Figs 1 and 18). The westward expansion may have coincided with a prograde thermal episode that resorbed any Glass Mountain crystals engulfed (including any zircon older than ~0·9 Ma) and promoted release of voluminous new batches of rhyolitic melt from deeper granitoid mush. Zircons analyzed from the Bishop Tuff are reported to be no older than 926 ± 36 ka, averaging ~850 ka (Reid & Coath, 2000; Simon & Reid, 2005), and compositionally they reflect the bulk Bishop zonation (Hildreth, 1977, 1979), indicating that expansion and integration of the caldera-wide reservoir had taken place during the younger Glass Mountain interval (1·1–0·8 Ma) and that the thermal and chemical zoning represented in the Bishop Tuff was present by ~850 ka.

Residence time of Bishop magma

Isotopic studies of the Bishop Tuff and its Glass Mountain predecessors have addressed questions of pre-eruptive residence times of the rhyolite magmas and of discrete datable differentiation events (DDDE, as opposed to secular fractionation), first formulated and explored by Halliday *et al.* (1989). Evidence includes (1) Rb–Sr model ages for various feldspar crystals and MIBQ in the Bishop Tuff, some of which are 0·3–1·7 Myr older than the 0·76-Ma eruption age (Christiansen & DePaolo, 1993; Christiansen & Halliday, 1996; Davies & Halliday, 1998); and (2) four pre-caldera sets of phenocryst-poor high-Rb/Sr rhyolite lavas that define four separate, tightly fit Rb–Sr isochrons, even though each set consists of several well-dated eruptions spread out over protracted time intervals, variously 270–450 kyr long by K–Ar and $^{40}Ar/^{39}Ar$ methods (Halliday *et al.*, 1989; Davies *et al.*, 1994; Davies & Halliday, 1998). The four isochronous multi-lava batches were interpreted to have originated during short-lived DDDEs (at 2·05, 1·89, 1·15, and 1·06 Ma) and to have thereafter each survived for hundreds of thousands of years as discrete closed-system magma bodies, isolated and little affected by their serial eruptions or by recharge, mixing, contamination, or any further fractional crystallization. Because a similar range of Rb–Sr model ages (2·5–1·1 Ma) was proposed for both MIBQ and feldspar crystals in the Bishop Tuff itself, the puzzle of these pre-caldera DDDEs, isochronous batches, and pre-eruptive model ages bears significantly upon the question of the time available for establishing the climactic compositional zonation.

Seemingly supportive evidence from apparent $^{40}Ar/^{39}Ar$ ages of 2·3–1·9 Ma for Bishop Tuff MIBQ (van den Bogaard & Schirnick, 1995) has now been discounted by recognition of excess radiogenic Ar in the magma body, inherited from crustal melting and trapped within MI during quartz crystallization (Winick *et al.*, 2001). On the other hand, the comparably great longevity of some MI and feldspars suggested by the Rb–Sr data would, if real, constitute a still-unresolved enigma. Few discussions of the Rb–Sr data, however, distinguish clearly enough among the separate questions of (1) gradual vs episodic vs abrupt accumulation of bodies of rhyolitic magma, (2) protracted vs punctuated crystallization intervals, (3) what processes could produce within a given crystal-poor magma body the wide range of Rb/Sr values needed to yield an isochron, and (4) how that range might be preserved, undisturbed, within the melt phase of a discrete phenocryst-poor body, lens, or layer for 10^5–10^6 years. For the last question, especially puzzling is how isochronous batches could have avoided disruption during withdrawal of any of the 17 plinian pumice eruptions recognized for Glass Mountain (Izett *et al.*, 1988; Sarna-Wojcicki *et al.*, 2005), some of which were far more voluminous (1–10 km^3) than any of the 50–60 rhyolite lavas exposed on the edifice.

A striking property of many Bishop pumices, Glass Mountain lavas, and comparable high-silica rhyolites is their ultra-low Sr content (0·1–10 ppm), which demands derivation from an underlying pluton-sized body dominated by feldspar-rich cumulates (Mahood, 1990). Extraction of crystal-poor (formerly interstitial) melt at or near the top of a batholithic body of quartz–feldspar mush is the simplest model for achieving such fractionation rapidly and, at the same time, buffering the low-Ba–Sr–Eu rhyolitic melt from contamination by recharge batches from below (Mahood, 1990; Hildreth, 2004). If the phenocryst-poor isochronous batches at Glass Mountain were truly long-lived, such melt extraction in brief DDDEs would dispense with any need for secular crystal fractionation that might defeat the isochronous relationships. Buoyancy of the extracted melt batch, as a result of its composition and (at least for the Bishop) vapor-saturation and gas bubbles, could prevent its remixing with the parental mush. Melt extraction from mush would not, however, alone protect the low-Sr melt from later contamination, nor is it obvious how it could account for long-term preservation of the required range of Rb/Sr values in a crystal-poor magma body subject to thermal convection. Perhaps the most realistic scenario is that each constituent melt batch of each isochronous set represented separation of an independent melt lens from largely the same parental mush domain (Fig. 18), much of the Sr-isotopic evolution having taken place within the mush prior to extraction.

For the Bandelier Tuff (New Mexico), which resembles the Bishop in having a wide range of high Rb/Sr values and comparable ranges in composition and crystal

content, Wolff *et al.* (1999) and Wolff & Ramos (2003) determined $^{87}Sr/^{86}Sr$ (calculated for the time of eruption) ranging from 0·7052 to 0·7076 for individual sanidine crystals, the ratios increasing roughly with 1/Sr and Rb/Sr. Matrix glasses and MIBQ gave eruption-age ratios ranging from 0·7052 to 0·7113. They also showed that Pb-isotope ratios for the same sanidine suite span ranges that could not have evolved by radiogenic ingrowth on the timescale required, thus demanding open-system behavior of Pb. Because of the greater susceptibility of Sr than of Pb to open-system modification in the low-Sr high-Pb rhyolite magma, the age significance of Sr-isotope variations is undermined, and any apparently isochronous $^{87}Sr/^{86}Sr$ vs Rb/Sr correlation in low-Sr rhyolites now needs to be scrutinized for alternative interpretation as a pseudoisochronous mixing array. Although not tightly fit like the Glass Mountain isochrons, the positive Rb/Sr vs $^{87}Sr/^{86}Sr$ array for the Bandelier Tuff (Wolff & Ramos, 2003) illustrates how interaction between low-Sr melt and a subtle contaminant can affect predominantly the roof-zone magma rather than deeper levels of a zoned reservoir. Comparable open-system models for Rb–Sr variations in low-Sr silicic magmas, attributed to a variety of processes, were advanced by Reece *et al.* (1990), Duffield *et al.* (1995), and Verplanck *et al.* (1995).

Nonetheless, as emphasized persuasively by Halliday and associates, assimilative contamination of the low-Sr rhyolite magmas by the pre-Cenozoic high-Sr country rocks at Long Valley is hard to reconcile with keeping either the ultra-low Sr contents or the tightly fit isochrons. If the interacting roof rocks, alternatively, were high-silica rhyolite predecessors—crystalline or mushy—only modestly older (say ~100 kyr) than any particular melt batch, then the contamination mechanism of low-temperature (~700°C), H_2O-saturated roof-zone melt might be of a different style than conventionally envisaged. The wide Rb/Sr ranges that define the isochrons principally reflect the wide variation in bulk and melt Sr contents (0·07–3·9 ppm), whereas the corresponding Rb contents range only twofold (156–312 ppm). Trace amounts of Sr-isotopic exchange with high-Rb/Sr roof-rind rocks (undergoing rapid ingrowth of radiogenic Sr), or simply dehydration of roof-rind (high-Rb/Sr) biotite carrying low Sr but elevated $^{87}Sr/^{86}Sr$, might suffice.

For the apparently isochronous sets of Glass Mountain lavas, an obstacle to accepting such a mixing-line hypothesis is not understanding what processes might coordinate changes in Rb/Sr and $^{87}Sr/^{86}Sr$ to maintain tightly fit (pseudo)isochrons. Resorption of earlier-formed biotite (from mushy predecessors or in indigenous floor or wall mush) and backmixing of its evolved Sr is a mechanism worth investigating. For the Bishop Tuff, however, there is no such tight-fit problem because there is no isochron at all. The numerous published (eruption-age) $^{87}Sr/^{86}Sr$ ratios (Halliday *et al.*, 1984; Christensen & DePaolo, 1993; Christensen & Halliday, 1996; Davies & Halliday, 1998) for glass separates, whole-pumices, and MIBQ (0·7060–0·7115) scatter widely, though they do show a very crude positive correlation with $^{87}Rb/^{86}Sr$ (2·3–298).

Although Bishop Rb–Sr data define no tightly fit array, the Bandelier results nonetheless provide a compelling reason to consider whether the Rb–Sr model ages for some Bishop feldspars and MIBQ reflect interactions with wall-rock components enriched in radiogenic Sr. Inheritance of quartz and feldspar crystals from remnants of earlier rhyolite batches by an expanding Bishop chamber might account (as would syneruptive ingestion) for the Glass Mountain model ages (2·5–1·1 Ma) and Nd-isotope signatures (ε_{Nd} down to −3·5) identified for a few crystals in Bishop plinian pumice. Moreover, most Rb–Sr model-age calculations assume an initial ratio of ~0·7060, but, if the magma had been modestly contaminated by roof-rock or roof-rind during chamber expansion, the effective initial ratio (at times of feldspar crystallization or MI enclosure) could have been higher and its period of ^{87}Sr ingrowth correspondingly shorter.

Irrespective of whether the supposedly old crystals in the Bishop Tuff were (1) xenocrysts syneruptively engulfed or (2) antecrysts inherited by incorporation of older Glass Mountain magma batches by the growing Bishop reservoir, or (3) whether they reflect roof-rind assimilation or exchange processes, it thus seems clear that the Rb–Sr data provide no firm evidence for Bishop magma residence times. Because zircons, one of the earliest-crystallizing phases in the Bishop Tuff (included within all other phenocrysts), crystallized no more than ~160 kyr before the climactic eruption (Reid & Coath, 2000; Simon & Reid, 2005), it seems unrealistic that one of the last-crystallizing phases, sanidine, should yield meaningful Rb–Sr model ages so much older. Dissolution of inherited zircon in proto-Bishop rhyolite magma should have been preceded by resorption of any accompanying sanidine.

It seems reasonable to infer, therefore, from the zircon age spectrum and the zonation-spanning gradient in zircon compositions (Hildreth, 1977, 1979), that the Bishop magma had been resident in an integrated reservoir for ~100–160 kyr and that much of its bulk compositional zonation had been established prior to the crystallization interval (which began with zircon) that produced the suite of phenocrysts ultimately erupted. Owing to recharge, chamber growth and melt evolution are nonetheless likely to have continued during the final 100 kyr before eruption.

Globally, there appears to be no simple relationship between magma residence time and development of zonation, although many have speculated on such an idea. Onset of chamber-wide convection can destroy existing zonation or prevent its development (Wilson *et al.*, 2006). Also, the monotonous crystal-rich intermediate ignimbrites (Best *et al.*, 1989; Lipman, 2000; Bachmann *et al.*, 2002)

demonstrate that some long-lived reservoirs failed to expel interstitial rhyolitic melt, zoned or not, even though they apparently had the capacity to do so.

DISCUSSION OF THE ORIGIN OF THE ZONING

It appears doubtful that the Bishop reservoir was ever strictly homogeneous, as implicit in (1) the ranges of phenocryst contents (0–20%) and ranges of trace-element concentrations (e.g. 150–300 ppm Rb) among the 60-odd rhyolites erupted at precaldera Glass Mountain (Metz & Mahood, 1991) and (2) the requirement that magma recharge from the deep crust and mantle thermally sustain so long-lived a system (Lachenbruch *et al.*, 1976). First-order questions are: (1) whether the zonation was produced by processes operative before, during, or after assembly of the magma body—or all three; (2) whether differentiation processes yielding zonation are continuous or episodic; (3) the relative importance of various processes contributing to the zonation; (4) how long it took.

Processes potentially contributing to zonation

Extraction and aggregation of rhyolitic melt (from a partially molten protolith or a crystallizing intermediate parent) needs to be distinguished conceptually from the concurrent or subsequent processes that bring about zonation within the rhyolite magma itself. Some rhyolites are fairly homogeneous (Hughes, 1993; Sutton *et al.*, 1995; Hildreth & Fierstein, 2000), but most large ones are zoned (Hildreth, 1981) or otherwise compositionally heterogeneous (Wilson *et al.*, 2006). Aggregation and development of zoning might or might not be concurrent.

Aggregation of a Bishop-scale reservoir of rhyolitic magma has variously been thought to result from: (1) amalgamation of successively ascending batches of rhyolitic partial melt segregated directly from crustal protoliths; or (2) fractional crystallization of a pluton-sized body of intermediate magma (by any of several modes of crystal removal from suspension or of crystal growth on surfaces enclosing the reservoir); or (3) protracted extraction of interstitial melt from a large subjacent reservoir of granitoid crystal mush; or (4) amalgamation of melt increments extracted from numerous discrete batches of crystallizing recharge magma. It is argued here that process (3) dominates, that (4) contributes, that (2) is subordinate, and that (1) has little direct relevance for Long Valley rhyolites.

As for zoning, although some voluminous ignimbrites are zoned from crystal-poor rhyolite to crystal-rich dacite (Lipman *et al.*, 1966; Hildreth, 1981), raising still other problems, the main questions for the Bishop Tuff concern how the compositional gradients were established within the rhyolitic magma body itself. Processes warranting consideration include the following. (1) Assembly of a zoned chamber *ab initio* by incremental stacking of melt batches according to relative buoyancy, whether derived by (1a) crustal partial melting, (1b) extraction from an underlying body of granitoid mush, or (1c) release from crystallizing batches of recharge magma lodged deeper in the reservoir. (2) Removal of crystals from suspension in a melt-dominant magma chamber, whether by settling, convective flow differentiation (plating out of schlieren at mushy margins), or avalanching from the walls. (3) Inward crystallization from the walls and/or roof. (4) Sidewall crystallization, producing buoyant batches of water-enriched residual melt that stack by density at higher levels. (5) Partial melting of roof rocks, and perhaps also of chamber walls or dike-laced basement domains beneath the chamber, if such melts could likewise rise to the top. (6) Bubble ascent through gas-saturated magma, potentially promoting upward transport of alkalis, halogens, B, Be, Cu, As, Mo, Sn, W, Hg, Pb, or U, and concurrently stabilizing a density gradient against rehomogenization. (7) CO_2 flux from mafic recharge into the roots of the reservoir, lowering H_2O activity in deeper parts of the rhyolitic magma, thereby inducing crystallization of lower zones and promoting escape of evolved interstitial melt to upper zones. (8) Magma mixing, probably recurrently in varied situations; for example, amalgamating rhyolite pods (Fig. 18), blurring interfaces between density-stratified layers, or blending resident magma with assimilant melts, recharge batches, and melt plumes rising from cumulate mush. We argue here that only process (1a) can be rejected; that processes (1b) and (1c) are important; and that all the rest can at times be secondary or local contributors.

Toward a realistic zoning model for the Bishop chamber

Several of the mechanisms listed above were discussed in Hildreth (1977, 1979, 1981). Assembly of the zoned Bishop chamber by stacking of melt batches from a progressively melting source region was ruled out by contradictions between partial-melting systematics and (1) low roof-zone abundances and extreme gradients in Ba, Sr, and Eu, (2) antithetical gradients in LREE and heavy REE (HREE), and (3) conflicting gradients among transition metals [Sc, Mn enriched roofward (Fig. 16); Ti, V, Fe, Co, Ni, and Cu depleted roofward; Cr and Zn erratic but effectively constant].

Wall-rock assimilation by low-temperature rhyolite magma, though certainly here a source of sparse xenocrysts and likely to be significant during initial assembly of any upper-crustal reservoir, is unlikely to contribute much to mature chamber-wide zoning, except perhaps during times of caldera collapse. For the Bishop Tuff, it was shown that most chemical gradients (for transition metals, REE, and alkaline earths) were opposite to those

expected for roof melting and that Sr, Nd, and O isotope ratios of the Mesozoic and Paleozoic roof rocks are too extreme for partial or bulk melts of such rocks to have made major contributions (Hildreth, 1979, 1981; Halliday *et al.*, 1984, 1989).

Hildreth (1979, 1981) proposed that thermal (Soret) diffusion at chamber walls was (in concert with buoyant roofward melt convection) a major control on gradients in the Bishop Tuff. Lesher (1986), however, demonstrated that the polarities of Soret separation for major and trace elements in silicate melts are largely antithetic to those in rhyolites. Michael (1983) and Cameron (1984) pointed out that gradients for many elements in the Bishop Tuff are consistent with crystal–melt equilibria if a credible mechanism for large-scale crystal–liquid separation could be identified. Miller & Mittlefehldt (1984) highlighted accessory-phase fractionation and similarities between trace-element patterns recorded for felsic dikes in granitoid plutons and those in zoned ignimbrites.

Aspects of the Bishop zonation that led Hildreth (1979) to appeal to unconventional processes included the following. (1) Sc and Mn were enriched roofward, in the glass (melt) phase (Fig. 16) as well as in the bulk magma, despite the strong mineral–melt partitioning ($D_i \sim 10$ to ~ 100) of both elements into biotite, allanite, oxides, and pyroxenes. (2) The distribution of (LREE-rich) allanite was apparently paradoxical—ubiquitous in roofward zones where LREE were depleted but sparse or absent in late-erupted magma from deeper levels where LREE were relatively enriched. (3) Compositional gradients existed in the liquid prior to crystallization of the observed phenocrysts (Fig. 16). (4) If established by loss of earlier phenocrysts, the trace-element gradients within the erupted rhyolite volume alone would require 50–75% of the rhyolitic magma to have been removed as crystals (Hildreth, 1977; Michael, 1983). Bishop pumice contains only rare crystals that might have survived from an earlier episode of crystal–melt fractionation, and the 12 mineral species present are largely unzoned and indigenous to zones of the bulk gradient from which they erupted (Hildreth, 1979, pp. 61–64). If the zonation had been established by crystal–melt fractionation, then what was the mechanism of separation and where are the hundreds of cubic kilometers of separated crystals? We argue below that a batholith-scale subjacent reservoir of crystal mush was the source of the zoned melt.

Stratification or gradient?

There is a need to reconcile the compositional and thermal zonation with the requirement that magmatic heat be supplied to the chamber roof to service the 700°C gradient through the 5 km thick roof plate, cooling of which was presumably intensified by a hydrothermal system. Convection involving large parts of the chamber would be expected, however, to have promoted mixing that would destroy gradients in suspended crystal content and in phenocryst, melt, and bulk compositions. Suppression of large-scale convection in a Bishop-sized chamber would demand a strong density gradient, and (within the rhyolitic zones of the magma body) only the gradient in water content (dissolved and as gas bubbles) would be adequate (Hildreth, 1977, pp. 145–149; Wallace *et al.*, 1999).

As an alternative to chamber-wide convection, heat loss through the roof and stabilization of a 100°C gradient (~714–819°C) within the magma volume tapped might have been accomplished by a system of many convecting layers (Sparks *et al.*, 1984). Layered convection could help keep crystals in suspension, minimizing sinking and mixing, and a buoyant gas-rich zone of low-temperature melt concentrated toward the top would ensure that little or no crystallization took place against the roof. In contrast to a few other large-volume zoned pyroclastic units (Fridrich & Mahood, 1987; Boden, 1989; Streck & Grunder, 1997), however, no evidence is recognized in the Bishop Tuff for compositional or thermal discontinuities that might reflect such pre-eruptive layering.

We do not, however, envisage a static magma chamber. Internal convection of some kind seems required to sustain the 100°C gradient. Repeated infusion of melt plumes (from a reservoir of crystal mush below and from crystallizing recharge batches), rising to various levels of the zoned melt-dominant chamber, would be one mode of convective heat transport. Ascent of gas bubbles would be another. Although the xp swirly and dark pumices are mostly in Ig2, penetration of small amounts of the lower-silica rhyolite that produced them into early erupted magma of Ig1 (Fig. 6) is consistent with such processes. Layered convection might, in principle, have also been a major heat transport mechanism, but if such cells (thick high-viscosity layers circulating slowly?) had been present, then any steps in composition, crystallinity, or temperature across layer boundaries must have been small, approaching continuous gradients (Figs 9–13), too subtle to recognize in our data. Chamber-wide convection (subsequent to crystallization of the phenocryst suite erupted) appears to be ruled out by the gradients in bulk and mineral compositions and by restriction of the quartz and sanidine overgrowths to the final part of the eruptive sequence.

Site of crystallization

If crystal–liquid fractionation were the main process for zoning the reservoir, where did crystallization take place and where did the crystals go? Production of ~500 km^3 of crystal-poor high-silica rhyolite melt strongly depleted in Ba, Sr, and Eu implicates at least 1000–1500 km^3 of feldspar and quartz crystals (Hildreth, 1977, 1979; Michael, 1983), which were somehow removed from contact with that melt and sequestered elsewhere.

The roof and sidewalls of the chamber are unlikely repositories for such a volume. The Bishop eruption did not

eject clasts or clots of mush or crystal-rich material interpretable as fragments torn from a crystallizing roof rind. Heat loss may well have been dominantly through the roof, but there is no evidence among the ejecta for significant crystallization along the roof contact or upper walls, the surfaces most susceptible to disruption during magma withdrawal and caldera collapse. Significantly, the early parts of the eruptive sequence contain pumice clasts (and sparse dense vitrophyre) that are nearly all crystal-poor. Crystallization at the roof must have been suppressed by the H_2O gradient, the adiabatic gradient, and (as the melt gradient evolved) decline in intrinsic liquidus temperature with time.

At Long Valley, the granodioritic, quartzitic, and silicic-hornfels country rocks, once dehydrated at the roof of the magma reservoir, could have remained solid at ~720°C, allowing the main inflection in the thermal gradient to migrate up into the roof plate, thereby leaving the gradient in the uppermost magma very small, right through the contact. Under such conditions, there need have been no roof melting after the Bishop expansion had supplanted the more distributed Glass Mountain rhyolite system (Fig. 18), and there need have been no crystallization along the roof contact. If the main temperature inflection were in the roof rocks, the thermal gradient within the uppermost magma may have been such that no roof-zone thermal boundary layer was capable of producing convective plumes cool enough to sink athwart the magmatic density gradient. Cooling of the gas-saturated uppermost melt through the dehydrated roof might have been slow and effectively conductive. Because hydrothermal cooling higher in the roof plate, particularly in response to regional extension, might be expected to promote intermittent upper-border crystallization, it must have been balanced by sporadic recharge from below, promoting reheating, resorption, and near-steady buffering of the water-saturated crystal-poor near-minimum melt close to the roof. Moreover, any degassing through the roof must have been (at least) compensated by secular replenishment of aqueous gas from below, so that roof crystallization would not have been induced by falling H_2O activity. Had there been a significant crystallization front advancing downward from the roof, one could expect some amount of settling, scour, or rind failure to have contaminated the gradient of suspended crystals below with lots of distinguishable crystals, but this is not seen.

Heat is likely to have been lost through chamber sidewalls as well. Convective fractionation (Sparks *et al.*, 1984) by sidewall crystallization and buoyant ascent of evolved melt may well have contributed, but the mass-balance problem is formidable for producing and zoning a body of crystal-poor high-silica rhyolite melt that averaged at least 9 km in radius by crystallization at sidewall boundary layers. For example, to yield the ~500 km^3 of crystal-poor Bishop high-silica rhyolite melt erupted would require 50–75% crystallization of a low-silica rhyolitic precursor (Hildreth, 1977, 1979; Michael, 1983), or a lot more if the parent were dacitic. If that melt had formed an upper layer 250 km^2 in area and 2 km thick (as estimated from the ring-fault zone and gas-saturation pressures in MI), then a putative crystalline sidewall counterpart could take the form of an enclosing cylindrical rind 2 km high and 6·5–9 km thick! Alternatively, if crystallization took place along a cylindrical sidewall 5 km high (i.e. extending well below the crystal-poor melt zone to the level of the deepest crystal-rich magma tapped), then the enclosing rind would still need to be 3–4·3 km thick.

Compounding skepticism about the importance of sidewall crystallization are the following. (1) Progressive heating of dehydrated sidewall country rocks and long-continuing production of latent heat of crystallization within a thick sidewall rind should soon retard further crystallization there. (2) Avalanching from steep sidewalls should scramble crystals from various points of origin, causing marginal resorption or zoning of crystals and disrupting the gradients in crystal compositions. (3) Upflow of buoyant sidewall melt should be a rapid process (relative to melt percolation out of floor mush), but rhyolitic systems strongly zoned in trace elements appear to require long time intervals to develop, characteristically ~10^5 years. (4) Fragments of crystal-rich mush or rigid sidewall rind are not present among the Bishop ejecta. This is hard to reconcile with 3 km of roof-plate subsidence and withdrawal of magma from a depth range of several kilometers, if sidewall crystallization had been a significant process occurring at the time of eruption. (5) The typical Bishop pumices that contain the most crystals yield the highest magma temperatures, consistent with vertical gradients in water content, composition, crystallinity, and temperature, but antithetic to crystallization at cooling sidewalls.

That leaves crystallization at the bottom. Unlike mafic magma chambers emplaced in the crust, rhyolitic chambers need have no floors as such, except where some spread shallow sill-like wings. Other than beneath such lateral protrusions, heat loss through the base is likely to be negligible (or generally negative because heat addition from below is required to maintain shallow rhyolitic magma for long timespans; Lachenbruch *et al.*, 1976). Factors promoting bottom crystallization would not therefore generally include a basal cooling surface but, instead, (1) a bulk compositional gradient from high-silica rhyolite above to less evolved silicic magma below; (2) a gradient in magmatic water activity, declining with depth owing to basal CO_2 input from recharge basalts; and (3) the general condition that in a chamber with a vertical dimension of several kilometers, the gradient in liquidus temperature would be significantly superadiabatic, even if the magma were homogeneous (Jackson, 1961; McCarthy &

Fripp, 1980). The compositional gradients would usually be more important but, even if compositionally and thermally uniform, a magma body 5 km thick should begin to crystallize at its floor at a temperature 13–18°C higher than it would at its roof (assuming an adiabatic gradient of 0·3°C/km and a liquidus gradient of 3–4°C/km).

A large rhyolitic reservoir must grade down into its quartz–feldspar mush progenitor, which in turn funnels down (at least centrally) into a complex root zone, a dike-and-mush column that ascends from zones of mid- to deep crustal partial melting. Upward escape of buoyant melt from such crystal mush provides the link between low-Ba–Sr–Eu rhyolite magmas and the ordinary granitoid plutons that subsequently solidify. Basaltic recharge from the mantle thermally sustains the whole crustal magma system as successive mafic and hybrid batches rise to various crustal levels that reflect rheological evolution of the system itself as well as the hybridization history and buoyancy of individual batches. Such recharge and the concomitant heat flux should maintain interstitial melt throughout great depths of a quartz–feldspar cumulate reservoir, as illustrated by the enormous volumes of 'monotonous intermediate' mush (Hildreth, 1981) sustained and rejuvenated by such recharge (Bachmann *et al.*, 2002) and erupted occasionally as great crystal-rich ignimbrites such as the Fish Canyon Tuff (Best *et al.*, 1989; Lipman, 2000).

For a rhyolitic chamber, most of the mush is not cumulate in the traditional sense of having settled out but, rather, a composite residue, assembled from below, of numerous crystallizing batches from which interstitial melt escaped upward. There need, therefore, be little crystal settling (other than by compaction), no layered floor sequence as in mafic intrusions, and little or no cooling at the base. Granitoid plutons commonly have marginal schlieren caused by convective flow, but they seldom display modal or cryptic layering consistent with settling of crystals to the floor.

Mafic and hybrid layers can form by insertion of recharge batches within the mush or at any transient melt–mush interface (Bacon & Druitt, 1988; Wiebe & Collins, 1998), contributing additional melt and mush by partial crystallization. If most crystallization thus takes place along or well beneath the transient floor of the melt-dominant zone, the melt itself could accumulate piecemeal and evolve with few phenocrysts in suspension, yielding at times of eruption the great volumes of crystal-poor ash and pumice observed. With such a model, there is no need to postulate any great chamber of mafic to intermediate magma extensively crystallizing to yield a modest fraction of derivative rhyolite. Most of the processing and multiparental blending of a hybrid line of descent takes place deeper in a variably molten crustal mush column (Hildreth, 1981; Hildreth & Moorbath, 1988; Marsh, 2000), which incrementally supplies upper-crustal growth of a mushy granitoid plutonic reservoir. Such a reservoir need never itself have been crystal-poor, but expulsion of its intergranular rhyolitic melt does, in some systems, lead to accumulation of voluminous capping zones of water-rich high-silica rhyolite.

As granitoid plutons ultimately do solidify completely, it is not disputed here that concentric inward crystallization does eventually take place at the roof and walls, leading to the relatively felsic cores commonly observed. During magmatically vigorous intervals when such systems are capable of erupting great volumes of water-saturated crystal-poor high-silica rhyolite, however, the evidence indicates that crystallization at the top can be minimal [compare Fig. 18 with chamber schematic illustrations with upper solidification fronts, as drawn, for example, by McCarthy & Groves (1979) or Bachmann & Bergantz (2004)].

Mush model of rhyolitic magmatism

Like the Bishop, many voluminous eruptions of zoned rhyolite start with high-silica crystal-poor magma and tap progressively or stepwise into less evolved magma with 20–30% crystals (Hildreth, 1981). Some such eruptions, however, are known to have terminated with withdrawal of far more crystal-rich (35–70% phenocrysts) mush or even rigid sponge (Fig. 18), suggesting that increasing magma viscosity sometimes plays a role in slowing and ending such events (Smith, 1979; Scaillet *et al.*, 1998). The general inference follows that large rhyolite reservoirs do not crystallize from the top down but, instead, accumulate at the roof the water-enriched highly evolved melt that progressively escapes from the mushy cumulate plutonic body below. Because granitoid mush crystallization is dominated by anhydrous feldspars and quartz, any interstitial melt percolating upward is strongly water-enriched, which inhibits crystallization of the high-silica roof zone in spite of its lower temperature (Hildreth, 1979). Many zoned ignimbrites include crystal-poor volumes of high-silica melt so great that a proximate source volume of cumulate mush many kilometers thick must have underlain the segregated melt. Solidification fronts at roof and sidewall, not unreasonable notions for mafic and intermediate magmas, are utterly inadequate repositories for the complementary feldspar + quartz demanded by hundreds of cubic kilometers of low-Ba–Sr–Eu melt. That such mush reservoirs can persist in granitoid plutons without solidifying is demonstrated by great eruptions of monotonous intermediate ignimbrites with 40–60% crystals and volumes of 500–5000 km^3.

The view that a large rhyolitic magma chamber evolves by separation of crystals from a largely liquid parent appears to be backwards. Instead, hybrid intermediate mush predates separation of silicic melt from its interstices, and such separation may be a recurrent process extended over 10^4–10^6 years or more in large plutons. Rather than a

great body of melt gradually crystallizing, there may be a great body of crystal mush that incrementally loses melt to lenses (Fig. 18) that collect at the roof, even as the pluton continues to grow by incremental addition of hybrid magma batches from deeper in the crust. Rhyolitic roof zones or lenses may grow large by serial accumulation of expelled melt batches, which might either homogenize convectively or stack by density, or (as during the Glass Mountain to Bishop expansion) by amalgamation of many such nearby lenses (Hildreth, 2004).

Secular escape of interstitial melt would be favored by the great thickness (several km) of permeable granitoid mush (Fig. 18), by the concomitant pressure differential, by long-term maintenance of permeability by hot recharge batches, by CO_2-rich vapor rising from mafic recharge below, by reduced melt viscosity owing to water enrichment with progressive crystallization, and by tectonic extension. As crystallizing mush makes the transition (at ~55% crystals) into a rigidifying, permeable but deformable crust, the magma viscosity increases greatly but viscosity of the water-enriching interstitial melt decreases, thus becoming potentially more mobile in response to gravity, shearing flow, gas-driven filter pressing, or external deformation. Work by Scaillet *et al.* (1998) has shown the viscosity range of hydrous rhyolitic melt at 700–800°C to be lower (10^4–$10^{5\cdot5}$ Pa s) than previously supposed, supporting the feasibility of interstitial melt extraction on realistic timescales.

Percolation velocities in mush would be increased by (1) melt-enhanced embrittlement (Davidson *et al.*, 1994) in the rigid-sponge facies (Fig. 18), especially during thermally prograde pulses of mafic recharge that promote dilation, favoring formation of the gash veins and leucogranite dikes ubiquitous in granitoids; (2) deformation-induced compaction, shear, or liquefaction of the mush facies, promoted variously by earthquakes, subsiding stope-blocks, eruptive disturbances, or mafic recharge batches from below; and (3) diking in the mush induced by regional tectonic extension. Unlike initial partial melting, the permeability-connectivity in a plutonic reservoir is primary, the rigid sponge grading into mush and thence into melt-dominant suspension (Fig. 18). When advancing crystallization causes interstitial melt to reach gas saturation [as argued for the Bishop magma by Wallace *et al.* (1995, 1999)], then gas-driven filter-pressing would help expel still more melt upward (Sisson & Bacon, 1999), and the bubbles would enhance buoyancy and maintenance of a stable melt layer at the roof.

Following presentation by Hildreth of the rhyolitic mush model (Fig. 18) at a 2001 Penrose Conference on Rhyolitic Magma Systems (Hildreth, 2004), Bachmann & Bergantz (2004) undertook a physical analysis of timescales within which such melt extraction from mush would be feasible. For static mush, they found that some combination of compaction, micro-settling, and hindered settling (from dense mushy suspension) favors percolative expulsion rates of the order of 500 km^3 of rhyolitic melt in 10^4–10^5 years, even without considering the additional melt contribution from convecting mush implicit in schlieren. Such melt accumulation rates appear to be reasonable for Glass Mountain and the Bishop Tuff. The rates of such processes might vary widely, however, in response to at least two factors. First, the fluxes of magma and heat in and out of the mush zone control the amounts of melt generated and its evolution relative to the bulk composition, with lower flux rates favoring extreme evolution (e.g. early Glass Mountain). Second, extensional stresses or rift-related faulting may help disrupt the mush and create pathways for efficient melt extraction. In areas of unusually high heat flux and active rifting, such as the Taupo Volcanic Zone, rhyolite melt accumulation can attain rates of 10–40 km^3/kyr for periods of 1–40 kyr (Sutton *et al.*, 2000; Wilson *et al.*, 2006). For the Bishop rhyolite, accumulation of 650 km^3 in ~160 kyr (as suggested by the zircon ages) yields a longer-term average rate of ~4 km^3/kyr.

Such a model helps resolve various puzzles. (1) The fairly uncommon 'reversely zoned' ignimbrites may simply tap marginal mush first (Fig. 18). (2) Repeated eruptions of similar batches of highly evolved rhyolite from a single pluton-scale reservoir (e.g. Glass Mountain, Coso, Mono Craters, Yellowstone, or the Valles caldera) could reflect serial disturbances or rejuvenations of the mush by recharge, or simply enough time and gas to drain more melt upward into another eruptible lens (Fig. 18). (3) The problem of multicyclic high-silica ignimbrites and sets of high-silica rhyolite lava flows arising from postcaldera reservoirs is resolved by serial extraction from mush, obviating the need to penetrate cleanly (had they been independent batches newly arriving from depth) any unerupted lower-silica magma left behind in the first cycle. (4) The extensive age ranges of zircon populations identified in some ignimbrites could reflect freeze–thaw cycles and entrainment (of crystals too small to settle) during melt expulsion from long-lived mush (e.g. Charlier *et al.*, 2005). (5) The notion of 'discrete datable differentiation events' (if real) in highly evolved rhyolite magma, first developed for Glass Mountain (Halliday *et al.*, 1989; Mahood, 1990), is better understandable if melt batches were to separate rapidly into isolated lenses (Fig. 18). The apparent longevity and stagnation of such isochronous batches might be real, if several coexisting melt lenses were enveloped by the same protective mush and sponge of crystals, part of a pluton-scale reservoir that buffered a near-steady heat flux, insulating the lenses both thermally and from physical recharge disturbances. (6) If large silicic magma chambers consist of mush and sponge most of the time, this may help account for the difficulty in imaging them seismically.

Trace-element distinctions between successively erupted batches of rhyolite from the same reservoir would be produced by changing accessory-mineral concentrations (e.g. zircon, apatite, monazite, allanite, chevkinite, perrierite, sphene, britholite) in the crystallizing source mush, with or without recharge effects. Such distinctions have misled some into conjuring up enormous new batches of alien rhyolite from deep sources instead of from the mushy reservoir intimately below. As a mush–sponge continuum (Fig. 18) advances from 40% to 95% crystals over a final cooling interval of only 20–30°C, the accessory mineral suites and thus the trace-element ratios (including Zr, Hf, Nb, Ta, Th, U, Sc, Y, and REE) of successive melt-escape batches would change drastically. A dozen or more phases might be resident in the crystallizing mush zone, and their relative contributions to trace-element partitioning into any particular melt-escape batch would vary with time, temperature, and recharge. Interstitially within the mush–sponge continuum (Fig. 18), a wide range of the potential liquid line would be present simultaneously, so the composition of any particular rhyolitic melt batch escaping should depend upon its location in the crystallinity gradient, the accessory phase assemblage, and the dynamics of extraction. Concurrently, over that wide crystallization interval, the dominant quartz–sanidine–plagioclase assemblage would buffer major-element composition within a limited range, while melt–feldspar partitioning yielded large ranges in concentrations of strongly compatible Ba, Sr, and Eu.

If melt batches extracted from the mush first segregated into veins and dikes, there need be little entrainment of major crystals from the mush into overlying melt-rich zones. A plume of buoyant melt escaping the mush might then rise through any pre-existing zones of crystal-poor rhyolitic melt in a laminar regime (at low Reynolds number) owing to small density difference and similar viscosity, thereby entraining little of the magma penetrated and ultimately spreading out at its level of neutral buoyancy, augmenting the zoned column. Serial batch escape may reconcile gradients with layering, as stepwise convective stratification (Fridrich & Mahood, 1987) might be favored temporarily, particularly if newly inserted melt layers were initially aphyric, crystallizing and exchanging or mixing with neighboring layers only rather slowly.

Physical evidence for rhyolitic melt extraction from granitoid mush is preserved in many plutons, most abundantly as leucogranite veins and dikes, some of which connect with melt pockets that grade nebulously into the host matrix. Granitoid schlieren—streaks and thin layers of melt-depleted mush, enriched in mafic crystals, typically in fascicles (1–15 m long) with internal branching and truncations, and commonly oriented steeply near the pluton walls—provide ubiquitous evidence for shearing suspension flow and crystal–melt fractionation in mushy slurries (e.g. Barrière, 1981). More internal to plutons but less commonly preserved are such melt-ascent structures as spoon-shaped schlieren, vortices, and diapiric upwellings shelled by schlieren (e.g. Weinberg *et al.*, 2001), evidence for localized (1–10 m) buoyant instabilities in ductile permeable mush. Upwellings in mush could be either compositionally driven (especially after gas saturation) or thermally driven by nearby recharge. Such features add to the evidence that much differentiation is driven internally, not dominantly by crystallization at the roof or walls. Locked-in only by ultimate consolidation of the mush, countless earlier generations of such melt extraction and ascent structures are likely to have been blurred or obliterated by convective stirring.

If ascending melt is extracted from mush variously by shear flowage, vein–dike networks, and upwellings that leave behind heterogeneous schlieren-residues, the implicit varieties of residual mode and melt composition may account for some of the messiness of the Bishop zonation; that is, its general departure from narrow linear compositional arrays (Figs 9–14). Moreover, melt batches may find their level of neutral buoyancy in the zoned rhyolitic reservoir principally on the basis of respective water contents (dissolved and as bubbles), and (if so) this suggests that the most evolved melt plumes should be the richest in water, rise farthest, have the longest ascent path through the magma body, and thus have the greatest opportunity for entraining suspended crystals from the column penetrated. In detail, the compositional variety of batches may depend on the mechanics of melt–mush segregation and the amount of crystal entrainment during melt extraction and ascent during each upwelling. Modest entrainment of mush crystals into overlying melt zones may well account for sparse Bishop antecrysts and for some of the compositional variability of melt inclusions in Bishop phenocrysts.

Why is mush not more often erupted? Many great eruptions are zoned from crystal-poor to crystal-rich, but the crystal-richest pumice released seldom has more than 25–35% phenocrysts. Even such abundant phenocrysts appear to have been in suspension because they are typically solitary (as in the Bishop Tuff), not clustered or intergrown. Less common examples exist, however, where true mushes of 40–55% clustered crystals were ejected following withdrawal of crystal-poor rhyolite, as at Novarupta in 1912 (Hildreth & Fierstein, 2000); and the last part of the caldera-forming Mazama (Crater Lake) eruption (7·7 ka) even ejected fragments of melt-bearing rigid sponge (Fig. 18) consisting of 60–70% crystals (Bacon & Druitt, 1988). Marsh (1996, 2000) discussed a rheological transition at ~25% crystals from viscous fluid suspension to crystal-laden mush (25–55% crystals) that has much greater viscosity owing to mutual crystal interference. Smith's (1979) 'viscosity barrier' may express such a transition or discontinuity in magma viscosity,

providing a crystal-rich viscous closer for many pyroclastic eruptions. The less common ignimbrite-forming events that advance still further to withdraw some of the truly crystal-choked mush and/or rigid sponge may additionally reflect the dynamics of roof collapse.

Incremental heterogeneous zonation of the Bishop magma

As the magmatic line leading to the Bishop Tuff included major crustal contributions and because crustal rocks around Long Valley are very heterogeneous in $\delta^{18}O$ (+2 to +29), the oxygen-isotope homogeneity of the entire main Bishop suite [$\delta^{18}O$ (magma) $= 7{\cdot}80 \pm 0{\cdot}05$; Bindeman & Valley, 2002] requires homogenization at some stage. Although Bindeman & Valley (2002) favored meter-scale homogenization by convective mixing of the entire chamber volume erupted, any such putative process would need to have preceded development of the gradients in bulk composition, crystallinity, T–fO_2, and in compositions of melt and phenocrysts. Moreover, their appeal to sidewall crystallization as the driving force for convective homogenization appears to conflict with their evocation of assimilation and isotopic exchange at the sidewalls. For a large chamber, sidewall mechanisms are unlikely to dominate, as discussed above in the section 'Site of crystallization'. More likely, the isotopic homogenization of Bishop O (and Pb and Nd) took place in the subjacent reservoir of crystal mush prior to extraction of the melt volume erupted.

The compositional and thermal gradients documented, attended by little mixing or zoning of crystals, can be explained straightforwardly by the model of secular upward accumulation of nearly aphyric melt. As melt increments escaped the mush reservoir, carrying varied amounts of gas (derived in part from crystallization of recharge batches in the invasive root zone beneath the mush), each would rise to its own appropriate level in the magmatic density gradient. There might be a tendency for more gas-enriched interstitial melt increments to be compositionally more evolved and thus to ascend to shallower levels of the accumulating melt body (Fig. 18). Owing to the thermal gradient, transient layered convection might ensue at each such level, but bubble ascent and interface exchange should combine to damp the convection and smooth the compositional gradient with time.

The quartz + feldspar-dominated mush body, many kilometers thick in the mature system, would have been largely homogenized (as observed for many large granitoid plutons) by convective mixing, repeatedly during long-lived piecemeal accumulation, as each batch ascending a mid-crustal mush column attained vapor saturation on reaching the upper crust, then crystallized extensively and liberated derivative melt and a gas phase into the mushy pluton-scale chamber under construction. Growth of a crystal-poor gas-saturated capping melt lens would thus accompany volumetrically greater growth of its parental mushy reservoir, and evolution of the compositional gradients within the melt lens would be an incremental secular process, largely internal to the mush–melt chamber. Variants specific to the Bishop system would include (1) growth of thin rims on Ig2 quartz and sanidine, associated with injection of the lower part of the melt-dominant domain by late batches of (lower-silica) rhyolitic melt enriched in Ba, Sr, Ti, and CO_2 (reflecting contributions derivative from still deeper mafic recharge) that also produced the dark and swirly pumice; and (2) development of the Sr-isotopic gradient, probably by slight roof-rock contamination of the low-Sr crystal-poor roof-zone melt (and perhaps also to some degree by secular ingrowth of ^{87}Sr in high-Rb/Sr melt). Both developments postdated establishment of the system-wide Bishop zonation.

Upward accumulation of melt extracted piecemeal from granitic mush is thus thought to have been the dominant process leading to zoning in the Bishop high-silica rhyolite magma chamber, but varied evidence suggests subordinate roles for concurrent or ensuing processes: (1) recharge; (2) roof contamination; (3) bubble ascent; (4) weak crystal–melt fractionation after melt/mush separation.

(1) For the Bishop, the influence of mafic recharge may have begun about 1 Ma with a major thermal pulse that partially remelted pre-Bishop (3·5–1·0 Ma) felsic intrusives, contributed to expansion and amalgamation of the silicic reservoir (Fig. 18), resorbed all the older zircons, and promoted convective homogenization prior to evolution of the zoning. Subsequently, mafic batches might have lodged beneath or spread as sills within the mush pile (Sisson *et al.*, 1996; Wiebe, 1996; Fig. 18). There is no evidence in the Bishop Tuff, however, for mafic recharge reaching the melt-dominant body itself, a process that could have convectively disrupted the rhyolite zoning (see Wilson *et al.*, 2006). Intrusion and crystallization of mafic batches beneath or within the mush pile should nonetheless contribute (a) their own derivative (Ba + Ti-enriched) melt and CO_2-rich gas, (b) expulsion of buoyant melt and gas from resident mush, (c) thermal pulses that induce local upwellings and transient marginal (near-eutectic) resorption of quartz and feldspar crystals, and (d) subsequent overgrowths on such crystals as a result of gradual reduction of H_2O activity in magma affected by CO_2 addition. The contributions of numerous mafic recharge batches during a chamber lifetime as long as 100 kyr could be profound.

Evidence is preserved for one or more such recharge batches not long before the Bishop eruption, represented by the higher-temperature (>800°C) lower-silica rhyolite that produced the swirly and dark pumices.

Enrichment in Ba, Sr, and Ti (and presumably CO_2) implicates basaltic recharge in the hybrid parentage of such rhyolite deeper in the mush pile. [Long Valley basalts generally have 1000–1500 ppm Ba and dacites 1400–1900 ppm (Cousens, 1996; Bailey, 2004).] Infusion of such magma accounts well for Ba-rich rims on sanidine, Ti-enriched rims on quartz, and the elevated Ba and CO_2 of late-entrapped MI in Ig2 phenocrysts, all of which were in magma at the deepest level withdrawn during the eruption. It may be no accident that the parts of Ig2 where such late overgrowths are common vented along the northerly segments of the ring-fault zone, adjacent to areas with a history of precaldera basaltic and dacitic volcanism. Continuing microbeam research to resolve the significance of repeated truncations of successive growth zones within Bishop quartz and sanidine crystals and of wide ranges in Ba concentration and thickness of the Ba-rich overgrowths on many late-erupted Ig2NW and Ig2N sanidines may eventually provide a clearer record and better understanding of secular recharge.

(2) Although roof contamination appears to have made at most a trivial contribution to the compositional zonation (Hildreth, 1977, 1979, 1981), modest Sr-isotopic effects have been identified in the Sr-impoverished magma thought to have been close to the chamber roof (see discussion of antecrysts, xenocrysts, and isotopic exchange in the section 'Residence time of Bishop magma'). Clearly not present, however, are polycrystalline clots (like those common in intermediate magmas) that might provide evidence for a crystallizing rind (solidification front) at the roof or upper walls.

(3) Bubble ascent from crystallizing zones of gas-saturated mush and recharge batches might have contributed to zoning of water, halogens, and such metals as Li, Be, B, Na, As, Mo, Sn, W, or U. Perhaps volatile complexing was also involved in the roofward enrichment of Sc and Mn, as in many pegmatites. Extraordinary enrichment of some Bishop biotites in Cs and Rb (Hildreth, 1977) might reflect interaction with a fluid phase before, during, or after eruption. Buoyant gas-rich upwellings or dikes escaping from crystallizing mush and mixing into overlying melt-dominant zones might entrain a few crystals, contaminating the phenocryst gradients already in suspension and introducing some disorder to sequences of MI entrapped in growing crystals.

(4) Weak internal crystal–melt fractionation (within the melt-dominant zones erupted), though not important enough to destroy overall zoning of the chamber, might account for some of the compositional scatter evident in Figures 9–14. This could involve at least four processes other than conventional crystal settling: (a) entrainment and sorting of crystals from floor mush or sidewall rinds by rising melt plumes; (b) mixing of crystals from various levels or layers of the zoned column when penetrated by melt plumes rising to and spreading out at their level of neutral buoyancy; (c) transient formation of schlieren or lenses relatively enriched or impoverished in suspended phenocrysts during convective flow; or (d) exchange of crystals across interfaces during layered convection. Although not overwhelming the gross zonation built by incremental accumulation, such effects could promote local departure from tight compositional arrays and might oblige some growing phenocrysts to bathe successively in a range of rhyolitic host melts, thereby producing unsystematic compositional sequences of MI trapped within them.

CONCLUSIONS

The Bishop Tuff was produced during a 6 day caldera-forming eruption that was the culmination of 4 Myr of activity in the Long Valley area. At least 600 km^3 of magma was ejected, forming a widespread fall deposit, ignimbrite outflow sheets, and intracaldera tuff with approximate bulk volumes of 250, 200, and 340 km^3, respectively.

The Bishop Tuff contains two broad groups of pumice. The first is a volumetrically dominant (>90%) main suite of 'normal' pumices that ranges from <1 to ~24 wt % crystals and defines a zoned rhyolitic array in which composition correlates roughly with FeTi-oxide temperature (714–818°C). Variation in major and trace elements among normal pumices correlates rather poorly with crystal content, supporting evidence from mineral data that the compositional zonation was established prior to crystallization of the phenocrysts erupted. The second, subordinate group includes several variant pumices distinguished by texture, color, and crystal content. Although also mostly rhyolitic, many such pumice clasts have elevated contents of Ba, Sr, and Ti that overlap but extend the ranges of the main-suite pumice. Batches of magma that yielded the variant swirly and dark pumices invaded the dominant (already-zoned) magma body shortly before the climactic eruption. Such material is mingled with main-suite pumice (as bands and blebs) throughout much of the eruptive sequence, but the main compositional effects attributable to the late injections are thin rims on sanidine and quartz and modest heating of resident magma in the deeper (Ig2) domains most strongly invaded.

Compositional diversity was marked at all stages of magma withdrawal and was greatest in the Ig2E packages, in which pumices span virtually the whole range of compositions found. The Bishop eruptive sequence nonetheless displays consistent overall trends toward greater proportions of less evolved pumice, more crystals, and higher FeTi-oxide temperatures. New field data indicate that the Ig2E packages were erupted in part coevally with the

northern ignimbrite packages and with an extended period of F9 fall deposition. Contrasts between pumice proportions emplaced north and east of the caldera during later parts of the F9/Ig2 interval thus indicate concurrent tapping of multiple domains or depths of a unitary magma body by separate vent segments along the ring-fault system.

The zoned magma that erupted to form the main-suite pumices amounted to roughly 600 km^3. It started to assemble around 1 Ma by extraction of rhyolitic melts from an expanding granitoid mush body that had been accumulating piecemeal during the long interval of Glass Mountain rhyolitic eruptions. Accumulation and zonation of the melt-dominant body of Bishop rhyolite was mature (if not complete) by ~850 ka, as inferred from zircon age spectra (Simon & Reid, 2005) and phenocryst compositional spectra (Hildreth, 1977). The earlier conclusion that melt was assembled and zoned before the observed phenocrysts had crystallized is reinforced by our new data. The compositional zonation defined by the main pumice array primarily reflects secular crystal–melt fractionation in the granitoid mush system beneath the accumulating rhyolitic melt body, but not to any significant extent at the walls or roof of the rhyolite chamber. Crystal–liquid separation took place as rhyolitic interstitial liquids were expelled batchwise from the mush zone.

ACKNOWLEDGEMENTS

A preliminary version of this work was presented orally as the opening keynote lecture at a Penrose Conference on rhyolitic magmatism held at Long Valley caldera in 2001. The manuscript was reviewed by Charlie Bacon, Chris Fridrich, Paul Wallace, and Ken Wohletz at a level of detailed scrutiny for which we are thoroughly grateful. John Wolff, Dan Morgan and an anonymous reviewer are thanked for thoughtful journal reviews, and Gareth Davies for careful editing and for originally inviting the contribution. Peggy Bruggman and the late Dave Siems produced the XRF data, attending meticulously to continuity of methods and standardization in USGS laboratories over the course of many years. Judy Fierstein accomplished most of the new electron-probe analyses of FeTi-oxide pairs and enhanced the quality of the diagrams. Fred Anderson, whose 15 years of stimulating dialogue exposed us to a third way of thinking about nature, contributed challenging, constructive, and friendly contrasts of perspective that helped hone the synthesis at hand. W.H. also thanks the numerous other colleagues who took up the challenge of the Bishop Tuff and contributed to our growing understanding, especially Ken Cameron, Nelia Dunbar, Alex Halliday, Calvin Miller, Peter Michael, Mary Reid, Bruno Scaillet, Paul Wallace, and Dave Wark. C.J.N.W. acknowledges support from the UK Natural Environment Research Council, the Royal Society of London, and the NZ Foundation for Research, Science & Technology. Along the braided stream of academic influence, our intellectual debts to I. S. E. Carmichael and the late G. P. L. Walker are truly immeasurable. We hope that each was amused and pleased at our collaborative confluence.

SUPPLEMENTARY DATA

Supplementary data for this paper are available at *Journal of Petrology* online.

REFERENCES

Andersen, D. J. & Lindsley, D. H. (1988). Internally consistent solution models for Fe–Mg–Mn–Ti oxides: Fe–Ti oxides. *American Mineralogist* **73**, 714–726.

Anderson, A. T., Jr (1991). Hourglass inclusions: theory and application to the Bishop rhyolitic tuff. *American Mineralogist* **76**, 530–547.

Anderson, A. T., Jr, Newman, S., Williams, S. N., Druitt, T. H., Skirius, C. & Stolper, E. (1989). H_2O, CO_2, Cl, and gas in Plinian and ash-flow Bishop rhyolite. *Geology* **17**, 221–225.

Anderson, A. T., Jr, Davis, A. M. & Lu, F. (2000). Evolution of Bishop Tuff rhyolitic magma based on melt and magnetite inclusions and zoned phenocrysts. *Journal of Petrology* **41**, 449–473.

Annen, C. & Sparks, R. S. J. (2002). Effects of repetitive emplacement of basaltic intrusions on thermal evolution and melt generation in the crust. *Earth and Planetary Science Letters* **203**, 937–955.

Bachmann, O. & Bergantz, G. W. (2004). On the origin of crystal-poor rhyolites: extracted from batholithic crystal mushes. *Journal of Petrology* **45**, 1565–1582.

Bachmann, O., Dungan, M. A. & Lipman, P. W. (2002). The Fish Canyon magma body, San Juan volcanic field, Colorado: rejuvenation and eruption of an upper crustal batholith. *Journal of Petrology* **43**, 1469–1503.

Bacon, C. R. & Druitt, T. H. (1988). Compositional evolution of the zoned calcalkaline magma chamber of Mount Mazama, Crater Lake, Oregon. *Contributions to Mineralogy and Petrology* **98**, 224–256.

Bacon, C. R. & Hirschmann, M. M. (1988). Mg/Mn partitioning as a test for equilibrium between coexisting Fe–Ti oxides. *American Mineralogist* **73**, 57–61.

Baedecker, P. A. (1987). *Methods for geochemical analysis. US Geological Survey Bulletin* **1770**, 132 pp.

Bailey, R. A. (1989). Geologic map of the Long Valley caldera, Mono–Inyo Craters volcanic chain, and vicinity, eastern California. *US Geological Survey Map* **I-1933**, scale 1:62 500.

Bailey, R. A. (2004). *Eruptive history and chemical evolution of the precaldera and postcaldera basalt–dacite sequences, Long Valley, California: implications for magma sources, current seismic unrest, and future volcanism. US Geological Survey, Professional Papers* **1692**, 75 pp.

Bailey, R. A., Dalrymple, G. B. & Lanphere, M. A. (1976). Volcanism, structure, and geochronology of Long Valley caldera, Mono County, California. *Journal of Geophysical Research* **81**, 725–744.

Barrière, M. (1981). On curved laminae, graded layers, convection currents and dynamic crystal sorting in the Ploumanac'h (Brittany) subalkaline granite. *Contributions to Mineralogy and Petrology* **77**, 214–224.

Bateman, P. C. (1965). *Geology and tungsten mineralization of the Bishop district, California. US Geological Survey, Professional Papers* **470**, 208 pp.

Beard, J. S. & Lofgren, G. E. (1991). Dehydration melting and water-saturated melting of basaltic and andesitic greenstones and amphibolites at 1, 3, and 6·9 kb. *Journal of Petrology* **32**, 365–401.

Beard, J. S., Abitz, R. J. & Lofgren, G. E. (1993). Experimental melting of crustal xenoliths from Kilbourne Hole, New Mexico, and implications for the contamination and genesis of magmas. *Contributions to Mineralogy and Petrology* **115**, 88–102.

Best, M. G., Christiansen, E. H., Deino, A. L., Grommé, C. S., McKee, E. H. & Noble, D. C. (1989). Eocene through Miocene volcanism in the Great Basin of the western United States. *New Mexico Bureau of Mines and Mineral Resources, Memoir* **47**, 91–133.

Bindeman, I. N. & Valley, J. W. (2002). Oxygen isotope study of the Long Valley magma system, California: isotope thermometry and convection in large silicic magma bodies. *Contributions to Mineralogy and Petrology* **144**, 185–205.

Boden, D. R. (1989). Evidence for step-function zoning of magma and eruptive dynamics, Toquima caldera complex, Nevada. *Journal of Volcanology and Geothermal Research* **37**, 39–57.

Buddington, A. F. & Lindsley, D. H. (1964). Iron–titanium oxide minerals and synthetic equivalents. *Journal of Petrology* **5**, 310–357.

Cameron, K. L. (1984). Bishop Tuff revisited: new rare earth element data consistent with crystal fractionation. *Science* **224**, 1339–1340.

Carle, S. F. (1988). Three-dimensional gravity modeling of the geologic structure of Long Valley caldera. *Journal of Geophysical Research* **93**, 13237–13250.

Carroll, M. R. & Wyllie, P. J. (1990). The system tonalite–H_2O at 15 kbar and the genesis of calc-alkaline magmas. *American Mineralogist* **75**, 345–357.

Charlier, B. L. A., Wilson, C. J. N., Lowenstern, J. B., Blake, S., van Calsteren, P. W. & Davidson, J. P. (2005). Magma generation at a large hyperactive silicic volcano (Taupo, New Zealand) revealed by U–Th and U–Pb systematics in zircons. *Journal of Petrology* **46**, 3–32.

Chiba, H., Chacko, T., Clayton, R. N. & Goldsmith, J. R. (1989). Oxygen isotope fractionations involving diopside, forsterite, magnetite, and calcite—application to geothermometry. *Geochimica et Cosmochimica Acta* **53**, 2985–2995.

Christensen, J. N. & DePaolo, D. J. (1993). Timescale of large volume silicic magma systems: Sr isotopic systematics of phenocrysts and glass from the Bishop Tuff, Long Valley, California. *Contributions to Mineralogy and Petrology* **113**, 100–114.

Christensen, J. N. & Halliday, A. N. (1996). Rb–Sr ages and Nd isotopic compositions of melt inclusions from the Bishop Tuff and the generation of silicic magma. *Earth and Planetary Science Letters* **144**, 547–561.

Conrad, W. K., Nicholls, I. A. & Wall, V. J. (1988). Water-saturated and -undersaturated melting of metaluminous and peraluminous crustal compositions at 10 kb: evidence for the origin of silicic magmas in the Taupo Volcanic Zone, New Zealand, and other occurrences. *Journal of Petrology* **29**, 765–803.

Couch, S., Sparks, R. S. J. & Carroll, M. R. (2001). Mineral disequilibrium in lavas explained by convective self-mixing in open magma chambers. *Nature* **411**, 1037–1039.

Cousens, B. L. (1996). Magmatic evolution of Quaternary mafic magmas at Long Valley caldera and Devils Postpile, California: effects of crustal contamination on lithospheric mantle-derived magmas. *Journal of Geophysical Research* **101**, 27673–27689.

Davidson, C., Schmid, S. M. & Hollister, L. S. (1994). Role of melt during deformation in the deep crust. *Terra Nova* **6**, 133–142.

Davies, G. R. & Halliday, A. N. (1998). Development of the Long Valley rhyolitic magma system: strontium and neodymium isotope evidence from glasses and individual phenocrysts. *Geochimica et Cosmochimica Acta* **62**, 3561–3574.

Davies, G. R., Halliday, A. N., Mahood, G. A. & Hall, C. M. (1994). Isotopic constraints on the production rates, crystallization histories and residence times of precaldera silicic magmas, Long Valley, California. *Earth and Planetary Science Letters* **125**, 17–37.

Duffield, W. A., Ruiz, J. & Webster, J. D. (1995). Roof-rock contamination of magma along the top of the reservoir for the Bishop Tuff. *Journal of Volcanology and Geothermal Research* **69**, 187–195.

Dunbar, N. W. & Hervig, R. L. (1992). Petrogenesis and volatile stratigraphy of the Bishop Tuff: evidence from melt inclusion analysis. *Journal of Geophysical Research* **97**, 15129–15150.

Fierstein, J. & Nathenson, M. (1992). Another look at the calculation of fallout tephra volumes. *Bulletin of Volcanology* **54**, 156–167.

Fridrich, C. J. & Mahood, G. A. (1987). Compositional layers in the zoned magma chamber of the Grizzly Peak Tuff. *Geology* **15**, 299–303.

Frost, B. R. & Lindsley, D. H. (1992). Equilibria among Fe–Ti oxides, pyroxenes, olivine, and quartz. Part II. Application. *American Mineralogist* **77**, 1004–1020.

Gardner, J. E., Sigurdsson, H. & Carey, S. N. (1991). Eruption dynamics and magma withdrawal during the plinian phase of the Bishop Tuff eruption, Long Valley caldera. *Journal of Geophysical Research* **96**, 8097–8111.

Ghiorso, M. S. & Sack, R. O. (1991). Fe–Ti oxide geothermometry: thermodynamic formulation and the estimation of intensive variables in silicic magmas. *Contributions to Mineralogy and Petrology* **108**, 485–510.

Gilbert, C. M. (1938). Welded tuff in eastern California. *Geological Society of America Bulletin* **49**, 1829–1862.

Goff, F., Wollenberg, H. A., Brookins, D. C. & Kistler, R. W. (1991). A Sr-isotopic comparison between thermal waters, rocks, and hydrothermal calcites, Long Valley caldera, California. *Journal of Volcanology and Geothermal Research* **48**, 265–281.

Halliday, A. N., Fallick, A. E., Hutchinson, J. & Hildreth, W. (1984). A Nd, Sr, and O isotopic investigation into the causes of chemical and isotopic zonation in the Bishop Tuff, California. *Earth and Planetary Science Letters* **68**, 379–391.

Halliday, A. N., Mahood, G. A., Holden, P., Metz, J. M., Dempster, T. J. & Davidson, J. P. (1989). Evidence for long residence times of rhyolitic magma in the Long Valley magmatic system: the isotopic record in precaldera lavas of Glass Mountain. *Earth and Planetary Science Letters* **94**, 274–290.

Helz, R. T. (1976). Phase relations of basalts in their melting ranges at $P_{H2O} = 5$ kb. Part II. Melt compositions. *Journal of Petrology* **17**, 139–193.

Hildreth, E. W. (1977). The magma chamber of the Bishop Tuff: gradients in temperature, pressure, and composition. Ph.D. thesis, University of California, Berkeley.

Hildreth, W. (1979). The Bishop Tuff: evidence for the origin of compositional zonation in silicic magma chambers. In: Chapin, C.E. & Elston, W. E. (eds) *Ash-flow tuffs. Geological Society of America, Special Paper* **180**, 43–75.

Hildreth, W. (1981). Gradients in silicic magma chambers: implications for lithospheric magmatism. *Journal of Geophysical Research* **86**, 10153–10192.

Hildreth, W. (1983). Comment on: 'Chemical differentiation of the Bishop Tuff and other high-silica magmas through crystallization processes'. *Geology* **11**, 622–623.

Hildreth, W. (1985). The Bishop Tuff: trace contents of dark pumice. *Geological Society of America, Abstracts with Programs* **17**, 361.

Hildreth, W. (2004). Volcanological perspectives on Long Valley, Mammoth Mountain, and Mono Craters: several contiguous but discrete systems. *Journal of Volcanology and Geothermal Research* **136**, 169–198.

Hildreth, W. & Fierstein, J. (2000). Katmai volcanic cluster and the great eruption of 1912. *Geological Society of America Bulletin* **112**, 1594–1620.

Hildreth, W. & Mahood, G. A. (1986). Ring-fracture eruption of the Bishop Tuff. *Geological Society of America Bulletin* **97**, 396–403.

Hildreth, W. & Moorbath, S. (1988). Crustal contributions to arc magmatism in the Andes of central Chile. *Contributions to Mineralogy and Petrology* **98**, 455–489.

Hildreth, W., Christiansen, R. L. & O'Neil, J. R. (1984). Catastrophic isotopic modification of rhyolitic magma at times of caldera subsidence, Yellowstone Plateau volcanic field. *Journal of Geophysical Research* **89**, 8339–8369.

Hildreth, W., Halliday, A. N. & Christiansen, R. L. (1991). Isotopic and chemical evidence concerning the genesis and contamination of basaltic and rhyolitic magma beneath the Yellowstone Plateau volcanic field. *Journal of Petrology* **32**, 63–138.

Hill, D. P. (1976). Structure of Long Valley caldera, California, from a seismic refraction experiment. *Journal of Geophysical Research* **81**, 745–753.

Hill, D. P., Kissling, E., Luetgert, J. H. & Kradolfer, U. (1985). Constraints on the upper crustal structure of the Long Valley–Mono Craters volcanic complex, eastern California, from seismic refraction measurements. *Journal of Geophysical Research* **90**, 11135–11150.

Hill, D. P., Dzurisin, D., Ellsworth, W. L., Endo, E. T., Galloway, D. L., Gerlach, T. M., Johnston, M. J. S., Langbein, J., McGee, K. A., Miller, C. D., Oppenheimer, D. & Sorey, M. L. (2002). *Response plan for volcano hazards in the Long Valley caldera and Mono Craters region, California. US Geological Survey Bulletin* **2185**, 57 pp.

Huebner, J. S. & Sato, M. (1970). The oxygen fugacity–temperature relationships of manganese oxide and nickel oxide buffers. *American Mineralogist* **55**, 934–952.

Hughes, R. E. (1993). Trace element geochemistry of volcanic glass from the Obsidian Cliffs flow, Three Sisters Wilderness, Oregon. *Northwest Science* **67**, 199–207.

Hurley, P. M., Bateman, P. C., Fairbairn, H. W. & Pinson, W. H., Jr (1965). Investigation of initial $^{87}Sr/^{86}Sr$ ratios in the Sierra Nevada plutonic province. *Geological Society of America Bulletin* **76**, 165–174.

Izett, G. A., Obradovich, J. D. & Mehnert, H. H. (1988). *The Bishop Ash Bed (middle Pleistocene) and some older (Pliocene and Pleistocene) chemically and mineralogically similar ash beds in California, Nevada, and Utah. US Geological Survey Bulletin* **1675**, 37 pp.

Jackson, E. D. (1961). *Primary textures and mineral associations in the ultramafic zone of the Stillwater Complex, Montana. US Geological Survey, Professional Papers* **358**, 106 pp.

Johnson, C. M. (1991). Large-scale crust formation and lithosphere modification beneath middle to late Cenozoic calderas and volcanic fields, western North America. *Journal of Geophysical Research* **96**, 13485–13507.

Johnson, M. C. & Rutherford, M. J. (1989). Experimentally determined conditions in the Fish Canyon Tuff, Colorado, magma chamber. *Journal of Petrology* **30**, 711–737.

Kane, M. F., Mabey, D. R. & Brace, R. L. (1976). Gravity and magnetic investigation of the Long Valley caldera, Mono County, California. *Journal of Geophysical Research* **81**, 754–762.

Lachenbruch, A. H., Sass, J. H., Munroe, R. J. & Moses, T. H., Jr (1976). Geothermal setting and simple heat conduction models for the Long Valley caldera. *Journal of Geophysical Research* **81**, 769–784.

Lesher, C. E. (1986). Effects of silicate liquid composition on mineral–liquid element partitioning from Soret diffusion studies. *Journal of Geophysical Research* **91**, 6123–6141.

Lipman, P. W. (1965). Chemical comparison of glassy and crystalline volcanic rocks. US Geological Survey Bulletin **1201-D**, 24 pp.

Lipman, P. W. (2000). Central San Juan caldera cluster: regional volcanic framework. In: Bethke, P. M. & Hay, R. L. (eds) *Ancient Lake Creede: its volcano-tectonic setting, history of sedimentation, and relation to mineralization in the Creede mining district. Geological Society of America, Special Paper* **346**, 9–69.

Lipman, P. W., Christiansen, R. L. & O'Connor, J. T. (1966). *A compositionally zoned ash-flow sheet in southern Nevada. US Geological Survey, Professional Papers* **524-F**, 47 pp.

Lu, F. (1991). The Bishop Tuff: origins of the high-silica rhyolite and its thermal and compositional zonations. Ph.D. thesis, University of Chicago.

Lu, F., Anderson, A. T., Jr & Davis, A. M. (1992). Melt inclusions and crystal–liquid separation in rhyolitic magma of the Bishop Tuff. *Contributions to Mineralogy and Petrology* **110**, 113–120.

Mahood, G. A. (1990). Second reply to comment of R. S. J. Sparks, H. E. Huppert, and C. J. N. Wilson on: 'Evidence for long residence times of rhyolitic magma in the Long Valley magmatic system: the isotopic record in the precaldera lavas of Glass Mountain'. *Earth and Planetary Science Letters* **99**, 395–399.

Mahood, G. A. & Halliday, A. N. (1988). Generation of high-silica rhyolite: a Nd, Sr, and O isotopic study of Sierra La Primavera, Mexican Neovolcanic Belt. *Contributions to Mineralogy and Petrology* **100**, 183–191.

Marsh, B. D. (1996). Solidification fronts and magmatic evolution. *Mineralogical Magazine* **60**, 5–40.

Marsh, B. D. (2000). Magma chambers. In: Sigurdsson, H., Houghton, B. F., McNutt, S., Rymer, H. & Stix, J. (eds) *Encyclopedia of Volcanoes*. San Diego and London: Academic Press, pp. 191–206.

McCarthy, T. S. & Fripp, R. E. P. (1980). The crystallization history of a granitic magma, as revealed by trace element abundances. *Journal of Geology* **88**, 211–224.

McCarthy, T. S. & Groves, D. I. (1979). The Blue Tier batholith, northeastern Tasmania. *Contributions to Mineralogy and Petrology* **71**, 193–209.

McConnell, V. S., Shearer, C. K., Eichelberger, J. C., Keskinen, M. J., Layer, P. W. & Papike, J. J. (1995). Rhyolite intrusions in the intracaldera Bishop Tuff, Long Valley caldera, California. *Journal of Volcanology and Geothermal Research* **67**, 41–60.

Metz, J. M. (1987). Physical and chemical evolution of Glass Mountain: precaldera high-silica rhyolites from the Long Valley magma system. Ph.D. thesis, Stanford University.

Metz, J. M. & Bailey, R. A. (1993). Geologic map of Glass Mountain, Mono County, California. *US Geological Survey Map* **1995**, scale 1:24 000.

Metz, J. M. & Mahood, G. A. (1985). Precursors to the Bishop Tuff eruption: Glass Mountain, Long Valley, California. *Journal of Geophysical Research* **90**, 11121–11126.

Metz, J. M. & Mahood, G. A. (1991). Development of the Long Valley, California, magma chamber recorded in precaldera rhyolite lavas of Glass Mountain. *Contributions to Mineralogy and Petrology* **106**, 379–397.

Michael, P. J. (1983). Chemical differentiation of the Bishop Tuff and other high-silica magmas through crystallization processes. *Geology* **11**, 31–34.

Michael, P. J. (1988). Partition coefficients for rare earth elements in mafic minerals of high silica rhyolites: the importance of accessory mineral inclusions. *Geochimica et Cosmochimica Acta* **52**, 275–282.

Miller, C. F. & Mittlefehldt, D. W. (1984). Extreme fractionation in felsic magma chambers: a product of liquid-state diffusion or fractional crystallization? *Earth and Planetary Science Letters* **68**, 151–158.

Myers, J. & Eugster, H. P. (1983). The system Fe–Si–O: oxygen buffer calibrations to 1500 K. *Contributions to Mineralogy and Petrology* **82**, 75–90.

Noble, D. C. (1967). Sodium, potassium, and ferrous iron contents of some secondarily hydrated natural silicic glasses. *American Mineralogist* **52**, 280–286.

Noble, D. C. & Hedge, C. E. (1969). Sr^{87}/Sr^{86} variations within individual ash-flow sheets. In: *Geological Survey Research 1969, Chapter C. US Geological Survey, Professional Paper* **650-C**, C133–C139.

Peppard, B. T., Steele, I. M., Davis, A. M., Wallace, P. J. & Anderson, A. T. (2001). Zoned quartz phenocrysts from the rhyolitic Bishop Tuff. *American Mineralogist* **86**, 1034–1052.

Perlman, I. & Asaro, F. (1969). Pottery analysis by neutron activation. *Archaeometry* **11**, 21–52.

Rapp, R. P. & Watson, E. B. (1995). Dehydration melting of metabasalt at 8–32 kbar: implications for continental growth and crust–mantle recycling. *Journal of Petrology* **36**, 891–931.

Reece, C., Ruiz, J., Duffield, W. A. & Patchett, P. J. (1990). Origin of Taylor Creek rhyolite magma, Black Range, New Mexico, based on Nd–Sr isotope studies. In: Stein, H. J. & Hannah, J. L. (eds) *Ore-bearing granite systems: petrogenesis and mineralizing processes. Geological Society of America, Special Paper* **246**, 263–273.

Reid, M. R. & Coath, C. D. (2000). In situ U–Pb ages of zircons from the Bishop Tuff: no evidence for long crystal residence times. *Geology* **28**, 443–446.

Roberts, M. P. & Clemens, J. D. (1993). Origin of high-potassium, calc-alkaline, I-type granitoids. *Geology* **21**, 825–828.

Rushmer, T. (1991). Partial melting of two amphibolites: contrasting experimental results under fluid-absent conditions. *Contributions to Mineralogy and Petrology* **107**, 41–59.

Sarna-Wojcicki, A. M., Reheis, M. C., Pringle, M. S., Fleck, R. J., Burbank, D., Meyer, C. E., Slate, J. L., Wan, E., Budahn, J. R., Troxel, B. & Walker, J. P. (2005). *Tephra layers of Blind Spring Valley and related upper Pliocene and Pleistocene tephra layers, California, Nevada, and Utah: isotopic ages, correlation, and magnetostratigraphy. US Geological Survey, Professional Papers* **1701**, 63 pp.

Scaillet, B. & Hildreth, W. (2001). Experimental constraints on the origin and evolution of the Bishop Tuff. In: Knesel, K., Bergantz, G. & Davidson, J. (convenors) *Geological Society of America Penrose Conference: Longevity and Dynamics of Rhyolitic Magma Systems*. Unpaginated volume of abstracts, 5 pp.

Scaillet, B., Holtz, F. & Pichavant, M. (1998). Phase equilibrium constraints on the viscosity of silicic magmas. *Journal of Geophysical Research* **103**, 27257–27266.

Sheridan, M. F. (1965). The mineralogy and petrology of the Bishop Tuff. Ph.D. thesis, Stanford University.

Sheridan, M. F. (1968). Double cooling-unit nature of the Bishop Tuff in Owens Gorge, California. In: *Abstracts for 1967. Geological Society of America, Special Paper* **115**, 351.

Sheridan, M. F. (1970). Fumarolic mounds and ridges of the Bishop Tuff, California. *Geological Society of America Bulletin* **81**, 851–868.

Siems, D. F. (2000). *The determination of 30 elements in geological materials by energy-dispersive X-ray fluorescence spectrometry. US Geological Survey, Open-File Report* **00-475**, 13 pp.

Simon, J. I. & Reid, M. R. (2005). The pace of rhyolite differentiation and storage in an 'archetypical' silicic magma system, Long Valley, California. *Earth and Planetary Science Letters* **235**, 123–140.

Simon, J. I., Reid, M. R. & Young, E. D. (2005). New isotopic measurements of zircon and feldspar constrain the magmatic evolution at Long Valley caldera. *Geochimica et Cosmochimica Acta* **69**, (10S, Goldschmidt Conference Abstracts), A234.

Sisson, T. W. & Bacon, C. R. (1999). Gas-driven filter pressing in magmas. *Geology* **27**, 613–616.

Sisson, T. W., Grove, T. L. & Coleman, D. S. (1996). Hornblende gabbro sill complex at Onion Valley, California, and a mixing origin for the Sierra Nevada batholith. *Contributions to Mineralogy and Petrology* **126**, 81–108.

Sisson, T. W., Ratajeski, K., Hankins, W. B. & Glazner, A. F. (2005). Voluminous granitic magmas from common basaltic sources. *Contributions to Mineralogy and Petrology* **148**, 635–661.

Skirius, C. M. (1990). Pre-eruptive H_2O and CO_2 content of plinian and ash-flow Bishop Tuff magma. Ph.D. thesis, University of Chicago.

Skjerlie, K. P. & Johnston, A. D. (1993). Fluid-absent melting behavior of an F-rich tonalitic gneiss at mid-crustal pressures: implications for the generation of anorogenic granites. *Journal of Petrology* **34**, 785–815.

Smith, R. L. (1979). Ash-flow magmatism. In: Chapin, C. E. & Elston, W. E. (eds) *Ash-flow tuffs. Geological Society of America, Special Paper* **180**, 5–27.

Snow, E. & Yund, R. A. (1985). Thermal history of a Bishop section as determined from the width of cryptoperthite lamellae. *Geology* **13**, 50–53.

Snow, E. & Yund, R. A. (1988). Origin of cryptoperthites in the Bishop Tuff and their bearing on its thermal history. *Journal of Geophysical Research* **93**, 8975–8984.

Sorey, M. L., Suemnicht, G. A., Sturchio, N. C. & Nordquist, G.A. (1991). New evidence on the hydrothermal system in Long Valley caldera, California, from wells, fluid sampling, electrical geophysics, and age determinations of hot-spring deposits. *Journal of Volcanology and Geothermal Research* **48**, 229–263.

Sparks, R. S. J., Huppert, H. E. & Turner, J. S. (1984). The fluid dynamics of evolving magma chambers. *Philosophical Transactions of the Royal Society of London, Series A* **310**, 511–534.

Sparks, R. S. J., Huppert, H. E. & Wilson, C. J. N. (1990). Comment on: 'Evidence for long residence times of rhyolitic magma in the Long Valley magmatic system: the isotopic record in precaldera lavas of Glass Mountain', by A. N. Halliday, G. A. Mahood, P. Holden, J. M. Metz, T. J. Dempster & J. P. Davidson. *Earth and Planetary Science Letters* **99**, 387–389.

Streck, M. J. & Grunder, A. L. (1997). Compositional gradients and gaps in high-silica rhyolites of the Rattlesnake Tuff, Oregon. *Journal of Petrology* **38**, 133–163.

Suemnicht, G. A. & Varga, R. J. (1988). Basement structure and implications for hydrothermal circulation patterns in the western moat of Long Valley caldera, California. *Journal of Geophysical Research* **93**, 13191–13207.

Sutton, A. N., Blake, S. & Wilson, C. J. N. (1995). An outline geochemistry of rhyolite eruptives from Taupo volcanic centre, New Zealand. *Journal of Volcanology and Geothermal Research* **68**, 153–175.

Sutton, A. N., Blake, S., Wilson, C. J. N. & Charlier, B. L. A. (2000). Late Quaternary evolution of a hyperactive rhyolite magmatic system: Taupo volcanic centre, New Zealand. *Journal of the Geological Society, London* **157**, 537–552.

Tait, S., Thomas, R., Gardner, J. & Jaupart, C. (1998). Constraints on cooling rates and permeabilities of pumice in an explosive eruption jet from colour and magnetic mineralogy. *Journal of Volcanology and Geothermal Research* **86**, 79–91.

Truesdell, A. H. (1966). Ion-exchange constants of natural glasses by the electrode method. *American Mineralogist* **51**, 110–122.

van den Bogaard, P. & Schirnick, C. (1995). $^{40}Ar/^{39}Ar$ laser probe ages of Bishop Tuff quartz phenocrysts substantiate long-lived silicic magma chamber at Long Valley, United States. *Geology* **23**, 759–762.

Verplanck, P. L., Farmer, G. L., McCurry, M., Mertzman, S. & Snee, L.W. (1995). Isotopic evidence on the origin of compositional

layering in an epizonal magma body. *Earth and Planetary Science Letters* **136**, 31–41.

Vigneresse, J. L., Barbey, P. & Cuney, M. (1996). Rheological transitions during partial melting and crystallization with application to felsic magma segregation and transfer. *Journal of Petrology* **37**, 1579–1600.

Wallace, P. J., Anderson, A. T., Jr & Davis, A. M. (1995). Quantification of pre-eruptive exsolved gas contents in silicic magmas. *Nature* **377**, 612–616.

Wallace, P. J., Anderson, A. T., Jr & Davis, A. M. (1999). Gradients in H_2O, CO_2, and exsolved gas in a large-volume silicic magma system: interpreting the record preserved in melt inclusions from the Bishop Tuff. *Journal of Geophysical Research* **104**, 20097–20122.

Wallace, P. J., Dufek, J., Anderson, A. T. & Zhang, Y. (2003). Cooling rates of Plinian fall and pyroclastic-flow deposits in the Bishop Tuff: inferences from water speciation in quartz-hosted glass inclusions. *Bulletin of Volcanology* **65**, 105–123.

Wark, D. A. & Watson, E. B. (2006). TitaniQ: a titanium-in-quartz thermometer. *Contributions to Mineralogy and Petrology* **152**, 743–754, doi: 10.1007/s00410-006-0132-1.

Wark, D. A., Hildreth, W., Watson, E. B. & Cherniak, D. J. (2004). Origin of thermal and compositional zoning in the Bishop magma reservoir: insights from zoned quartz phenocrysts. *EOS Transactions, American Geophysical Union* **85**(47), Fall Meeting Supplement, Abstract V53A-0623.

Wark, D. A., Hildreth, W., Spear, F. S., Cherniak, D. J. & Watson, E. B. (2007). Pre-eruption recharge of the Bishop magma system. *Geology* **35**, 235–238.

Weinberg, R. F. (1997). The disruption of a diorite magma pool by intruding granite: the Sobu body, Ladakh batholith, Indian Himalayas. *Journal of Geology* **105**, 87–98.

Weinberg, R. F. & Leitch, A. M. (1998). Mingling in mafic magma chambers replenished by light felsic inputs: fluid dynamical experiments. *Earth and Planetary Science Letters* **157**, 41–56.

Weinberg, R. F., Sial, A. N. & Pessoa, R. R. (2001). Magma flow within the Tavares pluton, northeastern Brazil: compositional and thermal convection. *Geological Society of America Bulletin* **113**, 508–520.

Wiebe, R. A. (1987). Rupture and inflation of a basic magma chamber by silicic liquid. *Nature* **326**, 69–71.

Wiebe, R. A. (1993). The Pleasant Bay layered gabbro–diorite, coastal Maine: ponding and crystallization of basaltic injections into a silicic magma chamber. *Journal of Petrology* **34**, 461–489.

Wiebe, R. A. (1996). Mafic–silicic layered intrusions: the role of basaltic injections on magmatic processes and the evolution of silicic magma chambers. *Transactions of the Royal Society of Edinburgh (Earth Sciences)* **87**, 233–242.

Wiebe, R. A. & Collins, W. J. (1998). Depositional features and stratigraphic sections in granitic plutons: implications for the emplacement and crystallization of granitic magma. *Journal of Structural Geology* **20**, 1273–1289.

Wilson, C. J. N. & Hildreth, W. (1997). The Bishop Tuff: new insights from eruptive stratigraphy. *Journal of Geology* **105**, 407–439.

Wilson, C. J. N. & Hildreth, W. (1998). Hybrid fall deposits in the Bishop Tuff, California: a novel pyroclastic depositional mechanism. *Geology* **26**, 7–10.

Wilson, C. J. N. & Hildreth, W. (2003). Assembling an ignimbrite: mechanical and thermal building blocks in the Bishop Tuff, California. *Journal of Geology* **111**, 653–670.

Wilson, C. J. N., Blake, S., Charlier, B. L. A. & Sutton, A. N. (2006). The 26·5 ka Oruanui eruption, Taupo volcano, New Zealand: development, characteristics and evacuation of a large rhyolitic magma body. *Journal of Petrology* **47**, 35–69.

Winick, J. A., McIntosh, W. C. & Dunbar, N. W. (2001). Melt-inclusion-hosted excess ^{40}Ar in quartz crystals of the Bishop and Bandelier magma systems. *Geology* **29**, 275–278.

Wolf, M. B. & Wyllie, P. J. (1994). Dehydration-melting of amphibolite at 10 kbar: the effects of temperature and time. *Contributions to Mineralogy and Petrology* **115**, 369–383.

Wolff, J. A. & Ramos, F. C. (2003). Pb isotope variations among Bandelier Tuff feldspars: no evidence for a long-lived silicic magma chamber. *Geology* **31**, 533–536.

Wolff, J. A., Ramos, F. C. & Davidson, J. P. (1999). Sr isotope disequilibrium during differentiation of the Bandelier Tuff, New Mexico: constraints on the crystallization of a large rhyolitic magma chamber. *Geology* **27**, 495–498.

Zhang, Y., Xu, Z. & Behrens, H. (2000). Hydrous species geospeedometer in rhyolite: improved calibration and application. *Geochimica et Cosmochimica Acta* **64**, 3347–3355.